Characterization of tumor-infiltrating B cells in solid tumors

Inaugural Dissertation
for
the doctoral degree of
Dr. rer. nat.

from the Faculty of Biology

University of Duisburg-Essen
Germany

Submitted by

Aparajita Singh

Born in Varanasi, India

Date of submission August 2020

The experiments underlying the present work were conducted at the Research and Development Department of Miltenyi Biotec B.V. & Co. KG (Bergisch Gladbach) in close collaboration with the University of Duisburg-Essen.

1. Examiner: Prof. Dr. Ralf Küppers

2. Examiner: Prof. Dr. Jan Dürig

Chair of the Board of Examiners: Prof. Katharina Fleischhauer

Date of the oral examination: 25.11.2020

Contents

List of abbreviations

A	
APCs	antigen-presenting cells
AID	activation-induced cytidine deaminase
ADCC	antibody-dependent cell-mediated cytotoxicity
ADCP	antibody-dependent phagocytosis
B	
BCR	B cell receptor
B-ALL	B-cell acute lymphoblastic leukemia
BMDCs	bone marrow-derived dendritic cells
Bregs	regulatory B cells
C	
CTLs	cytotoxic T lymphocytes
CLP	common lymphoid precursors
CSR	class switch recombination
CAR	chimeric antigen receptor
CICs	circulating immune complexes
D	
D	diversity
E	
EBF	early B cell factor
F	
FDCs	follicular dendritic cells
H	
K	
K	kappa
L	
LCA-2	common lymphoid 2 progenitor
L	lambda
M	
MHC	major histocompatibility complex
MPPs	multipotent progenitor cells
MALTs	mucosa-associated lymphoid tissues
MICS	multiparameter imaging cell screen
N	
NK cells	natural killer cells
O	
Ovca	ovarian carcinoma
P	
PRRs	pattern recognition receptors
PAMPs	pathogen-associated molecular patterns
PAX5	paired box gene 5
PPs	Peyer’s patches
S	
SLOs	secondary lymphoid organs
SHM	somatic hypermutation
scBCR	single-cell BCR sequencing data

HEVs	high endothelial venules	**T**	
I		TH	helper T cells
IF	immunofluorescence	TI	thymus-independent
IHC	immunohistochemistry	TD	thymus-dependent
ICB	immune checkpoint blockade	TNF-α	tumor necrosis factor-alpha
Ig	immunoglobulin	TILs	tumor infiltrating lymphocytes
IRF	interferon regulatory factor	TIBs	tumor-infiltrating B cells
ICAM1		TLOs	tertiary lymphoid organs
IL	interleukin	TLSs	tertiary lymphoid structures
J		**V**	
J	joining	V	variable

List of Figures

1. Introduction

1.1 B cells in the human immune system

Our first line of defense against foreign pathogens is provided by physical barriers, such as skin or mucous membrane. Any pathogen which crosses the physical barrier encounters the innate immune system – our second line of defense. The term "innate" signifies that it is a defense that all humans naturally have from birth. The key player of the innate immune system are macrophages who are "professional phagocytes", dendritic cells, mast cells, neutrophils, basophils, eosinophils, complement proteins and natural killer cells. They have pattern recognition receptors (PRRs) on their surface and can recognize pathogen-associated molecular patterns (PAMPs) such as peptidoglycans, oligosaccharides on the bacterial cell wall. The response generated through innate immunity occurs rapidly on exposure to an infectious organism. Pathogens which cannot be killed by the innate immune system are handled by the third level of defense: the adaptive immune system. As the name "adaptive" suggests, this is a defense system which can adapt specifically to guard the host against any pathogen, including viruses, bacteria or fungi (Janeway, 2012).

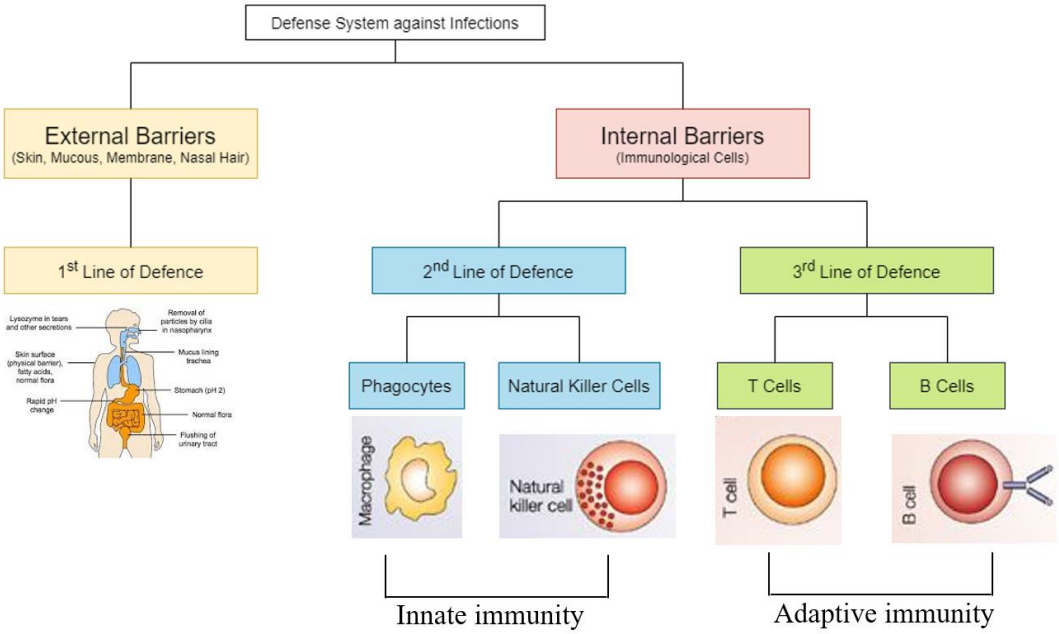

Figure 1: Overview of the human defense system against infections.
Schematic representation of key players involved in the defense system. The first line of barrier is provided by physical membranes followed by the innate and adaptive immune system.

The key players of the adaptive immune system are B cells and T cells which were both essentially discovered simultaneously. Max Cooper and Robert Good proposed a functional division of labor among cells in the chicken bursa of Fabricius accountable for antibody production and cells that required an intact thymus for the manifestation of delayed-type hypersensitivity (Cooper and others, 1965; Cooper and others, 1966).

Although B and T cells are similar in many ways, there are also major differences. B cells make antibodies which can identify any organic molecule, T cells specialize in identifying proteins. Also, B cells can secrete their receptors in soluble form as well as express them as cell membrane receptors, while T cell receptors are only expressed as membrane-inserted receptors. Most importantly, a B cell can recognize an antigen "by itself", on the contrary, a T cell can only recognize an antigen if it is "properly presented" by professional antigen-presenting cells (APCc). T cells can identify fragments of protein antigens which have been partly digested inside APCs. The peptide fragments are then transported to the surface of APC on a special molecule called major histocompatibility complex (MHC) proteins, which present peptides to T cells. There are two kinds of MHC molecules, MHC class I and class II. MHC class I molecules are expressed by mostly all nucleated cells and they present peptides from pathogens, mainly viruses to CD8 cytotoxic T cells, which have the capability to kill almost any cell. On the other hand, MHC class II molecules are expressed by APCs such as dendritic cells, B cells and macrophages and they present antigens to $CD4^+$ T cells, which mainly activate other effector cells of the immune system. B cells and T cells work in close interaction. B cells can function as APCs, where the fragmented peptide is displayed by MHC-II molecules on the surface of B cells, which is recognized by the helper T (T_H) cells, leading through a signaling cascade to its activation. With this signal alone, T cells may become anergic or undergo apoptosis. The second co-stimulatory signal for T cell activation is non-antigen specific and mediated by binding of B7 molecule on the surface of B cells or other activated APCs with CD28 on the surface of T cells. Mostly, these interactions take place in secondary lymphoid organs such as lymph nodes or spleen. These structures provide proper niches for the interaction of foreign antigens with B and T cells circulating from peripheral blood through the body into the secondary lymphoid organs. In the case of an antigen-specific encounter, they can undergo clonal expansion and provide antigen-specific immune reaction (Alberts B, 2002).

1.2 B cell development and differentiation

B cell development starts with the migration of multipotent progenitor cells (MPPs) initially into the fetal liver and then into the bone marrow. MPPs then differentiate into the common lymphoid precursors (CLP) that finally produce the common lymphoid 2 progenitor (LCA-2) which is responsible for the B cell lineage (Tobón and others, 2013). Following this, LCA-2 receives signals from stromal bone marrow cells to induce the further development of B cells. Transcription factors like early B cell factor (EBF) 1, paired box gene (PAX) 5, and interferon regulatory factor (IRF) 8 are important signal molecules for efficient B cell development. The pro-B cell stage is the earliest stage in B cell development. One important characteristic of a B cell is its B cell receptor (BCR). A functional BCR is essential to specifically recognize and respond to pathogens. The BCR consists of two light and two heavy chains, as well as cofactors (CD79a and CD79b). Functional rearrangement of the heavy chain together with V_L-J_L rearrangement of the light chain makes complete BCR. Presence of multiple copies of the variable (V), diversity (D) and joining (J) gene segments corresponding to each light and heavy chains (D only for the heavy chain), results in providing millions of different antibody specificities in humans. The high variance and therefore flexibility of B cell specificity is obtained by the wide range of VDJ gene segments which are combined during B cell development. Here, first, the D_H and J_H segment of the immunoglobulin (Ig) heavy chain (IgH) locus and subsequently the V_H to D_HJ_H are joined with the help of recombination activating genes 1 and 2 (RAG1/2) (Oettinger and others, 1990; Schatz and others, 1989). After successful $V_HD_HJ_H$ recombination, the heavy chain pairs with a surrogate light chain (λ5-Vpre-B) and along with the expression of signal-transducing components Ig-α and Ig-β, it completes the formation of pre-BCR (Karasuyama and others, 1994; Pillai and Baltimore, 1987). As a quality control, a positive selection is conducted checking successful Ig heavy chain expression. For B cell survival and continuous differentiation signaling through the pre-BCR is critical. Only B cells which have a functional and responsive BCR expressed on their surface obtain these signals while the others undergo apoptosis (Kitamura and others, 1992). Following this, RAG proteins are produced again in pre-B cells and rearrangement of a light chain locus starts. The light chain has two genes, kappa (κ) and lambda (λ) and light chains display isotypic exclusion, meaning the expression of only one type of light chain – κ or λ - by a single B cell. Complete rearrangement of light chain results in the formation of IgM-bearing immature B cells (Figure 2).

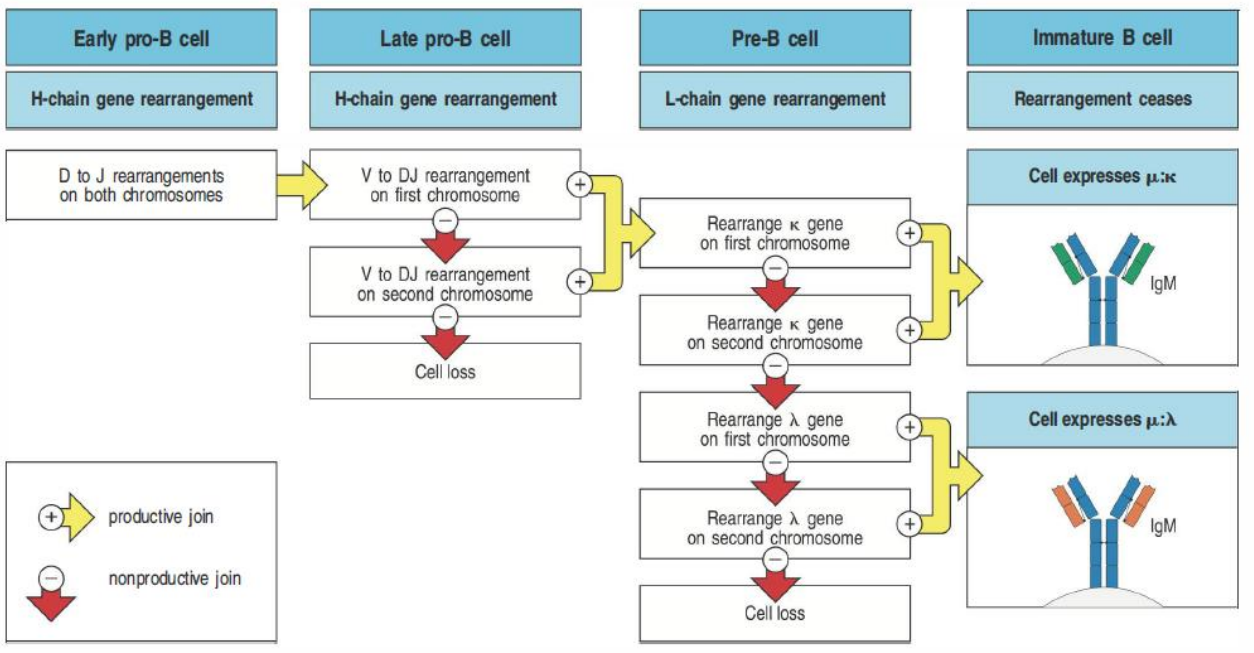

Figure 2: B cell receptor rearrangement during B cell development

B cell development begins in the bone marrow, where first rearrangements of the heavy chain occur followed by rearrangement of light chain genes which display isotypic exclusion. After the complete rearrangement of heavy and light chains, IgM-bearing immature B cell leaves the bone marrow (Janeway, 2012).

On encounter with antigen, signaling via the BCR induces B cell activation. The real mechanism by which antigen binding activates the BCR remains an active topic of investigation. One hypothesis is that antigen binding leads to clustering of BCRs on the membrane to induce signaling (Liu and others, 2016). On the contrary, another model is that BCR clusters preexist already before antigen encounter, and antigen-binding separates these clusters allowing signaling to occur (Yang and Reth, 2016). Naive B cells have membrane-bound immunoglobulins of the IgM and IgD isotypes, in which intracellular domains are missing. Therefore signal transduction is dependent on linked molecules. Igα and Igβ are the signaling subunits of the BCR, which contain intracellular ITAM motifs that can be phosphorylated by tyrosine kinases (Kurosaki, 2011; Yang and Reth, 2016). After tyrosine phosphorylation, a cascade of downstream signaling events begins, including the activation of multiple pathways. One example is CD19 which interacts with IgM and IgD and is involved mainly in prompting the PI3 kinase-Akt pathway (Kurosaki and others, 2010). Altogether, signals transduced downstream of the BCR complex result in alteration in the

expression of many genes, including upregulation of costimulatory molecules (CD86, CD80), adhesion molecules (e.g. ICAM1), migration receptors, pro-survival molecules, and cell-cycle-related genes.

Depending on the nature of the antigen, there can be two ways for B cell activation: thymus-independent (TI) and thymus-dependent (TD), based on if they require direct contact with helper T cells (T_H) or not. When naïve B cells come in contact with antigens like polysaccharides from bacterial capsules, it leads to clustering of surface immunoglobulins that can lead to activation of B cells, such response is called TI response as they occur without co-stimulation from T_H cells. On the other hand, soluble protein antigens which after binding with BCR gets internalized, processed and are displayed as peptides on MHC-II molecules, are recognized by T_H cells. T_H cells further express CD40L and produce cytokines like interleukin (IL)-21, which provides signal for B cell activation, such responses are called TD as they required assistance from T_H cells for activation (Liao and others, 2017). Usually, naïve B cells home to secondary lymphoid organs such as spleen or lymph nodes (Nieuwenhuis and Opstelten, 1984). In the case of antigen encounter, germinal centers are formed in the spleen or lymph nodes within 3 days. Germinal centers possess distinct zones, the dark and the light zones. The dark zone is composed of centroblasts undertaking fast cycles of proliferation. In proliferating B cells, activation-induced cytidine deaminase (AID) expression is induced which is essential for somatic hypermutation (SHM), the process of introducing base-pair changes in V_H and V_L regions of IgH and IgL genes. Subsequently, the centroblasts exit the dark zone to enter the light zone, as centrocytes. The light zone contains antigen-antibody complex-bearing follicular dendritic cells and $CD4^+$ T cells and mainly is the area for clonal selection of high affinity and self-tolerant clones. B cells also undergo class switch recombination (CSR) of IgH chains to IgG, IgA, and IgE in the light zone. Following this, B cells recirculate between dark and light zones and undergo several rounds of proliferation-mutation-selection before the cells differentiate to become memory B cells or plasma cells. Any clone which shows autoreactivity or high-affinity to self-antigens is eliminated to avoid autoimmune diseases (Brink, 2014; Heise and others, 2014; Königsberger and others, 2015). Following this, B cells can differentiate into memory B cells, owing to the ability to mount rapid responses when secondary exposure to antigen happens, as memory B cell have a lower threshold of activation (Bar-Or and others, 2001). Besides this B cells can terminally differentiate into plasma cells, which protects by secretion of antigen-specific antibodies. When cells continue proliferating, they are denoted as

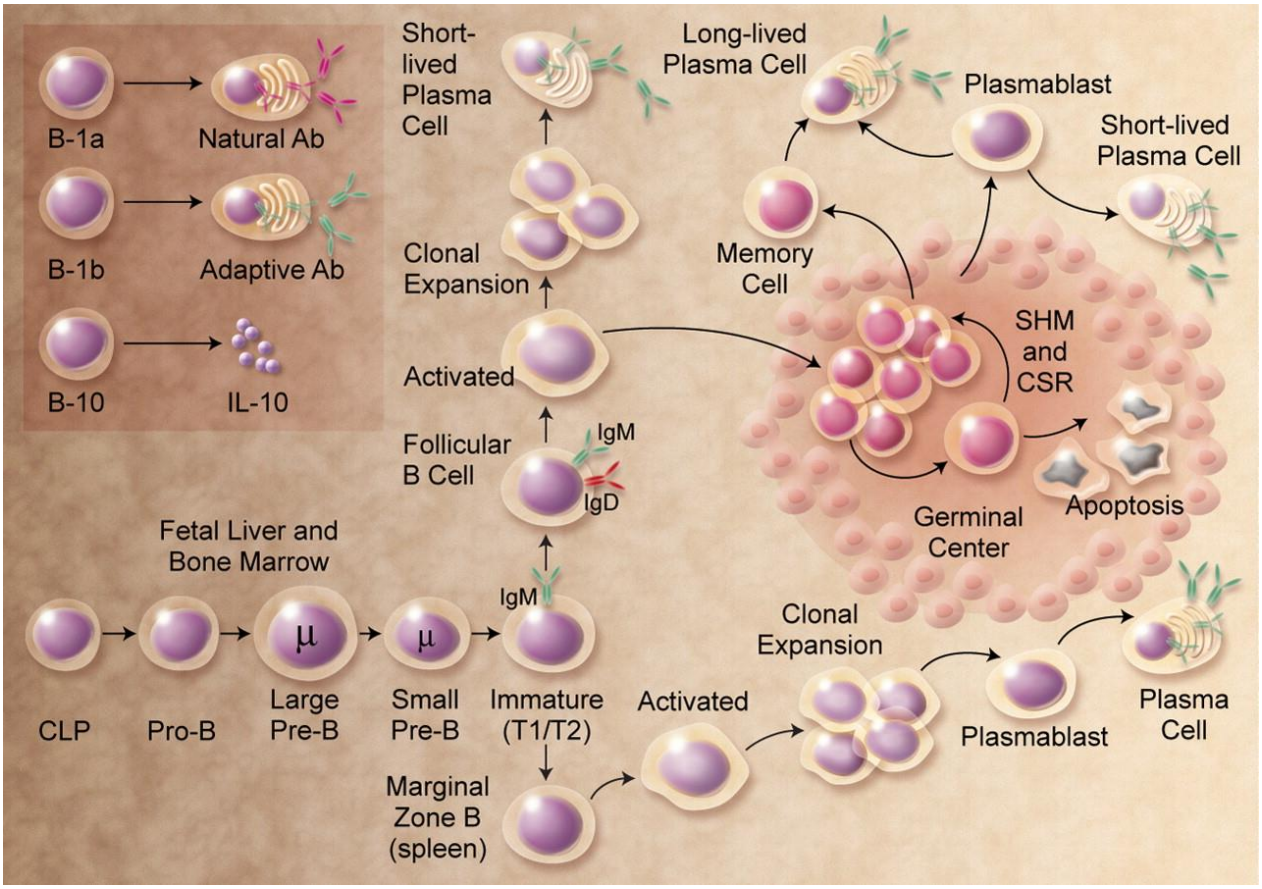

Figure 3: B cell differentiation.

Schematic diagram representing different stages throughout B cell development. In bone marrow from common lymphoid progenitor first, pro-B cells are formed, following initiation of heavy and light chain rearrangements. A functional BCR expressing naïve B cell then leaves the bone marrow and migrates via blood to secondary lymphoid organs where it undergoes upon encounter with its specific antigen germinal center reaction to finally differentiate to memory or plasma cells (Lebien and Tedder, 2008).

plasmablasts (Nutt and others, 2015). Only after they stop dividing and fully mature, they differentiate to plasma cells (Figure 3). These differentiation states are prejudiced by a diversity of signals, such as those from the BCR, co-receptors, and cytokines. B cells having a greater affinity for their respective antigen develop a stronger plasma cell response in comparison to B cells having a lower affinity towards antigen (Kräutler and Suan, 2017).

B cells are primarily known for producing antigen-specific antibodies, but apart from this classical role, B cells can also work as potent APCs resulting in antigen-specific T cell expansion, cytokine release and memory generation (Batista and Harwood, 2009; Crawford and others, 2006).

Costimulatory molecules like CD40, CD80 and CD86 are expressed by B cells and provide ideal T cell activation (Linton and others, 2003). B cells also maintain effector immune functions via the secretion of several cytokines, such as tumor necrosis factor-alpha (TNF-α) and IL-6 for supporting inflammatory functions or IL-10 and IL-35 for regulatory, immunosuppressive functions (Fillatreau and others, 2002; Shen and others, 2014).

1.3 B cells in diseases

As mentioned in the previous section, the development of B cells is tightly regulated and errors can lead to severe malfunction and diseases. Depending on which mechanisms are affected this can be divided into autoimmune diseases or leukemia and lymphoma. In case of autoimmune diseases, the immunoglobulin production and B cell development are affected leading to an abnormal immune response to the so-called self-antigens, while B cell leukemia and lymphoma are developing if cells are proliferating in an uncontrolled manner leading to malignancy (Casola and others, 2019).

1.3.1 B cells in cancer

Besides their role in autoimmune disease, leukemia and lymphoma where B cells can be the primary cause of disease pathogenesis, B cells can also have an indirect effect as part of the tumor microenvironment in other tumors. Multiple studies have shown prolonged survival in patients with melanoma and other cancers after undergoing immunotherapy (Coventry and others, 2015; Hsueh and others, 2002) and the field is commencing to gain perception into the mechanisms of therapeutic responses as well as biomarkers of response and resistance. Substantial progress has been made especially with the identification of numerous confirmed biomarkers, particularly for immune checkpoint blockade (ICB) (Cottrell and Taube, 2018; Jacquelot and others, 2017). It is evident that cytotoxic T cells have a leading part in responses to ICB and other forms of immunotherapy. Nevertheless, there is an increasing appreciation of additional components of the tumor microenvironment that can have an impact on the therapeutic response—including myeloid cells and other types of immune cells (Fridman and others, 2017). It has been shown in primary tumors that the presence of $CD8^+$ tumor infiltrating lymphocytes (TILs) carries a >2-fold increased probability of survival (Hwang and others, 2012). However, $CD8^+$ TILs do not work in isolation. It has been observed that tumors with $CD8^+$ TILs present are often infiltrated with $CD20^+$ B cells as well (Milne and others, 2009). Notably, in some instances, tumors containing both $CD8^+$ and $CD20^+$ TILs are associated with a better prognosis than $CD8^+$ TILs alone (Nielsen and others, 2012). Similar findings have been reported in a variety of others cancers (Iglesia and others, 2014; Richards and others, 2012), suggesting that effective tumor immunity requires cooperative interactions between T cells and B cells.

Apart from immune-regulatory functions of antibody and antibody-antigen complexes, B cells can assist the functions of other immune cells by presenting antigens, providing

costimulation, and secreting cytokines (Martin and Chan, 2006). Through global gene expression profiles, B cell gene signatures have been associated with a better outcome for several cancer types, including breast and ovarian (Iglesia and others, 2014; Schmidt and others, 2008). However, B cells illustrate a diverse population with functionally distinct subsets, contributing to both pro- as well as antitumor immune responses, and the balance among the subsets might impact tumor development and behavior (Fremd and others, 2013; Nelson, 2010). Therapeutic ICB therapy which mainly focuses on activated T cells might also target activated B cells, as PD-1, PD-L1, CTLA-4, and the B7 molecules are also expressed by B cells. Both, CTLA-4 and PD-1 hinder B cell activation and blockade of either molecule increases the proliferation of memory B cells and the production of antibody, either by directly or indirectly acting on B cells (Fanoni and others, 2011; Intlekofer and Thompson, 2013; Okazaki and others, 2001; Pardoll, 2012; Pioli and others, 2000; Postow and others, 2015; Thibult and others, 2013). The ability to elicit an antibody-dependent anti-tumor immunity by a B cell involves a wide variety of molecular and cellular mechanisms, some of which may represent novel therapeutic targets in oncology.

1.3.2 Anti-tumor specific response by B cells

Significant B cell populations have often been reported in solid tumors, suggesting a role of these cells in cooperation with other resident cells to influence the tumor microenvironment (Schmidt and others, 2008). Adoptive-transfer studies in mice and correlative studies in human cancer have also described a protective and antigen-specific role to TIL B cells. Studies have shown that the presence of B cells in cervical cancer (Nedergaard and others, 2008) and in lung cancer (Al-Shibli and others, 2008) correlate with increased survival and reduced relapse rates. Furthermore, in different human cancer patients, antibodies directed against intracellular tumor antigens like MUC1, NY-ESO-1, MYC, survivin, and p62 have been detected (Reuschenbach and others, 2009). In medullary breast cancer patients, antibodies against aberrantly exposed B-actin have been reported which was associated with better outcome (Hansen and others, 2002). Besides this, studies in lung cancer have shown that the presence of anti-p53 antibodies corresponds with

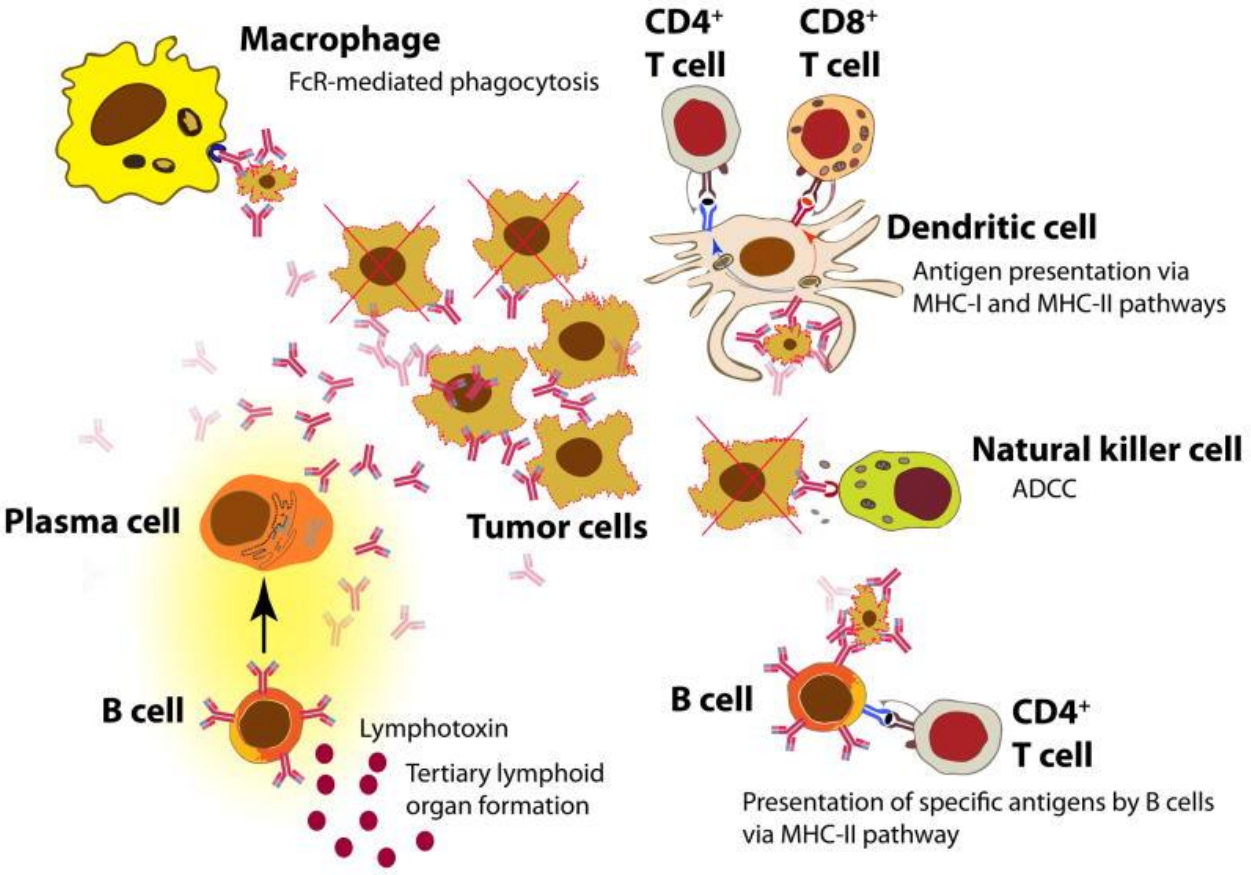

Figure 4: Role of B cells in antitumor response.

Antibodies secreted by plasma cells can contribute in antitumor response in many ways: By promoting antibody- and complement-mediated killing of tumor cells, Fc-mediated phagocytosis by macrophages, and ADCC by natural killer (NK) cells. Antibody bound tumor cells can also be taken up and processed by dendritic cells, which can present antigens to $CD4^+$ T cells and cross-present to $CD8^+$ T cells. B cells can also process tumor antigens, and present them to $CD4^+$ T cells. Lymphotoxin, produced by B cells, can have a role in the formation of tertiary lymphoid organs, which is correlated with better outcome in patients. Picture adapted from (Yuen and others, 2016).

better prognosis (Kumar and others, 2009). Interestingly, a combined study on single-cell transcriptomics together with bulk gene expression data has shown that the expression of complement genes correlated with T cell enrichment in several tumors (Tirosh and others, 2016). It has been shown that human tumor cells coated with allogenic natural IgG induce activation of bone marrow-derived dendritic cells (BMDCs) from mesothelioma patients, which then in turn was able to drive the proliferation of $CD4^+$ T cells (Carmi and others, 2015).

B cells are efficient antigen prsenting cells, owing to their ability to take up specific antigen even at low concentration using their BCRs. Memory B cells are a subset of long-lived B cells and hence can present antigens to T cells even after the first wave of dendritic cells drops (Yanaba and others, 2008)and in this way further drive T cell expansion and memory formation. B cells can directly regulate the functions of target proteins, or provide anti-tumor effect through opsonization of tumor antigens, the complement-mediated killing of tumor cells, or by antibody-dependent cell-mediated cytotoxicity (ADCC) and antibody-dependent phagocytosis (ADCP). Besides, tumor cells can also be attacked by B cells through secretion of granzyme B and TRAIL signaling when stimulated with IL-21 and IFN-γ or TLR, respectively, which can have cytotoxic effects against tumor cells (Hagn and others, 2009; Kemp and others, 2004). Through CD27-CD70 interactions, B cells can also mediate the generation of $CD4^+$ T cell memory (Whitmire and others, 2009) and promote the survival and proliferation of activated $CD8^+$ T cells (Deola and others, 2008). Under the impact of $CD4^+$ Th1 and Th2 cells, B cells can be differentiated into subsets that produce IFN-γ, TNF-α, IL-6, and IL-2 (Lund, 2008), which can further regulate other immune cells. Lymphotoxin can mediate tumorigenesis (Ammirante and others, 2010), but when it is produced by B cells, it can also mediate the formation of ectopic tertiary lymphoid organs (TLOs) (Luther and others, 2000; Schrama and others, 2001).

1.3.3 Tumor promoting role of B cells

Despite the promising role of tumor-infiltrating B cells (TIBs) in the anti-tumor response within different tumor entities, there have been contrasting findings as well. Human B cells have been also described to promote tumor progression. $CD19^+$ B cell infiltration in patients with metastatic ovarian carcinoma was found to be associated with poor disease outcome (Dong and others, 2006). Furthermore, with partial B cell depletion using rituximab, reduction in tumor burden was observed in 50% of patients with advanced colorectal cancer (Barbera-Guillem and others, 2000). The correlation between antitumor antibodies and tumor progression can be linked with the capability of these antibodies to form circulating immune complexes (CICs). While these CICs are mostly discussed in the context of diseases such as systemic lupus erythematosus and serum sickness, they also play a role in tumor advancement (Gunderson and Coussens, 2013). CICs in humans do not mostly correlate with antitumor immunity, instead, they show poor outcome (Kumar and others, 2009). In a study using a mouse model of squamous cell carcinoma, CICs were found to be accumulated in premalignant tissue and activate Fcγ receptors on infiltrating myeloid cells (mostly

macrophages and mast cells) (Andreu and others, 2010) inducing myeloid suppressor cell activity. Besides that, they also stimulate the complement pathway which triggers a pro-angiogenic program of tissue remodeling that leads to keratinocyte hyperproliferation and malignant progression (de Visser and others, 2005; Gunderson and Coussens, 2013) (Figure 5).

Induction of lymphangiogenesis is an important characteristic of cancer to promote metastasis of neoplastic cells (Folkman, 1971). It can be enhanced by inflammation and thus facilitate immune cell migration into the lymphatics. It has been recently described that B cells can provide lymphotoxin, a growth factor which can trigger angiogenesis. In a mouse prostate cancer model, following androgen ablation, production of the chemokine CXCL13, probably by T follicular helper cells, was associated with tumor CXCL13 expression and recruitment of B cells into the tumor (Bindea and others, 2014; Bindea and others, 2013; Gu-Trantien and others, 2013; Teng and others, 2015). These TIBs were then reported to produce lymphotoxin which triggers canonical and non-canonical NF-κB signaling and STAT3 in the tumor cells, consequentially leading to tumor progression (Ammirante and others, 2010; Luo and others, 2007; Woo and others, 2014).

Regulatory B cells (Bregs) are another B cell subset that in itself can be defined as a heterogeneous population of B cells that produce a diversity of immunoregulatory cytokines, which are capable of suppressing inflammatory responses, either directly or indirectly by inhibiting effector cells such as $CD8^+$ cytotoxic T lymphocytes (CTLs) and NK cells (Lund, 2008). Bregs are mostly characterized as cells that secrete IL-10, but Breg cells can also secrete IL-35 or TGF-β (Bodogai and others, 2015; Shen and Fillatreau, 2015; Shen and others, 2014). There can be phenotypic and functional variations between different Breg subsets: there can be IL-10 producing Bregs that suppress inflammation and facilitate cancer growth (de Visser and others, 2005), B cells that restrict $CD4^+$ T cell responses (Olkhanud and others, 2011) and distinct tumor-induced Bregs (Wejksza and others, 2013). It has been shown that TGF-β produced by Bregs can switch naïve $CD4^+$ T cells into $Foxp3^+$ Tregs, which can further restrict NK cells and effector $CD8^+$ CTLs, leading to metastasis (Bodogai and others, 2015; Olkhanud and others, 2009). The conversion of B cells to Bregs has been shown to be induced by IL-21, a cytokine produced by Tregs, as IL-21 endorses the upregulation of IL-10, IDO and granzyme B (Lindner and others, 2013). While granzyme B is mostly associated with NK cells, as well as with $CD8^+$ and $CD4^+$ CTLs, it has been found that Bregs can transfer this serine protease molecule (granzyme) from B to T cells, degrading the T cell receptor chain ζ without inducing T cell apoptosis, resulting in inhibition of antitumor T cell-mediated activity (Lindner and others, 2013).

Experiments done on the development of murine mammary tumors implanted in mice have shown the association of TIBs with less recruitment and proliferation of $CD49^+$ NK and $CD8^+$ T cells, even irrespective of IL-10 secretion by B cells (Zhang and others, 2013). Bregs also produce TGF-β, which activates the monocyte and granulocyte subsets of MDSCs to increase reactive oxygen species and nitric oxide production. These are essential for efficient inhibition of $CD4^+$ and $CD8^+$ T cells mediated antitumor response (Bodogai and others, 2015; Lee-Chang and others, 2019).

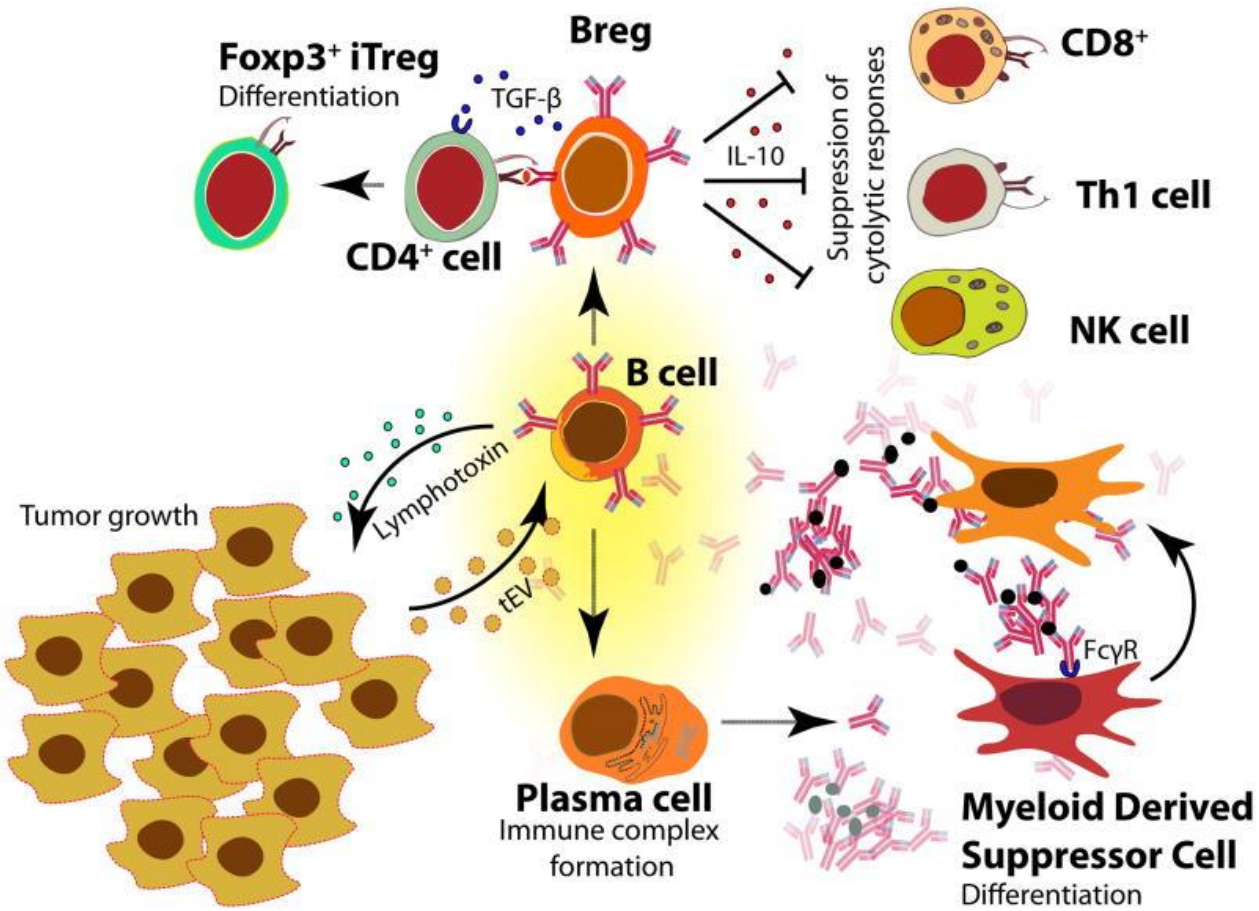

Figure 5: Role of B cells in promoting tumor progression.

Antibodies produced by B cells can bind to antigen and form circulating immune complexes (CICs) which can activate Fcγ receptors on myeloid cells, stimulating them to MDSCs which can inhibit $CD4^+$ and $CD8^+$ T cells. B cells can also produce lymphotoxin, which can induce angiogenesis. Bregs can secrete several immunoregulatory cytokines such as IL-10 and TGF-β which can suppress effector cells like $CD4^+$ T cells, NK cells or $CD8^+$ cytotoxic T cells (Yuen and others, 2016).

1.3.4 B cells in tertiary lymphoid structures

Canonical secondary lymphoid organs (SLOs) encompass spleen, lymph nodes, tonsils and the mucosa-associated associated lymphoid tissues (MALTs) including intestinal Peyer's patches (PPs). SLOs are highly specialized, organized structures especially adapted to mediate immune cell interactions which are essential for proper immune response initiation. Tertiary lymphoid structures (TLSs) are ectopic SLO-like structures, mainly discrete, structured organization of infiltrating immune cells (Messina and others, 2012), formed at the site of chronic inflammation such as autoimmune diseases, allograft rejection, and in cancer (Dieu-Nosjean and others, 2014; Pimenta and Barnes, 2014). They are topologically composed of tightly packed B cells and follicular dendritic cells (FDCs), surrounded by T cells, dendritic cells and high endothelial venules (HEVs) (Sautes-Fridman and others, 2019). HEVs are highly specialized capillary venules, whose function is homeostatic delivery of lymphocytes from the neighboring bloodstream.

In several studies, tumor-infiltrating B cells have been found to be linked with better outcomes when they are found to be associated with TLSs (Cabrita and others, 2020; Helmink and others, 2020; Sautès-Fridman and Petitprez, 2019; Sautes-Fridman and others, 2019). These TLSs are thought to be a modulator of anti-tumor response. There is evidence where mature TLSs show formation of germinal center-like structures characterized by CD23 expression in lung squamous cell carcinoma (Siliņa and others, 2018). In cutaneous melanoma and metastases (Cipponi and others, 2012; Selitsky and others, 2019) oligoclonal B cell responses were identified, suggesting B cell-driven active immune response within TLSs. More investigations are required to find out the exact role of B cells in the TLSs and their correlation with anti-tumor response.

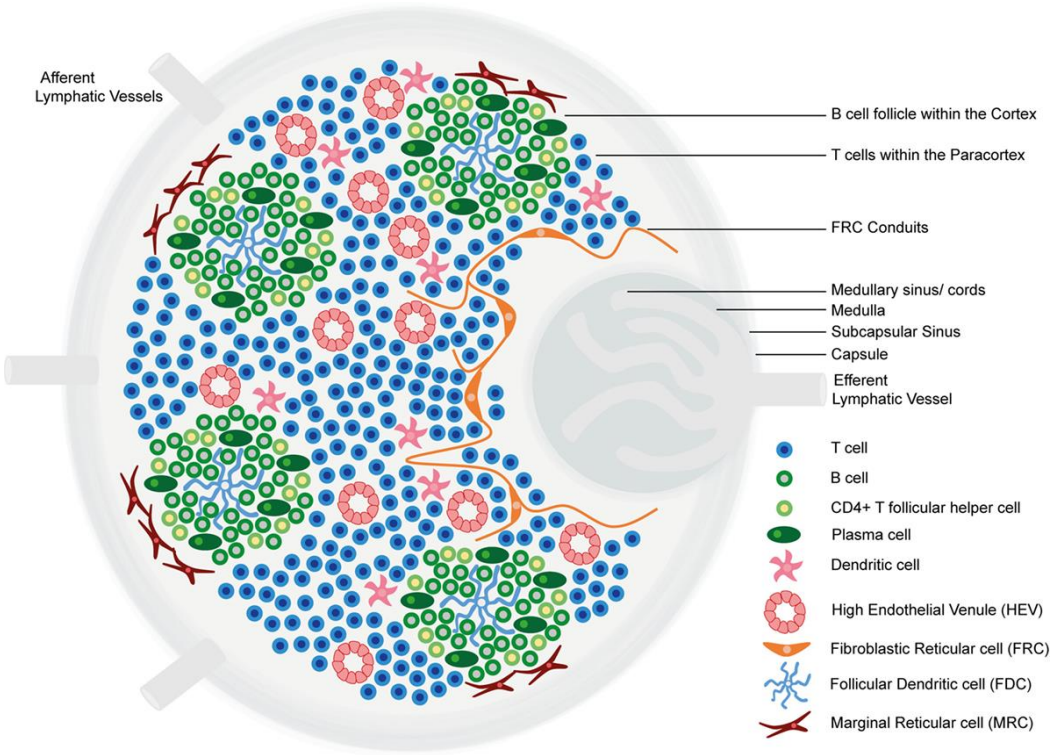

Figure 6: Model of the composition of TLS.

T and B cells are segregated into distinct zones. Mature DCs are located within T cell zone, while B cells cluster to form B-cell follicles around FDCs. HEVs allow extravasation of immune cells from circulation. (Colbeck and others, 2017)

1.4 Aim of the study

As mentioned in the sections above, B cells perform widely diverse roles in tumor immunity as part of the tumor microenvironment. In different cancer entities, B cells can act either tumor growth-promoting or as mediators of antitumor responses. However, further characterization of pro- vs. anti-tumor B-cell subsets will assist to pinpoint the exact roles of B cells in the tumor and the factors which are responsible for the distinct B cell subset generation. By identifying specific markers for pro- as well as for anti-tumor B cells, we can target depletion of only protumorigenic B cells using CAR therapy. Also, as CAR therapies comprise an antibody part for target recognition, identification of a potential new tumor-specific antigen by BCR sequencing could be used for evolving new and more effective CAR treatments. Knowledge about markers expressed by B cells can also open doors for ICB therapy, by which specific activation of B cells in tumor microenvironment might be achieved.

Therefore, this project aimed to shed light on the phenotypes of the B cells infiltrating solid tumors, in context to their spatial localization within the tumor. The purpose was to investigate the exact surface marker profiling of these TIBs, followed by validation of their gene expression profiling. As B cells produce tumor antigen-specific antibody, analysis on BCR sequencing was performed to screen for tumor-specific antibody. With regular microscopy techniques, there are limitations to obtain information about multiple cell-cell interactions, and protein co-expression on single tissue. Approaches allowing information about several marker combinations on single cell provides accurate and precise knowledge about the phenotypical and functional status of the cells in the tissue. For that reason, MACSima technology was developed and optimized during the study to decipher more insights about B cells infiltrating solid tumors. Also, single cell BCR sequencing and RNA sequencing was deployed using the 10X genomics platform to characterize the exact status of B cells in fresh solid tumors, which can be a very useful information to develop or improve therapies. As B cells can secrete antibodies against tumor antigens, this property was applied to generate tumor specific antibody and its validation.

2. Material and methods

2.1 MACSima imaging system

MACSima™ Imaging System, an instrument developed by Miltenyi Biotec, Bergisch Gladbach, Germany, is based on MICS (MACSima Image Cyclic Staining) technology, enabling highly multiplexed immunofluorescence imaging. The basic principle of the technology is the cyclic acquisition of images (stain-image-erase) with a bleaching step involved after each antibody staining. Bleaching is performed with help of white LED light to erase fluorescence signals via photobleaching. The advantage of the technology is that it allows staining of more than 100 markers on single tissue sections, meaning one can look at multiple markers of interest along with keeping their spatial information in the tissue.

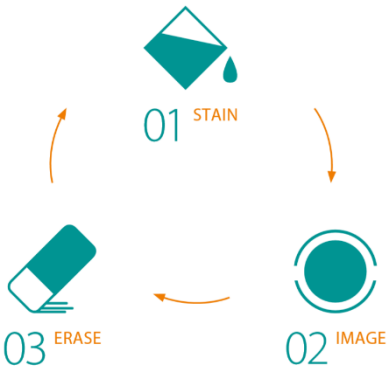

Figure 7: Principle of MACSima imaging platform.

2.1.1 Cryosectioning

Fresh frozen solid tumor tissues, healthy ovary and tonsil tissues of various entities were bought from ProteoGenex or arranged from collaborators and stored at -80°C. Sectioning of the tissues was performed using the Cryostat instrument (Leica Biosystem, Germany). Sectioning was performed at -18°C to -22°C in 8 µm thickness. Serial sections were taken for various experiments: for immunohistochemistry (IHC) staining and MACSima technology. Slices were fixed for 3 minutes in ice-chilled acetone and then stored at -80°C until the day of the run.

2.1.2 Preparation of antibody plate

A detailed list of markers was made covering all subsets of B cells, activation markers, general immune cell markers, tumor microenvironment and TLS related markers, as mentioned in the table below:

Table 1: List of antibodies used for MACSima run

S.No.	Marker	Clone	Conjugate	Provider	Titer
1	CD19	REA675	PE	Miltenyi Biotec	50
2	CD326	REA635	FITC	Miltenyi Biotec	50
3	IgG	M1310G05	PE	Bio legend	5
4	CD20	REA780	PE	Miltenyi Biotec	50
5	CD27	M-T2T1	PE	Miltenyi Biotec	50
6	CD38	IB6	PE	Miltenyi Biotec	50
7	CD138	44F9	PE	Miltenyi Biotec	50
8	CD22	REA340	PE	Miltenyi Biotec	10
9	IgD	REA740	PE	Miltenyi Biotec	50
10	CD279	PD1.3.1.3	PE	Miltenyi Biotec	50
11	CD80	REA661	PE	Miltenyi Biotec	10
12	CD23	M-L23.4	PE	Miltenyi Biotec	10
13	CD24	REA832	PE	Miltenyi Biotec	50
14	CD28	REA612 (L293)	PE	Miltenyi Biotec	10
15	Bcl-2	REA872	PE	Miltenyi Biotec	50
16	IgM	PJ2-22H3	PE	Miltenyi Biotec	10
17	CD45	5B1	PE	Miltenyi Biotec	50
18	CD273	REA985	PE	Bio legend	30
19	CD40	HB14	PE	Miltenyi Biotec	10
20	CD79a	REA1168	PE	Miltenyi Biotec	50
21	CD79b	REA120	PE	Miltenyi Biotec	10
22	CD86	REA968	PE	Miltenyi Biotec	50
23	CD95	LT95	PE	Life span Biosciences	5
24	CD21	REA940	PE	Miltenyi Biotec	50

25	CD183	2AR1	PE	Miltenyi Biotec	10
26	HLA-ABC	REA230 (G46-2.6)	PE	Miltenyi Biotec	50
27	CX3CR1	REA385	PE	Miltenyi Biotec	10
28	CD154	REA238	PE	Miltenyi Biotec	10
29	Bcl-6	REA373	PE	Miltenyi Biotec	50
30	BAFFr_1	11C1	PE	Bio legend	15
31	PAX5_1	1H9	PE	Bio legend	50
32	TSPAN8	REA443	PE	Miltenyi Biotec	50
33	Ki-67	REA183 (B56)	PE	Miltenyi Biotec	10
34	HLA-DQ	REA303 (SPVL3)	PE	Miltenyi Biotec	10
35	CD102	REA878	PE	Miltenyi Biotec	50
36	CD200	REA1067	PE	Miltenyi Biotec	10
37	CD45RA	T6D11	PE	Miltenyi Biotec	50
38	CD45RO	UCHL1	PE	Miltenyi Biotec	10
39	CD208	REA295	PE	Miltenyi Biotec	10
40	CD34	AC136	PE	Miltenyi Biotec	10
41	HLA-DR	REA805	PE	Miltenyi Biotec	50
42	CD72	REA231	PE	Miltenyi Biotec	10
43	CD52	REA164	PE	Miltenyi Biotec	10
44	IgA		PE	Life span Biosciences	5
45	CD3	REA613	PE	Miltenyi Biotec	50
46	CD8	REA734	PE	Miltenyi Biotec	50
47	CD4	VIT4	PE	Miltenyi Biotec	50
48	CD39	REA739	PE	Miltenyi Biotec	50
49	CD25	REA570	PE	Miltenyi Biotec	10
50	CD137	REA756	PE	Miltenyi Biotec	50
51	CD69	FN50	PE	Miltenyi Biotec	10
52	CD11a	REA378	PE	Miltenyi Biotec	10
53	CD366	REA635	PE	Miltenyi Biotec	50
54	KLRG1	REA261	PE	Miltenyi Biotec	10
55	CD58	TS2/9	PE	Miltenyi Biotec	10

56	CD1c	AD5-8E7	PE	Miltenyi Biotec	50
57	CD196	REA190	PE	Miltenyi Biotec	10
58	CD223	REA351 (17B4)	PE	Miltenyi Biotec	10
59	CD49e	NKI-SAM1	PE	Miltenyi Biotec	10
60	CD15	VIMC6	PE	Miltenyi Biotec	10
61	CD11c	MJ4-27G12	PE	Miltenyi Biotec	10
62	CD10	REA877	PE	Miltenyi Biotec	50
63	CD163	GHI/61.1	PE	Miltenyi Biotec	10
64	CD56	REA196 (NCAM16.2)	PE	Miltenyi Biotec	50
65	CD150	REA151	PE	Miltenyi Biotec	10
66	CD64	10.1.1	PE	Miltenyi Biotec	50
67	CD14	REA599	PE	Miltenyi Biotec	50
68	CD49f	GoH3	PE	Miltenyi Biotec	10
69	CD161	REA631	PE	Miltenyi Biotec	10
70	CD164	67D2	PE	Miltenyi Biotec	10
71	CD73	AD2	PE	Miltenyi Biotec	50
72	CD62L	145/15	PE	Miltenyi Biotec	10
73	MECA-79		FITC	Thermo fischer	50
74	CD274	28-8	FITC	Abacm	50
75	CD16	REA423	FITC	Miltenyi Biotec	50
76	CD103	ACT8	FITC	Miltenyi Biotec	10
77	CD31	REA730	FITC	Miltenyi Biotec	50
78	CD244	REA112	FITC	Miltenyi Biotec	10
79	FoxP3	236A/E7	FITC	Invitrogen	10
80	CD193	REA574	FITC	Miltenyi Biotec	50
81	CD197	REA546	FITC	Miltenyi Biotec	10
82	CD127	REA614	FITC	Miltenyi Biotec	10
83	CD134	REA621	FITC	Miltenyi Biotec	10
84	CD105	REA794	FITC	Miltenyi Biotec	50
85	CD192	REA624	FITC	Miltenyi Biotec	10
86	CD119	REA161	FITC	Miltenyi Biotec	10

87	CD122	REA167	FITC	Miltenyi Biotec	10
88	CD55	JS11	FITC	Miltenyi Biotec	10
89	CD81	REA958	FITC	Miltenyi Biotec	50
90	CD30	Ki-2	FITC	Miltenyi Biotec	10
91	CD51	REA181	FITC	Miltenyi Biotec	10
92	CD222	REA187	FITC	Miltenyi Biotec	10
93	CD217	REA290	FITC	Miltenyi Biotec	10
94	CD218a	H44	FITC	Miltenyi Biotec	10
95	CD148	REA204	FITC	Miltenyi Biotec	10
96	CD275	MIH12	FITC	Miltenyi Biotec	10
97	CD182	REA208	FITC	Miltenyi Biotec	10
98	CD66e	REA876	FITC	Miltenyi Biotec	50

All the antibodies were pipetted in their respective titers along with Hoechst (Hoechst 33342 Sigma-Aldrich, Germany), FcR block (Miltenyi Biotec) and AutoMACS Running Buffer (Miltenyi Biotec). Antibody plate was sealed and placed in 4 °C.

2.1.3 Loading of the tissue plate and starting the run

Tissue plate previously-stored at -80°C was placed in ice-chilled acetone for 10 minutes for fixation. Following this, the tissue plate was dried and glued with a frame of a 24-well plate prepared with double-sided adhesive tape, and 1 ml of AutoMACS Running Buffer was added. Pre-staining was performed using anti-CD19-PE (clone: REA675, Miltenyi Biotec), anti-CD326 – FITC (clone: REA635, Miltenyi Biotec) and Hoechst for 10 minutes. 1 ml of AutoMACS Running Buffer was added and the tissue plate was placed in a respective slot in the MACSima instrument. Similarly, antibody plate was also placed in MACSima instrument before the start of the run. The region of interest was selected using pre-staining markers and the run was started by the facility member. 20X magnification is used to acquire images.

2.1.4 Processing of the data

After successful completion of the run, images were processed using an in-house developed pipeline, called MTP.exe (MICS Preprocessing Tool). With this tool, the images are prepared for subsequent image analysis. The procedure consists of 4 steps:

1. Dark-frame subtraction: helps in the correction of noise and pixel errors of the CCD camera chip.
2. Flat-field correction: cancels the effects of image artifacts e.g. caused by uneven illumination through the optical path.
3. Image registration: The image registration transforms the images of all cycles into one coordinate system with the help of the Hoechst images (stained nuclei) of each cycle.
4. Bleach correction: After the photobleaching step there might be residual fluorescence signals that would distort the signal of the subsequent cycle. To correct this the bleaching image of the previous cycle is subtracted from the fluorescence image of the current cycle.

2.2 Immunohistochemistry staining

Sectioning of the tissues was performed using the Cryostat instrument (Leica Biosystem, Nussloch), at -18°C in 8 µm thickness. Slices were fixed for 10 minutes in ice-chilled acetone, and then blocking was performed using Dako peroxidase blocking solution (Agilent, Ratingen). After washing, anti-human CD19, clone SJ25 (Miltenyi Biotec) primary antibody, raised in mouse was added for 10 minutes at room temperature. HRP labelled anti-mouse secondary antibody (Agilent) was applied for 60 minutes at room temperature in dark. Following this, freshly prepared substrate-chromogen (Agilent) was added for 10 minutes. Hematoxylin counterstain was performed for 3 minutes and then slides were mounted using Dako Fluorescence Mounting Medium (Agilent). Images were acquired at 20X magnification using Sensocope (Sensovation AG, Radolfzell am Bodensee).

2.3 Immunofluorescence (IF) staining

Ovarian cancer tissue stored at -80°C from two different patients were sectioned using a cryostat instrument (Leica Biosystem), at -18°C in 8 µm thickness. Slices were fixed for 10 minutes in ice-chilled acetone, and then staining was performed using anti-OvCa_1-PE-conjugated antibody along with anti-CD326–FITC (clone: REA635, Miltenyi Biotec) and Hoechst for 10

minutes. 1 ml of AutoMACS Running Buffer was added and the tissue plate was placed in a respective slot in MACSima instrument. The entire tissue was imaged with 10X magnification and images were analyzed using ImageJ software (ImageJ 1.52p, USA).

2.4 Image analysis using ImageJ software

All images that were generated from the MACSima instrument, by IHC staining or by IF staining were analyzed using ImageJ software. After loading of the images in the tool, using Image function and then adjust function, brightness and contrast were adjusted for individual images. Various composites were made using Image and then color-merge channels option. Final images were saved in TIFF format and used for illustrations.

2.5 Bioinformatic analysis

2.5.1 Image segmentation

Raw images obtained from MACSima technology were loaded in QI Tissue software. QI Tissue is a commercial image processing software from QI and is distributed by Miltenyi Biotec for image analysis and visualization. It has a database covering the most commonly used markers with information about their localization within cells, expression pattern and their function. Using the in-built segmentation platform, individual cells in the tissues were segmented. Mean intensity values corresponding to each marker was automatically extracted in the form of CSV files for further analysis. Information about X and Y coordinates was stored to keep spatial information of cells.

2.5.2 Clustering and t-SNE plot generation

For further bioinformatic analysis, Orange software was used. Orange is an open-source software for data visualization and analysis. Mean intensity values for each marker for the corresponding cell was loaded in the software. Hierarchical clustering was performed and visualized as a t-SNE plot. Clustering data was saved in the form of CSV files and exported back to QI Tissue software, where clusters could be visualized in terms of their localization in the tissue.

2.5.3 Manual segmentation and analysis with Inspector cell tool

Images were initially segmented using an automated software called Cell Profiler. Following this, images were loaded in the Inspector cell tool, along with a segmentation mask. Cell segmentation was corrected manually cell by cell using surface marker staining. DAPI was used as a reference. Each cell was annotated for its respective marker expression. Annotated data was then extracted in an Excel file and the respective population of cells were calculated using marker combinations and represented using pie-chart.

2.6 Tumor tissue dissociation

Fresh solid tumor tissues were received in MACS Tissue Storage Solution (Miltenyi Biotec) and were dissociated following the standard protocol as mentioned in the datasheet of tumor dissociation kit (Miltenyi Biotec). Enzyme R was not used as it might affect the expression of cell surface epitopes. Cells were resuspended in RPMI 1640and used for further analysis.

2.7 Flow cytometry analysis

For cell phenotyping, antibodies were used according to manufacturer's recommendations. The following antibodies were used: anti-CD326 (REA764), anti-CD9 (REA107), anti-CD235a (REA175), anti-CD90 (REA897) (1:50), anti-CD31 (REA730), anti-CD163 (REA812), anti-CD14 (REA599), anti-CD45 (REA747), anti-CD3 (REA613), anti-CD8 (REA734), anti-CD19 (REA675), anti-CD138 (44F9). Cells were incubated with the antibody mix for 15 minutes at 4°C. After washing, the measurement was done using MACS Quant® X (Miltenyi Biotec). The flow cytometer is equipped with three lasers (405 nm, 488 nm, 640 nm) and 10 emission detectors. Standard calibration using MACSQuant® calibration beads was performed, along with the setting of suitable compensation employing a multicolor compensation panel. Analysis of acquired flow data was accomplished using the FlowLogic 7.2.1 software (Inivai Technologies Pty.Ltd., Mentone Victoria, Australia). The gating strategy was based on the identification of target cells in forward scatter (FSC) and side scatter (SSC), exclusion of cell aggregates by forward scatter height (FSC-H) and forward scatter area (FSC-A) plot and live cells (7AAD-negative). With the help of negative controls or FMO (fluorescence minus one) controls, gating was set up.

2.8 B cell culture and expansion

B cells were isolated using CD19 microbeads, human and CD138 microbeads, human (Miltenyi Biotec). Steps for isolation were followed as mentioned in the datasheet. After isolation, cells were plated as per B cell expansion kit, human (Miltenyi Biotec). Cells were stimulated with CD40-ligand (80 U/ml) and IL-21 (25 ng/ml) for 14 days. Flow staining was performed using the following antibodies: anti-IgG (clone IS11-3B2.2.3), anti-CD38 (IB6), anti-CD138 (44F9), anti-CD27 (M-T271), anti-CD20 (LT20), anti-IgD (IgD26) and anti-CD326 (HEA-125) at day 7 and day 14.

2.9. Single-cell sequencing for BCR sequencing and expression profiling using the 10X platform

2.9.1 Materials

Table 2: List of reagents used for scBCR sequencing and expression profiling

Product	Product No.	Vendor
Chromium™ NEXT GEM Chip G Single Cell Kit, 16 reactions	1000224	10x Genomics
Chromium™ Controller	1000202	10x Genomics
Single Index Kit T Set A	1000213	10x Genomics
Chromium™ Single Cell V(D)J Enrichment Kit, Human B Cell, 96 reactions	1000016	10x Genomics
Chromium™ NEXT GEM Single Cell 5' Library and Gel Bead Kit 4 reactions	1000167	10x Genomics
Nuclease-free water	AM9937	Thermo Fisher Scientific
Ethanol, pure (200 Proof, anhydrous)	E7023-500ML	Millipore Sigma
SPRIselect Reagent Kit	B23318	Beckman Coulter
10% Tween 20	1662404	Bio-Rad
Glycerin (glycerol), 50% (v/v) aqueous solution	3290-32	Rica Chemical Company
Qiagen Buffer EB	19086	Qiagen
Vortex mixer		VWR
High Sensitivity DNA Kit	5067-4626	Agilent
Qubit 4.0 Fluorometer	Q33226	Thermo Fisher Scientific
Qubit dsDNA HS Assay Kit	Q32854	Thermo Fisher Scientific
NextSeq High-Output Cartridge 2x75 bp	0024907	Illumina
NEBNext® Library Quant Kit for Illumina®	E7630L	New England Biolabs

2.9.2 Methods

1) Library Preparation

For the preparation of B cell-specific V(D)J as well as gene expression profiling libraries 10x Genomics reagents and protocols were used. The workflow was performed according to the manufacturer's protocol. Gel Bead-In Emulsions (GEMs) were generated by a combination of gel beads containing 10x barcodes with a reverse transcription master mix and sample material (targeting the recovery of 10,000 cells per sample). GemCode technology employs ~750,000 barcodes to distinguish between each cell's transcriptome and to track single molecules back to their cell of origin. This is achieved by delivering the cells in a limited dilution so that one cell is paired with one bead in one drop. All cDNA generated from a single cell then share a common 10x barcode. In the final libraries, 10x barcodes are used to associate individual reads back to the individual partitions.

Immediately following GEM generation, reverse transcription was performed according to the manufacturer's protocol; resulting in 10x barcoded cDNA first strands. Silane magnetic beads (Dynal MyOne Silane beads) were used to purify the 10x barcoded first-strand cDNA from the post-GEM-RT reaction mixture. Following the clean-up, cDNA was amplified to obtain enough material for all subsequent applications. Full-length V(D)J segments were enriched from amplified cDNA via PCR amplification with primers specific for Ig constant regions. For the enriched library construction as well as gene expression profiling library construction, 50 ng of cDNA of each sample was subjected to enzymatic fragmentation and size selection, which were then applied to optimize the cDNA amplicon sizes before finalizing the different libraries. Final steps included the addition of P5, P7, a sample index, and Illumina R2 sequence (read 2 primer sequence) via End Repair, A-tailing, adaptor ligation, and sample index PCR. P5 and P7 priming sites used in Illumina sequencers.

2) Agilent QC steps

For quality control during the process of library preparation (cDNA amplification, Ig gene enrichment and finalization of library construction) as well as for determination of average base-pair size, distribution of the produced libraries was checked through Agilent bioanalyzer High Sensitivity DNA assays according to the manufacturer's protocol. The on-chip DNA electrophoresis was performed on an Agilent 2100 Bioanalyzer instrument

and evaluated with High Sensitivity DNA assay available with the Agilent 2100 Expert software (Version B.02.08.SI648 (SR3)).

3) Fluorometric DNA quantification of the first-strand cDNA

After first-strand synthesis, the cDNA concentration of the samples was determined with Thermo Fisher's Qubit HS DNA Assay for further use. The assay is highly selective for double-stranded DNA (dsDNA) over RNA and is accurate for initial sample concentrations from 10 pg/µL to 100 ng/µL. The measurements were conducted according to the manufacturer's protocol.

4) Final Library quantification with qPCR

The quantification of the libraries produced was performed with NEB NEXT Quantification Kit for qPCR analysis according to the manufacturer's protocol. To increase the precision of the quantification each sample was analyzed in triplicates of three different dilutions (1:100,000, 1:1,000,000 and 1:100,000,000). Analysis of samples was performed on an ABI 7900ht real-time cycler employing Sequencing Detection System Version 2.4.1 software.

5) Sequencing

Sequencing of the samples was performed according to 10x Genomics recommendations: 20,000 reads per cell for Gene Expression Profiling and 5,000 reads per cell for V(D)J libraries (10XGenomics, 2020). Assuming 10,000 cells were recovered during GEM generation arithmetically 200,000,000 reads for each GEX and 50,000,000 reads for each V(D)J sample were applied during sequencing.

2.10 Analysis of BCR repertoire using Loupe V(D)J browser

Data obtained from the 10X Genomics platform were initially processed with the modules "mkfastq" and "vdj" of "cellranger 3.1.0", a Linux-based command line tool provided by 10x Genomics, using the V(D)J reference "GRCh38-alts-ensembl-2.0.0". "Cellranger VDJ" generates input files for Loupe V(D)J Browser, which is an application provided by 10x Genomics that allows in-depth analysis and visualization of V(D)J sequences and clonotypes from single-cell 5′ data. Data from B cell isolated fraction and unisolated fraction were loaded in the software and

using the clonotype abundance function, the frequency of shared clones was checked among both fractions. With the help of the B cell isotype function, information about dominant isotypes and their respective frequency was extracted. The sequences of the heavy and light chains from the dominant clone, referred here as consensus sequence, were matched with the reference sequence to check for mutation from the germline sequence. The consensus sequence is a sequence that represents the most likely sequence for a receptor chain within the clonotype. The reference sequence, is a concatenation of the sequences of each gene detected in the chain. Finally, on top of the reference and consensus sequences are the gene annotations, which indicate where the detected gene segments start and end. (Adapted from 10X genomics support page). The sequences of the heavy and light chains from the dominant clone were extracted and used for antibody production.

2.11 Analysis of gene expression profiling using Loupe Cell Browser

Data obtained from the 10X Genomics platform were initially processed with the modules “mkfastq” and “count” of “cellranger 3.0.2”, a Linux-based command line tool provided by 10x Genomics, using the reference “GRCh38”. “Cellranger count” generates input files for Loupe V(D)J Browser, which is an application provided by 10x Genomics that provides interactive visualization functionality for various applications such as analysis of 3’ and 5’ single-cell gene expression data.. Here, using the t-SNE function, gene expression-based clusters were visualized. Lists of the top 50 significant genes per cluster were extracted and used for defining the cell type representing individual clusters. With the help of the gene/feature expression function, expression of various genes of interest was visualized among different clusters. Using the V(D)J clonotype function, single-cell BCR sequencing data (scBCR) was loaded, and localization of individual cells from scBCR data was visualized in the t-SNE plot. Gene expression profiling of the cells expressing the top BCR clone was performed using the Gene/expression feature.

3. Results

3.1 Screening of solid tumor tissues for B cells

In order to characterize the tumor-infiltrating B cells, solid tumor tissue was identified which was infiltrated with B cells. B cells have been reported to infiltrate several tumor entities, so a variety of solid tumors like ovarian, pancreatic, breast and melanoma samples was screened in the course of this study. To cover whole tumor sections for screening, IHC staining was used as a method utilizing an anti-human CD19 antibody to identify B cells and hematoxylin to stain the nuclei. First, tumor tissues were sectioned in 8 µm width in the cryostat, followed by fixation with acetone. Then, IHC staining and microscopy was performed as described in the Materials and Methods section. Samples showing staining for CD19 (brown spot) were considered positive for B cell infiltration. Taken together all investigated tumor samples, in 27% of the samples B cells were detected. Due to supply reasons, the focus was set on ovarian carcinoma (Ovca). Here, 19 ovca samples were screened from which 21% (4 cases) of the cases possessed B cells, an illustrative image is shown in Figure 8. These B cell rich four samples were selected and used for further experiments.

A.

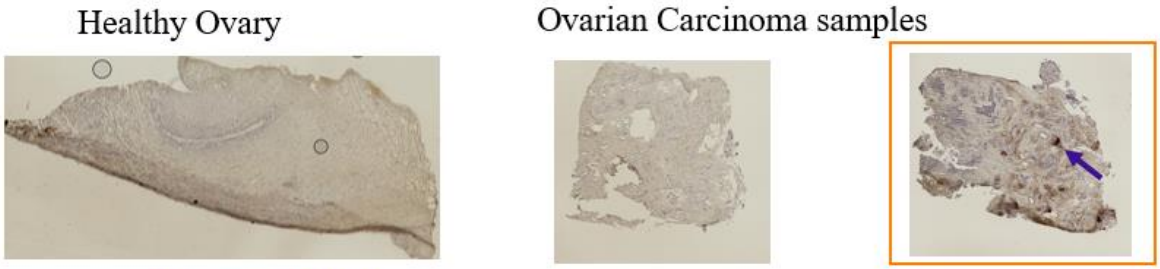

Brown = CD19

B.

Sr. No.	Tumor entity	No. of samples	B cell infiltration
1.	Pancreatic Tumor	4	2
2.	Ovarian carcinoma	19	4
3.	Melanoma	2	0
4.	Breast carcinoma	1	1
	Total	26	7

C.

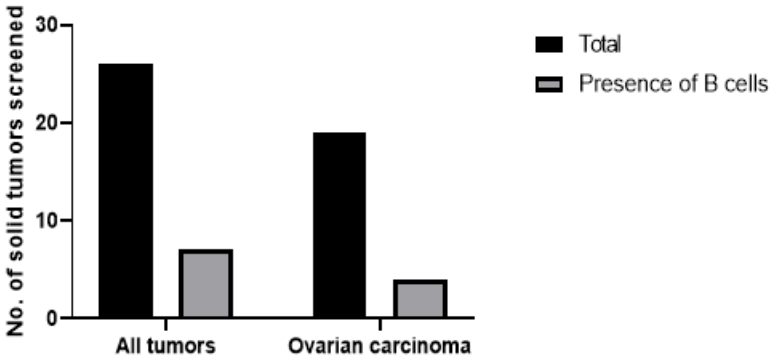

Figure 8: Screening of tumor samples for B cell infiltration

A. IHC staining using anti-CD19 antibody in human ovarian carcinoma samples. Healthy ovary was used as a control. Brown signal indicates presence of $CD19^+$ B cells in the sample, two exemplary samples shown here. Images were taken in 20X magnification. B. List of different human entities used for screening of B cells. C. Bar graph representing presence of B cells in 27% of all tumor samples investigated, and in 21% of all ovarian carcinoma samples screened. Criado-Moronati E. assisted in screening of B cells.

3.2 Ultrahigh-content imaging based on the MACSima™ Imaging System identifies the lymphoid structure and distinct cell types in ovarian carcinoma tissue

For phenotypical characterization of tumor-infiltrating B cells in their local compartment, detailed microscopy was conducted using the MACSima™ Imaging System, an instrument developed in-house based on MICS (multiparameter imaging cell screen) technology enabling highly multiplexed immunofluorescence imaging. A list of relevant B cell markers, covering

diverse developmental subsets of B cells, activation markers, different immune cell type markers, tumor and its microenvironment related markers was selected and prepared. For B cells subset characterization, markers like IgD, CD27, CD38, CD138, IgG, IgM, IgA were tested, for activation status markers like CD80, CD86, HLA-DR, HLA-DQ, CD95, BCL-2, CD77, AID and for inhibitory status like CD200, CD279, IL-10, CD5 were used. For immune cell phenotyping markers like CD45, CD45RA, CD45RO, CD3, CD4, CD8, CD14, CD56, CD163, CD11c, CD208, CD62L, CD39 were incorporated, for tumor cells and stroma markers like CD326, CD90, CD31, CD273, CD274, cytokeratin were taken. Several chemokines and their ligands were also tested like CXCL13, CXCL12, CCL19, CCL21. Followed by testing of different clones and titers for antibodies, a final panel of 98 antibodies was made. Different tumor sections were screened with this panel of 98 antibodies, as mentioned in material and method section. Afterimage acquisition, pre-processing, and quality control of the images, cell segmentation was performed using internal software. Mean intensity values were extracted and further bioinformatic analysis was performed using a clustering tool. The complete workflow is illustrated in Figure 9.

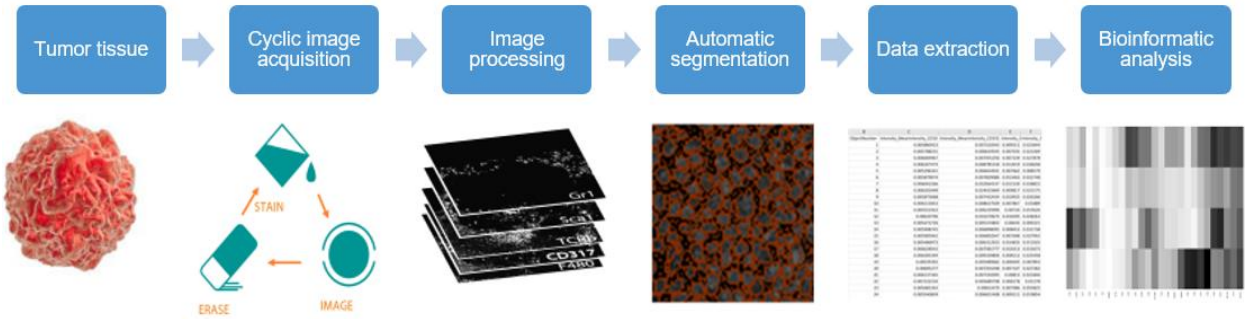

Figure 9: Workflow of MACSima™ imaging system

Tumor tissues were sectioned and fixed in acetone, followed by cyclic staining and image acquisition which was performed using standard MACSima system. After processing the images, cells were segmented an d analyzed using bioinformatics tools.

To characterize the B cells infiltrating solid tumors, four ovarian carcinoma tissues were processed and imaging was performed using MACSima™ Imaging System. Single images were obtained corresponding to individual marker, in a total of 98 images. Representative collage is shown in Figure 10, with the use of 20 markers. After processing the data, single images corresponding to each marker were obtained. Exemplary collage to show final data received for

individual markers, the name on the top left corner of each image specifies the marker displayed. Images were taken in 20X magnification.

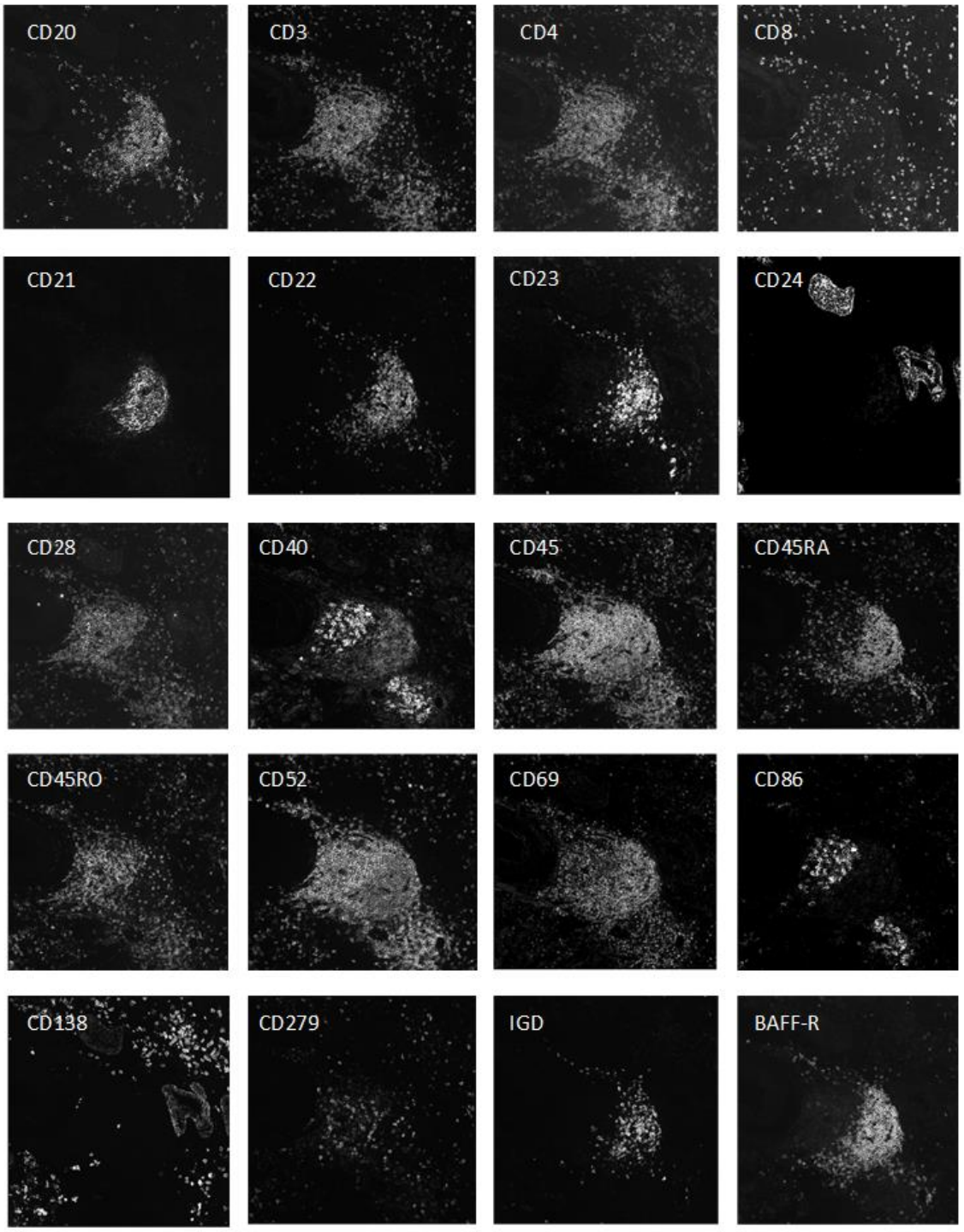

Figure 10: Illustration of images obtained on human ovarian carcinoma sample from MACSima technology.

Furthermore, to confirm B cell infiltration into the tissue, image composites were made using markers for B cells (CD20), T cells (CD3) and tumor cells (EpCAM). In some tissues, dense B cells clusters were observed, while in some very few B cells were infiltrating (Figure 11).

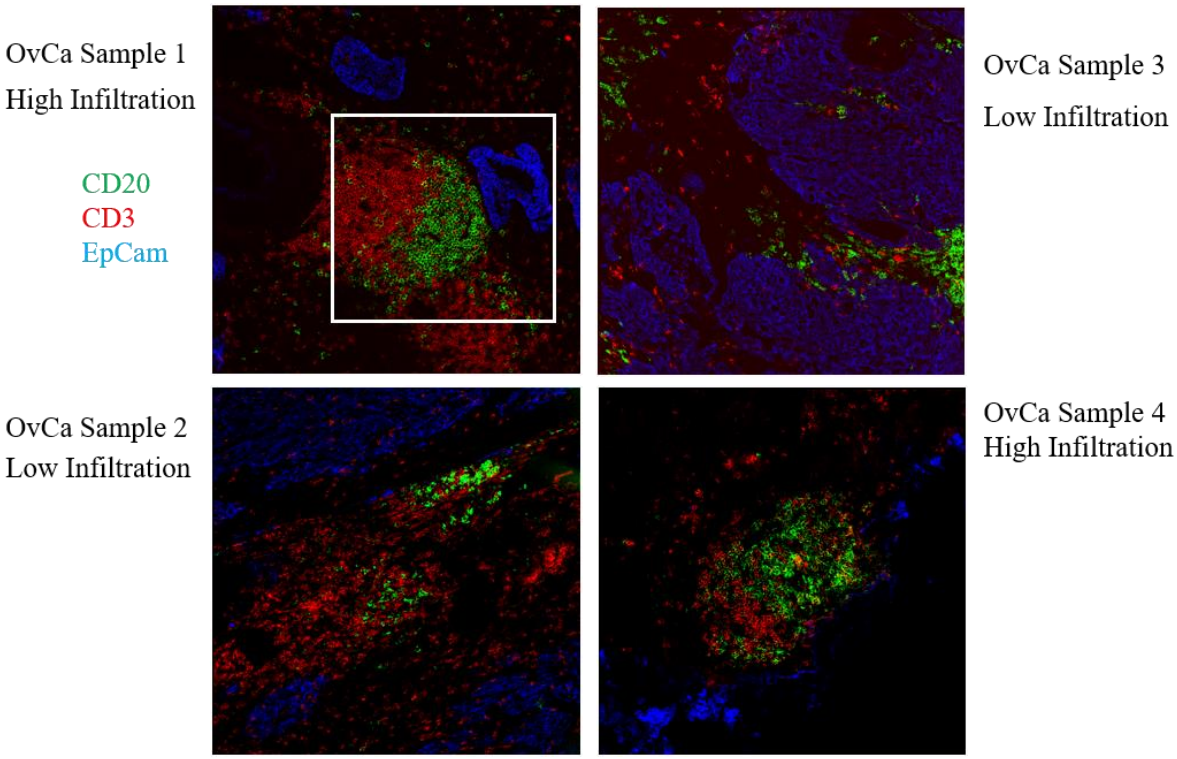

Figure 11: Low density and high-density areas of TIBs infiltrating human ovarian carcinoma

B cell presence was investigated in different ovarian carcinoma sample by making composite images using Image J software. B cells are marked in green ($CD20^+$), T cells ($CD3^+$) in red and tumor cells ($CD326^+$) in blue. Based on the amount of B cells, samples were categorized into high to low infiltrated.

From the 4 samples displaying B cell infiltration, 2 had high infiltration and 2 had low infiltration. One of the samples with low B cell infiltration showed also low T cell infiltration while one sample still exhibited high T cell presence. The strong B cell infiltrated sample also had relatively high T cell infiltration, especially the one marked with the white box in Figure 11, displayed ectopic lymphoid like structure. For this reason, this sample was selected for in-depth analysis. Interestingly, infiltrating $CD45^+$ leukocytes were observed next to $CD326^+$ tumor cells (epithelial cell adhesion molecule, EpCAM), surrounded by $CD14^+$ myeloid cells, $CD163^+$ macrophages and $CD105^+$ blood vessels (Figure 12A). The tumor microenvironment was

predominantly composed of $CD4^+$ T cells, surrounded by $CD20^+$ B cells (Figure 12B). $CD138^+$ plasma cells were found in the vicinity, together with $CD8^+$ T cells.

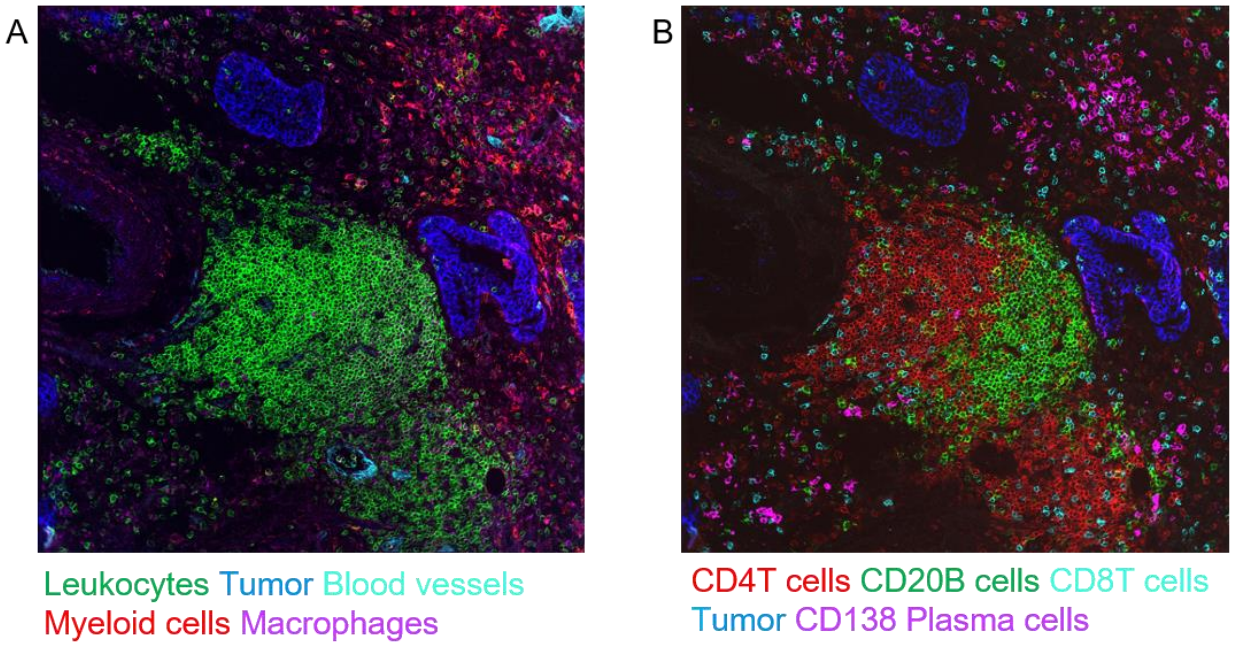

Figure 12: Identification of distinct cell types within TIB cell areas

Human ovarian tumor sample processed with MACSima technology and analyzed regarding cell-type composition. A. Infiltrating $CD45^+$ leukocytes shown in green, $CD326^+$ tumor cells in blue, $CD14^+$ myeloid cells in red, $CD163^+$ macrophages in magenta and $CD105^+$ blood vessels in cyan. B. Immune cell composition shown by $CD4^+$ T cells in red, $CD20^+$ B cells in green, $CD138^+$ plasma cells in magenta, and $CD8^+$ T cells in cyan.

TLS has been reported in many solid tumors and mostly they are considered a hallmark of ongoing immune reaction. Generally, they are characterized by clusters of B within network of follicular dendritic cells and T cells in the surrounding, often contain high endothelial venules (HEVs). Furthermore, to check for the presence of ectopic lymphoid structure in the sample, expression of classical markers defining TLS were checked upon. In the ovarian carcinoma sample, clusters of $CD20^+$ B cells were observed adjacent to $CD21^+$ follicular dendritic cells (FDCs) and $CD3^+$ T cells. Moreover, MECA-79–expressing high endothelial venules (HEVs) were found. (Figure 13).

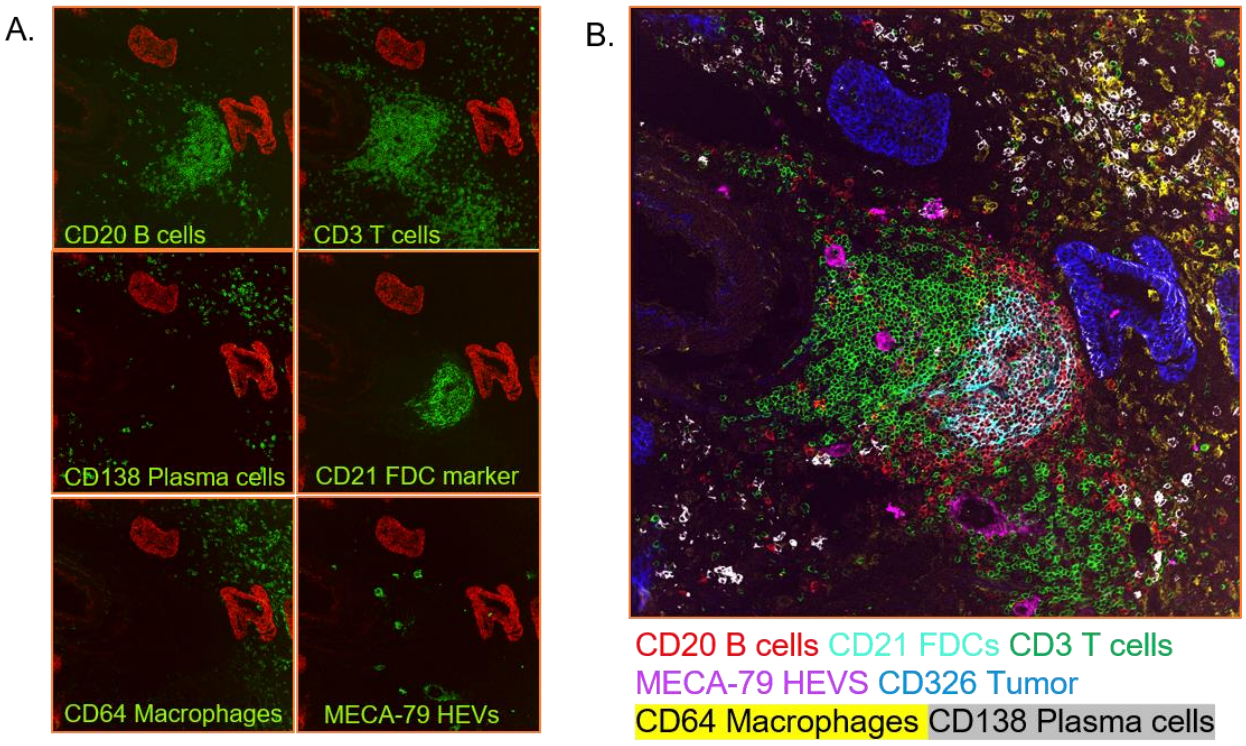

Figure 13: Identification of TLS in human ovarian carcinoma sample

Human ovarian tumor sample processed with MACSima technology and analyzed regarding ectopic lymphoid structures. A. Individual staining was shown for cell types (in green): B cells with CD20, T cells with CD3, plasma cells with CD138, follicular dendritic cells (FDCs) with CD21, macrophages with CD64 and high endothelial venules with MECA-79, merged with the tumor in red, CD326. B. A composite image representing tertiary lymphoid structure, with $CD20^+$ B cells in red, $CD21^+$ FDCs in cyan, $CD3^+$ T cells in green, MECA-79^+ HEVs in magenta, $CD326^+$ tumor in blue, $CD64^+$ macrophages in yellow and $CD138^+$ plasma cells in grey.

3.3 Subset analysis of infiltrating B cells

Besides the identification of TLS like structures and cell composition of the tumor microenvironment also the subset distribution of the B cells was investigated in more detail. B cells undergo different stages of differentiation during their development. Here it was analyzed which B cell subsets, i.e. naïve, memory, plasmablast or plasma cells are infiltrating the respective tumor tissues. For this, IgD along with CD20 was used to determine naïve B cells, CD27 was used to check IgD^+CD27^+ unswitched memory B cells. Few IgD^+CD20^+cells (shown in yellow) were found in the B cell cluster (Figure 14A), no IgD^+CD27^+ unswitched memory B cells (shown on magenta) were detected. Next, to check for the memory B cells CD27 in combination with CD20 was used as T cells also express CD27. CD3 was used to mark out T cell areas. The majority of $CD20^+$ cells were positive for CD27, indicating enrichment of B cells with a memory phenotype (Figure 14A). Many $CD27^+$ cells present in the periphery were $CD20^-CD3^-$. To confirm if these cells were plasmablasts or plasma cells, it was investigated if these cells were expressing the plasma cell markers CD38 and CD138. Cells expressing $CD138^+CD38^+CD27^+$ (yellow/white) confirmed a dominance of plasma cells in the periphery followed by few $CD27^+CD38^+CD138^{dim/-}$ plasmablasts (Figure 14A). Taken together, this suggests a structure of few naïve B cells resident more in the center of the TLS like structure and enrichment of memory B cells at the outside margin of the cluster, while plasma cells and plasmablasts are present in the periphery outside of the cluster, but within the tumor. Noticeable is also the relatively high amount of plasma cells detectable in the periphery.

For further characterization, it was screened which other markers were expressed by $CD20^+$ B cells in the tumor. Along with the expression of classical B cell markers like CD22, IgM, B cells were also expressing CD79a which is a signaling subunit for the BCR (Figure 14B). Also, B cells were shown to express BCL2 which is an anti-apoptotic protein and a marker generally reported to be not expressed by the germinal center, indicating that these B cells may not be germinal center B cells. Expression of BAFF-R was also found on the B cells within the cluster, but not outside of it strengthening the observation made before that mature B cells accumulate within the cluster, but plasma cells and plasmablasts residing in the periphery. In addition to that, CD40 was also found to be expressed on the B cells. CD40 is an important costimulatory molecule for B cells, suggesting that these B cells might function as APCs in the tumor.

A.

IgD
CD20
CD27
Naïve B cells

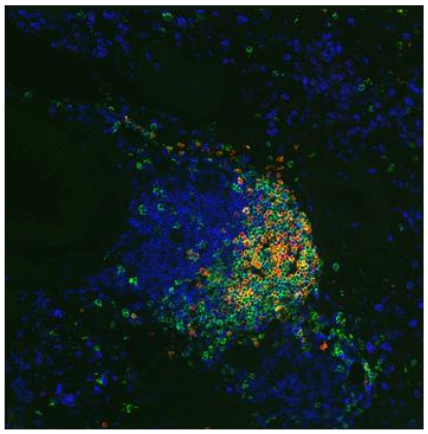

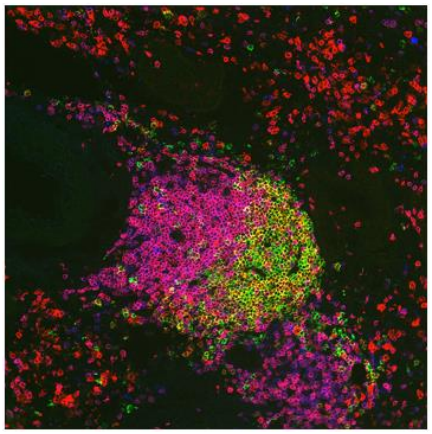

CD27
CD20
CD3
Memory B cells

CD38
CD20
CD27
Plasma blast

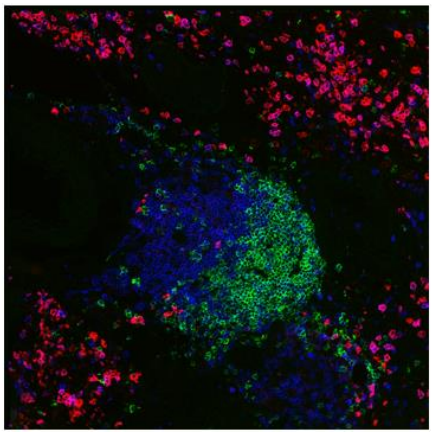

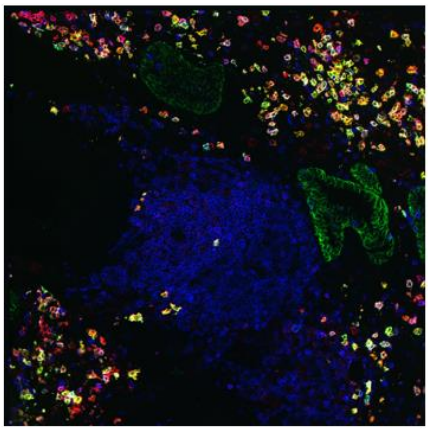

CD38
CD138
CD27
Plasma cells

B.

CD79aCD20

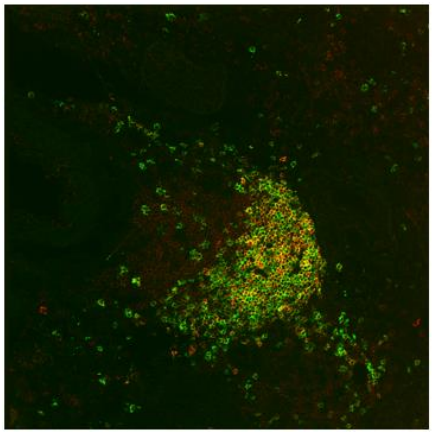

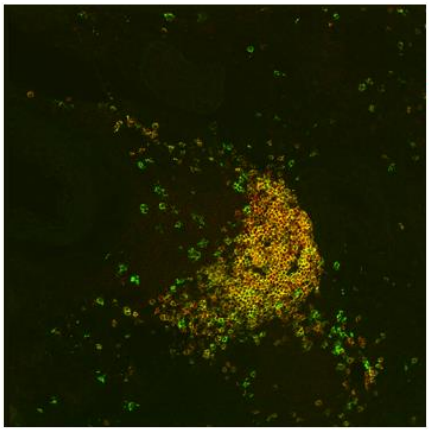

BAFF-RCD20

BCL2CD20

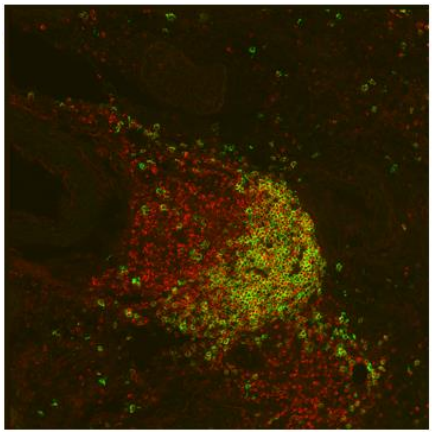

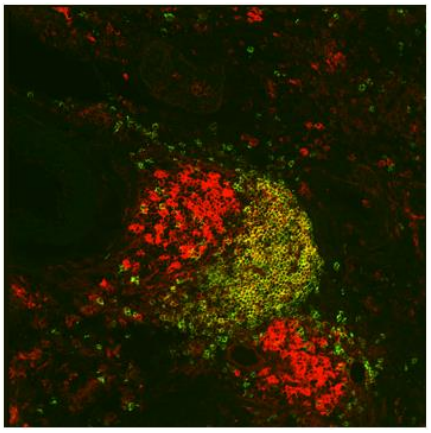

CD40CD20

Figure 14: **Phenotypic characterization and subset analysis of tumor infiltrating B cells**

Human ovarian tumor sample processed with MACSima technology and analyzed for B cells. Markers were selected based on the staining quality of the antibody and composites were made using ImageJ software. A. Using classical marker combinations, B cell subsets were defined. Along with CD20, IgD was used as naïve B cell marker (top row left image), CD27 as memory B cell marker (top row right image) and the combination of CD38 and CD138 plasma cells identification (bottom row). B. Expression of CD79a, BCL2, BAFF-R and CD40 was represented in red in combination with $CD20^+$ B cells in green. Yellow represents expression of dual markers.

3.4 Bioinformatic analysis

For more in-depth characterization of TIBs, different software were tested for image segmentation and clustering and data visualization. The acquired images were analyzed by using QI tissue software, and segmentation of individual cells from the whole tissue was performed. Along with other common cell surface markers included in the software, CD20 was added for identification of B cells by its cell surface expression. In total, 7234 cells were segmented from the whole image and mean expression values for each of the 96 markers were extracted, keeping cell IDs and X-Y coordinates for each cell (Figure 15a). Following this, using the Orange tool, cells were hierarchically clustered into 7 different clusters and visualized on a t-SNE plot. Different clusters were defined based on dominant marker expression patterns (Figure 15b). Major cell types could be identified in alignment with the visual analysis. $CD20^+$ clusters were classified as B cells, $CD4^+$ clusters as $CD4^+$ T cells, $CD8^+$ clusters as $CD8^+$ T cells, $CD138^+CD38^+$ clusters as plasma cells, $CD14^+$ as monocytes, $CD326^+$ as tumor cells. Mapping of the clusters onto the original image was performed using QI tissue software to decipher the spatial information of the clusters in the tissue (Figure 15c). Representative microscopy image of TLS has been added from Figure 13, to visualize the distribution of different clusters into image resembles with the TLS-like structure observed in visual analysis.

Marker profiling of B cell cluster was then carried out. In alignment with the visual analysis, cells in B cell cluster were positive for classical B cell markers like CD22, CD45RA, and CD19 (data not shown). Also, cells in the B cell cluster were clearly expressing CD79b, BAFF-R, BCL2 and CD40 (Figure 15d). This visual analysis can be confirmed using this automated analysis strategy. As cells are localized in very close proximity to each other within the tissue, exact

quantification was challenging. Global expression profiling of the B cell cluster was possible, but further classification into smaller B cell subsets was leading to results, which were not reliable enough up to this time point and remains to be optimized further.

A.

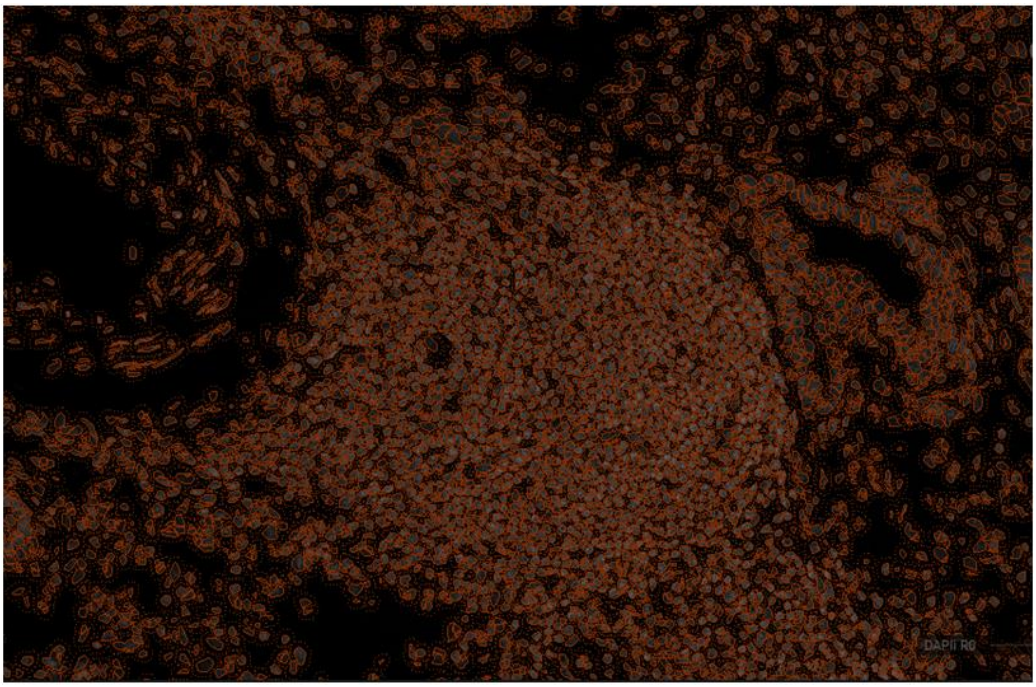

B.

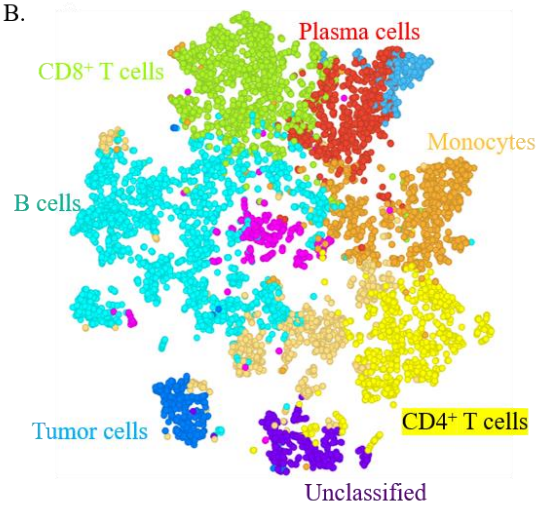

C.

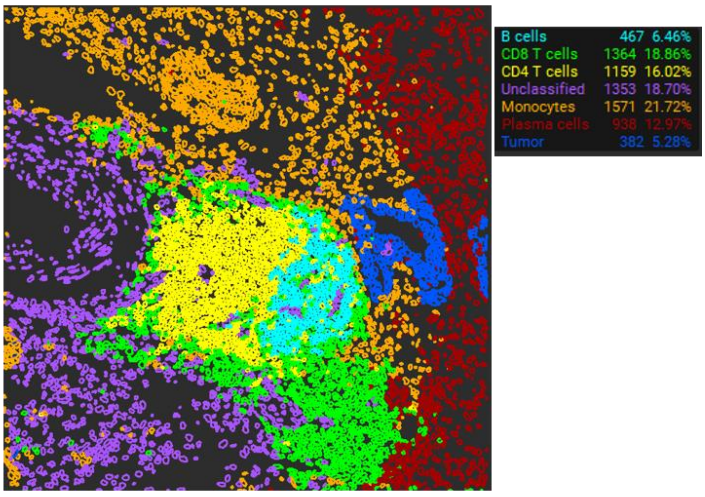

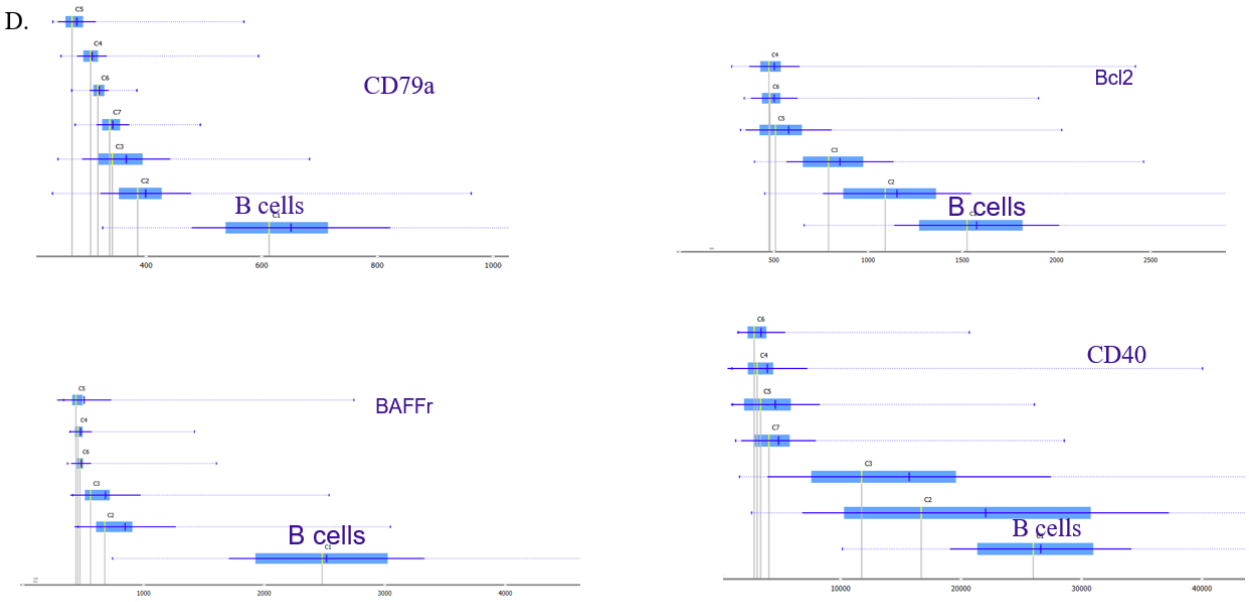

Figure 15: Bioinformatic analysis using automated tools

A. Segmented cells from the whole tissue using DAPI and surface markers. B. t-SNE plot showing seven different clusters obtained from hierarchical cluster using the Orange tool, clusters were labelled based on abundant marker expression. C. The clusters were mapped back to original image to show localization of clusters within the tissue. Representative microscopy picture can be used from Figure 13 for comparison of cell types localization within tissue. D. Markers expression among different clusters.

3.5 Manual cell annotation strategy for quantification purposes

Cells in tissues are very tightly organized, leading to difficulties in the quantification of marker expression from individual cells using automated software. To address this problem, a tool called Inspector Cell, developed in-house for visualization of multiplexed immune staining images was used. Individual cell segmentation followed by a detailed annotation of all markers expressed on each cell was planned. To make it easy to handle, the image was evenly divided into 16 splits (Figure 16a) and handed over to specialists which corrected the initial segmentation done with Cell Profiler (public software). First, cell boundaries were corrected using a defined set of cell surface markers such as CD3, CD20, CD45, CD45RA, CD45R0, CD4, CD8, CD22, CD138, CD27, CD56, CD163, which majorly cover all the cell types present in the tissue. Following this, each individual cell was annotated for each marker (48) as positive or negative. An exemplary image is shown below (Figure 16b), where highlighted the cell (marked with a pink circle) is expressing CD45, CD20, CD22, CD27 and so on.

This approach was tested to investigate if this strategy would allow the identification of smaller B cell subsets consisting of lower cell number which would otherwise not be visible with the other techniques. From the first analysis, it was found that B cells were accounting for 17% of all annotated cells (4561 total number of cells), after CD4 T cells which constituted 32% of all annotated cells (Figure 17A). Among different subsets, B cells with a memory phenotype ($CD20^+CD27^+$) were found to be present at a frequency of 62%, while naïve B cell ($CD20^+IgD^+$) s were found with a frequency of 16% of all $CD20^+$ B cells (Figure 17B.). Plasma cells ($CD138^+CD38^+$) were representing 22% of all annotated B cells. Many $CD20^+$ cells were found to be expressing HLA-DQ or HLA-DR, but also common lymphocyte activation markers such as CD69 and CD72.

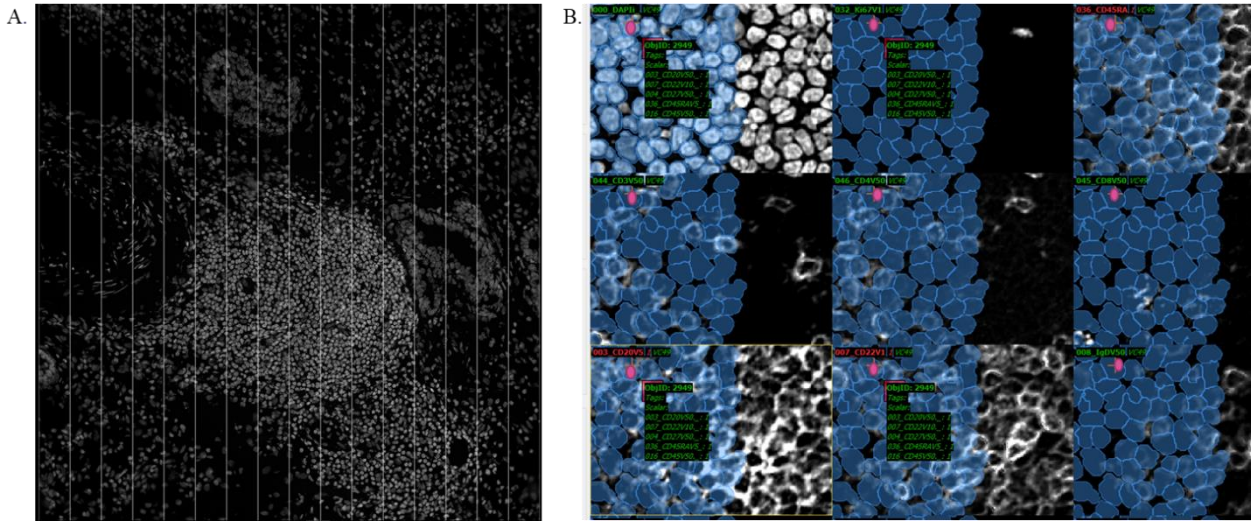

Figure 16: Image segmentation with Inspector tool

A. Images were initially segmented using automated software called Cell Profiler. Images were divided into 16 grids for segmentation and annotation. Cell segmentation was corrected manually cell by cell using surface marker staining, using DAPI as reference. B. Each cell was annotated for its respective marker expression. An exemplary image showing expression pattern of highlighted cell after annotation of markers. Segmentation and annotation was done together with Gosselink A. and Criado-Moronati E. from T cell group.

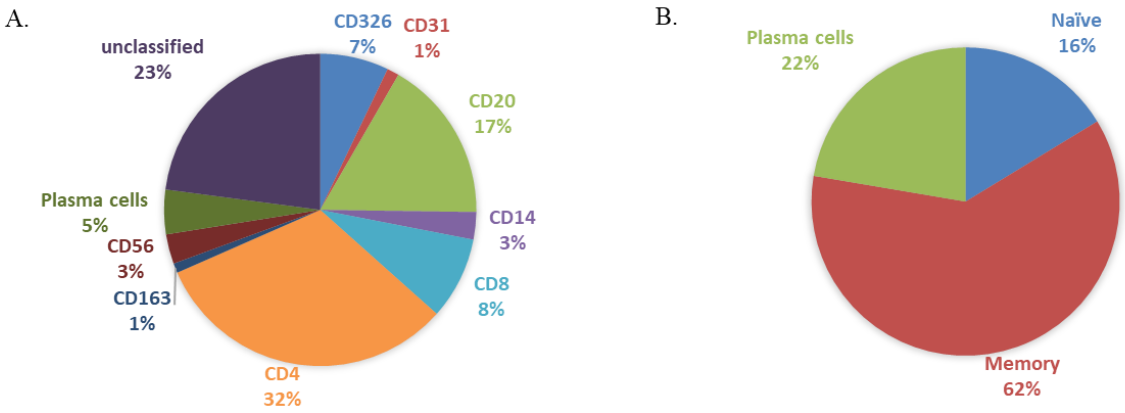

Figure 17: Quantification of manually annotated data

A. Pi-chart showing the distribution of prominent cell types within the tumor tissue. Using classical markers, subsets were labelled, identified and their relative abundance within the annotated cells was calculated. The B cell population was calculated and displayed as 17% frequency of CD20 and 5% as plasma cells. B. Subset analysis of B cells using classical marker combinations: memory B cell phenotype (CD20+CD27+), plasma cells (CD138+CD38+), and naïve B cells (CD20+IgD+).

3.6 Flowchart for isolation of B and T cells from the fresh tumor sample

To develop efficient targets for immunotherapy, knowledge about viable cell population infiltrating solid tumor, their activation/inhibition state, might help in mimicking the tumor microenvironment and aid in developing effective therapies. For instance, with the finding of surface markers like PD-1 and CTLA-4 and their role in inhibition of T cells by the tumor, promising targets like Ipilimumab could be developed and have been successfully used for CAR therapy (Farkona and others, 2016). Therefore, the aim of this part was to look at viable B cells from fresh solid tumor samples, to characterize their marker profile, BCR repertoire and gene expression profile. After analyzing the phenotype of B cells on frozen tissue sections, B cells were isolated from fresh tumor samples, characterized by flow cytometry and single-cell sequencing and compared to the results obtained from frozen, fixed tissue. To optimize the output and the efficacy a workflow was developed that enables the isolation and analysis of T as well as B cells with different techniques (Figure 18).

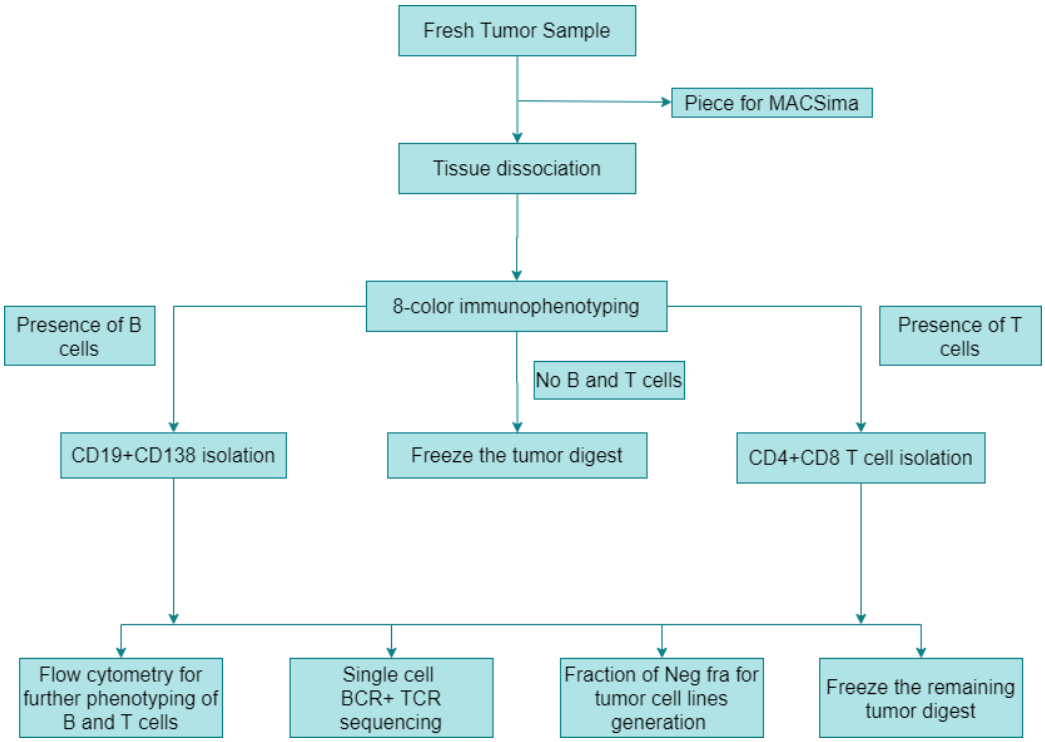

Figure 18: Workflow for isolation of B and T cells from the fresh tumor sample

Workflow depicting plan from the dissociation of the fresh tumor sample, sequential magnetic isolation of B and T cells, processing for flow analysis and single-cell sequencing. Tumor cell line generation and freezing a piece for microscopy were also combined.

3.7 Flow analysis of human tumor tissue digests

Solid tumor tissues were dissociated using the established Gentle MACS tumor dissociation protocol. Following this, flow staining was performed to determine the presence of B cells, T cells and the quality of the material by assessing the amount of viable cells. This is a crucial parameter, especially for the subsequent single-cell sequencing. Several attempts were made to isolate B cells from fresh solid tumors, Table 19 summarizes the list of tissues dissociated and screened for B cells.

Sr. No.	Tumor entity	% B cells (among total viable cells)
1	CRC TS20190919	0.031
2	CRC TS20200428	0.417
3	CRC TS20200714	0.902
4	EndoCa TS20191114	0.372
5	OvCa TS20190524	0.000
6	OvCa TS20190806	0.000
7	OvCa TS20191122	0.070
8	OvCa TS20200108	0.010
9	OvCa TS20200514	1.290
10	OvCa TS20200708	0.042

Table 3: List of human solid tumor tissues dissociated for screening B cells.

Tumor tissues were dissociated and among the viable population the percentage of B cells in the total tumor digest was calculated using CD19 and CD138 fluorochrome conjugated antibodies, enabling the detection and assessment by flow cytometry. Dissociation and screening was done together with Criado-Moronati E. from T cell group.

In the processed colon carcinoma sample, after tumor dissociation, the total cell viability of 51% could be detected. Among the viable population, excluding red blood cells, 42% were leukocytes and 44% tumor cells. Among leukocytes, T cells accounted for 45% of cells, while B cells accounted for 2% (Figure 19).

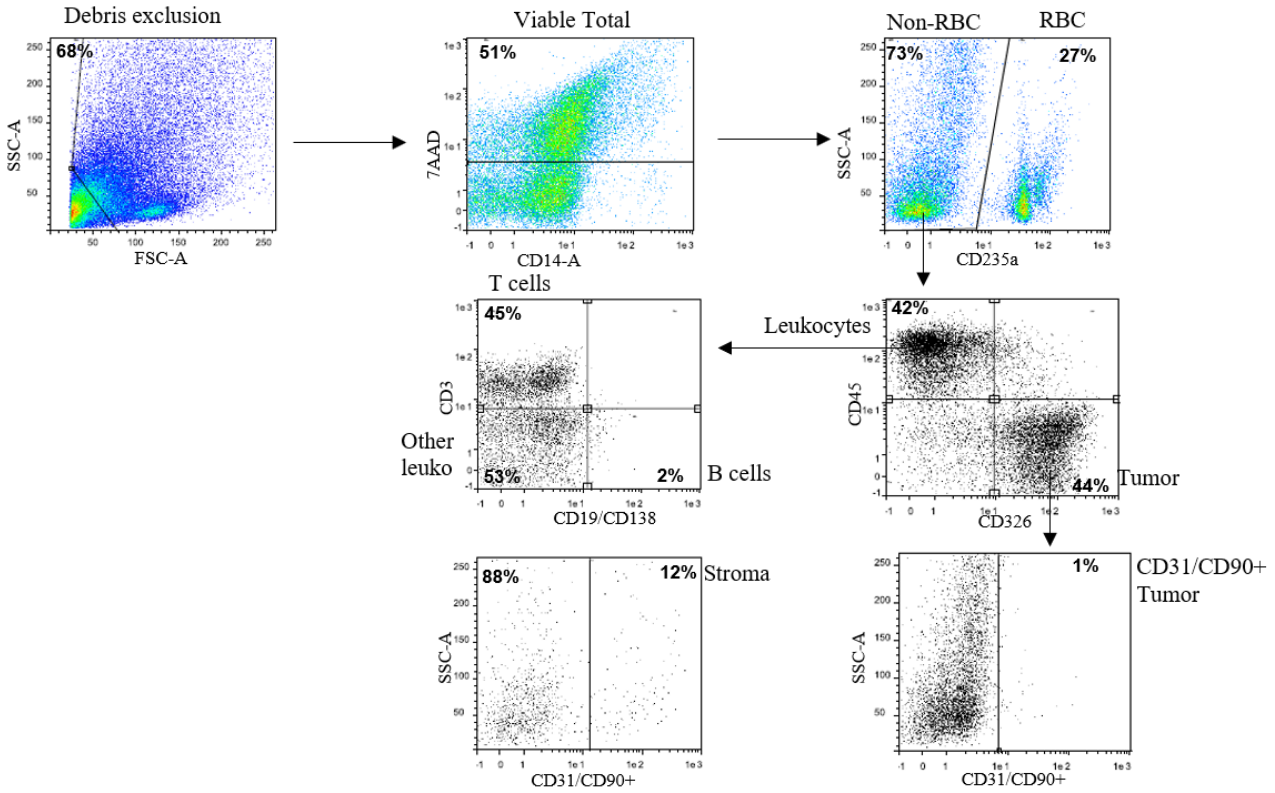

Figure 19: Flow analysis of human, colorectal carcinoma tumor digest

First, debris is gated out, then viable cells are gated based on 7AAD staining. Following this, live cells are gated for CD235a, a marker for red blood cells (RBCs). Then, Non-RBCs are selected and gated for $CD326^+$ tumor cells and $CD45^+$ leukocytes. Leukocytes are further selected and sub-gated for $CD19/CD138^+$ B cells/plasma cells and $CD3^+$ T cells. Around 2% of B cells/plasma cells were present in the leukocyte population. Tumor cells and $CD326^-CD45^-$ cells were further sub gated for CD31/CD90 to check for fibroblasts and stromal cells. Dissociation, screening and analysis was done together with Criado-Moronati E. from T cell group.

To enrich the B cell fraction, B cells were isolated using CD19 and CD138 microbeads. As plasma cells downregulate CD19, this dual combination approach was applied to obtain as many B cells and plasma cells as possible. After isolation, flow analysis was performed to determine B cell purity and yield and to subdivide them into subsets (Figure 20). 7% of B cells could be found in the isolated fraction, which was further gated for CD27 and IgD expression. 31% of B cells were $CD27^+IgD^+$ suggesting the presence of unswitched memory population. 10% had a naïve phenotype, determined by IgD^+, but no CD27 expression, 47% had a switched memory phenotype defined by $CD27^+$IgD- surface expression and 12% were double negative for CD27 as well as for

IgD. To determine the amount of plasma cells and plasmablasts, all $CD326^-$ cells were gated for CD27 and CD38 expression. $CD27^+CD38^{++}$ was then accordingly sub gated for their CD20 expression. 71% displayed CD20 expression, suggesting a plasmablast phenotype, around 23% were negative for CD20 signifying a plasma cell phenotype. In the CD19 and CD138 isolated fraction, 86% of tumor cells were present.

The isolated cell fraction was not further processed by single-cell BCR sequencing, due to limited viability and B cell frequency. Instead, the isolated cell fraction containing tumor cells as well as B cells was cultured *in vitro* along with CD40-ligand and IL-21 for 14 days according to a B cell expansion protocol to examine if the B cell population could be expanded further to obtain a higher purity. Flow analysis was done on day 7 (d7) and day 14 (d14) to discriminate the respective B cell subsets and determine the total B cell numbers. No B cell proliferation could be observed. Instead, the B cell number dropped from $5x10^5$ at d0 to $9x10^4$ at d7 and $9x10^3$ at d14. The frequency of naïve B cells dropped from 10% to 3% at d7 and of unswitched memory B cells from 31% to 5%, while the frequency switched memory B cells increased from 47% to 56%. Plasma cells and plasmablasts were not detectable at d7 and d14, and are therefore not shown below (Figure 21). Noticeably, as mentioned above, at d0 the majority of the B cells exhibited a memory phenotype and only 10% a naïve phenotype. This tendency was also observed at d7 and d14 with only 3% naïve cells at d7 and 16% at d14. But, in contrast to d0 also the frequency of $CD27^-IgD^-$ cells increased strongly accounting for the majority of B cells at d7 and d14.

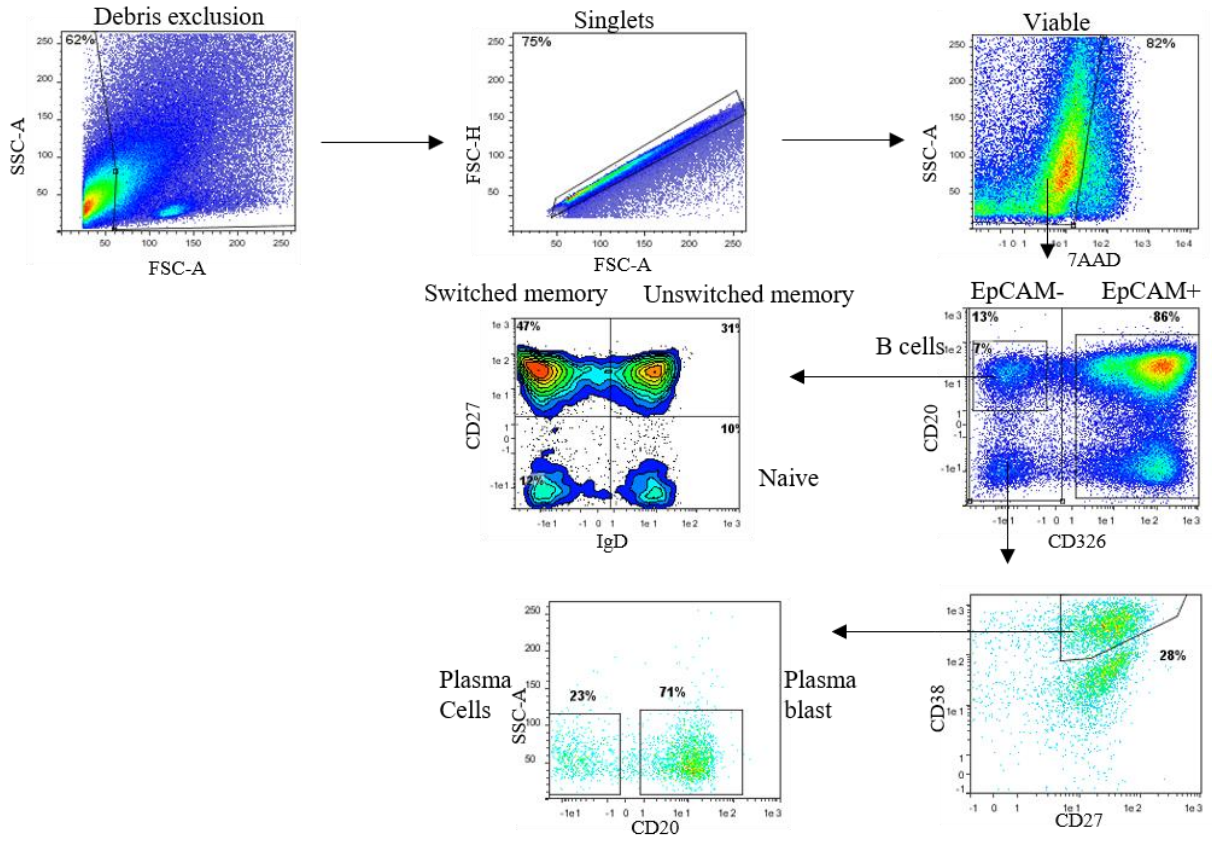

Figure 20: Flow analysis after B cell isolation

At day 0, using CD19 and CD138 microbeads, B cells were isolated and gated for subset identification. Firstly, debris is gated out, then singlets are selected. Viable cells are gated based on 7AAD staining. Following this, live cells are gated for EpCAM, a marker for tumors and CD20, a marker for B cells. Then, B cells are selected and gated for IgD+ naive and CD27+ memory. EpCAM- are further selected and sub-gated for CD27 and CD38. The double-positive population were selected and sub-gated for CD20.

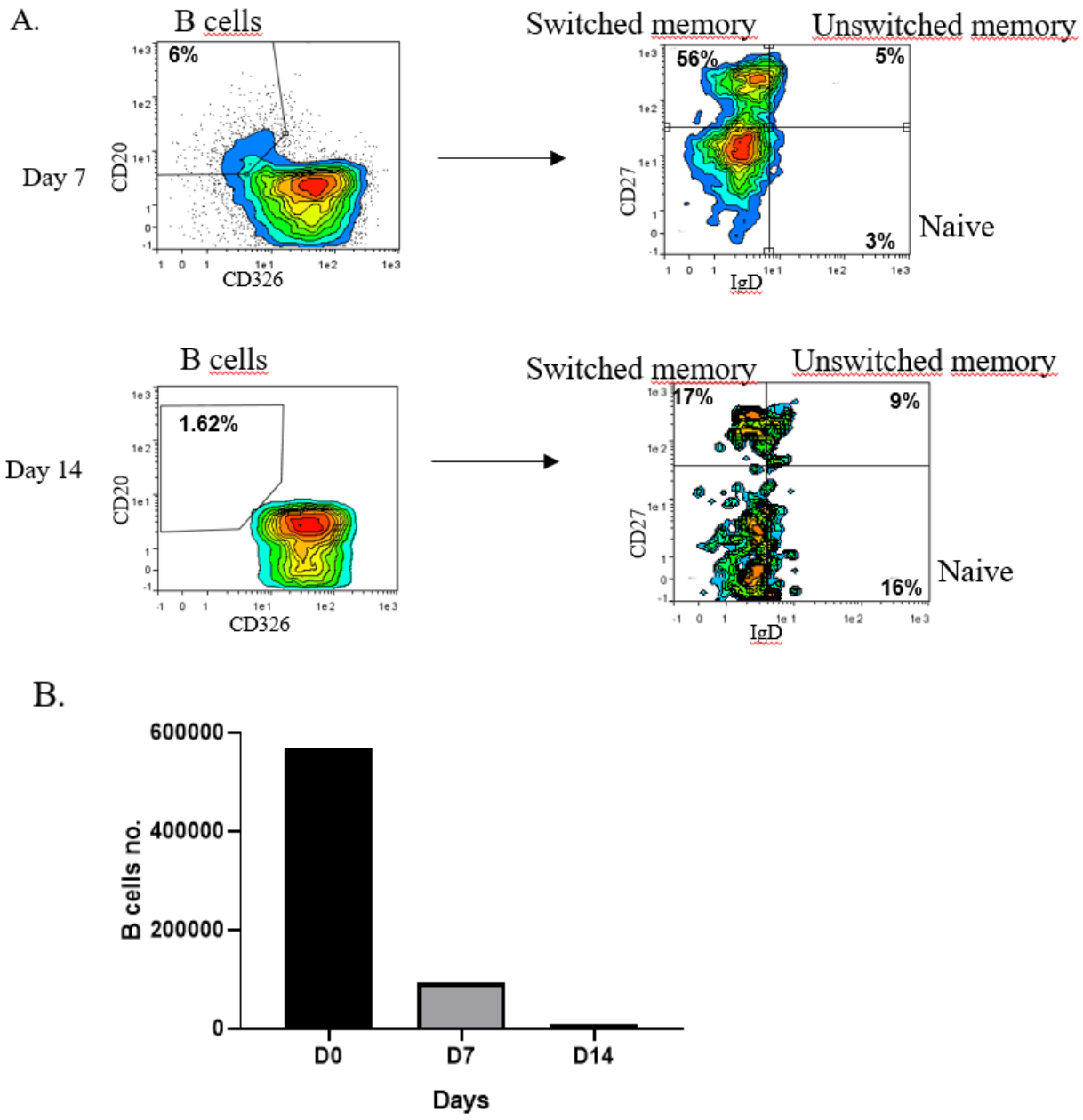

Figure 21: Flow analysis after B cell culture

A. and B. Cells were cultured at density $1X10^6$ per ml along with CD40-ligand (80 U/ml) and IL-21 (25 ng/ml) for 14 days and stained at day 7 (a) and day 14 (b). As shown before in Figure14 gating was made in order from debris exclusion, singlet selection, viable population (data not shown), then $CD20^+$ B cells were gated and $CD326^+$ tumor cells were gated, to gate out tumor cells. Then, B cells are selected and gated for IgD^+ naive and for $CD27^+$ memory. B. Graph showing number of B cells during culture at day 0, day 7 and day 14.

3.8 Single cell BCR sequencing from ovarian carcinoma sample

As described above fresh tumor material was processed accordingly. The fresh ovarian carcinoma tissue was received after surgery. The tissue was dissociated using the standard Gentle MACS tumor tissue dissociation protocol. Dead cells were removed using a dead cell removal kit and analyzed by flow analysis. B cells were present with a frequency of 15% in the original sample. Using CD19 and CD138 magnetic beads, B cells and plasma cells were isolated (Figure 22). In total, 34,000 cells were isolated and used for single cell BCR sequencing, using the 10X chromium platform, as explained in material and methods section.

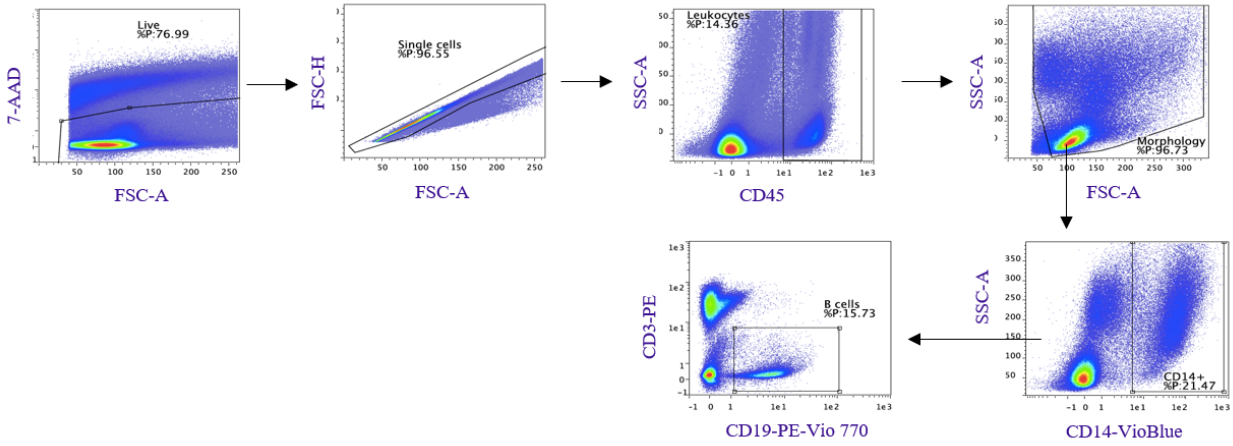

Figure 22: Flow analysis of ovarian carcinoma sample after Gentle MACS dissociation

Human ovarian carcinoma sample was processed as described before. The gating strategy was conducted starting with viable cells then singlets. Among singlets, $CD45^+$ leukocytes were gated followed with morphological gating and then on $CD14^+$ monocytes excluded gate $CD19^+CD3^-$ B cells were selected. Dissociation and screening was done together with Criado-Moronati E. from T cell group.

Upon interaction with their cognate antigen B cells undergo clonal expansion. Based on this, the hypothesis was made that a high abundant BCR clone within the B cell fraction of an infiltrated tumor sample would therefore indicate a clone with tumor specificity. To test this, isolated B cells were processed by BCR single cell sequencing. Data was analyzed using 10X Loupe VDJ browser software which allows users to analyze, search, and visualize V(D)J sequences and clonotypes from single cell data produced by the 10x Chromium Platform. In total, 1,265 cells were sequenced from the isolated B cell fraction. First, it was investigated if an abundant clonotype

could be detected in the data. Next, the abundant clonotype of the BCR was compared between B cells from a total tumor bulk and B cells from the isolated fraction (Figure 23A). In case of the total bulk, no distinct clonotype enrichment was observed, shared clones were present only in 2-3 cells, while in case of the isolated fraction, a clear enrichment (ranging from 10-60 cells) of distinct clones was detectable. The isolated fraction contains a higher percentage of B cells and therefore allows a more in depth analysis of the B cell clones. Thus, sequencing of the pre-enriched B cell fraction was established as strategy to look for dominant, potentially tumor specific clones.

The top clone in the isolated B cell fraction of an ovarian carcinoma sample which encompassed 60 B cells was selected for further experiments. For this, it was initially checked if there are any point mutations/variations for this clone present among different cells (Figure 23B). The row marked consensus above the contigs is the chain consensus sequence, a sequence that represents the most likely sequence for a receptor chain within the clonotype (Figure 23B). Above the consensus is the reference sequence, which is a concatenation of the reference sequences of each gene detected in the chain (referred from 10X Loupe page). It was found that all the 60 B cells from the top clone fraction were sharing the exact same sequence with common mutations in comparison to the reference sequence. Other sequences, which were shared in 8 or 6 cells, also displayed mutations in comparison to the germline sequence. Mutational status of IgHV genes have been correlated with prognosis. Interestingly, in the dominant clone we find mutation in the IGHV3-23 gene, which has also been correlated with specific subset of B-cell chronic lymphocytic leukemia (Bomben and others, 2010). Furthermore, it was investigated how the isotypes are distributed among the sequenced cells (Figure 23C). We found that IGHM was present in highest abundance, being detected in 497 clones including the top clone. IGHG and IGHD were present in 139 and 132 cells, respectively, and IGHA was present in 74 cells. More Igκ light chains were present than Igλ light chains, in a ratio of 8:1.

A.

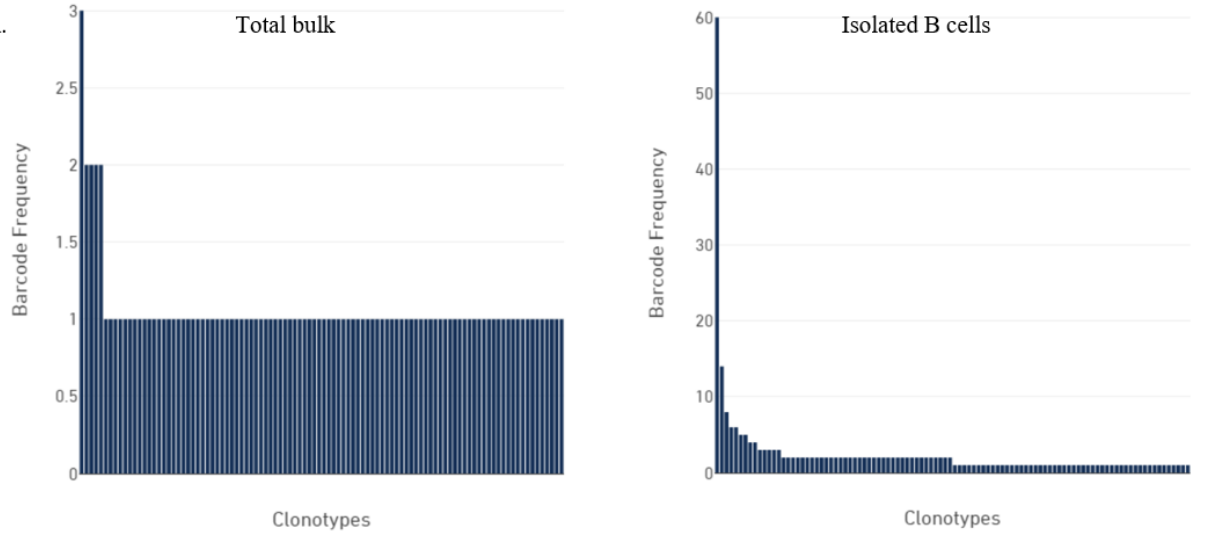
Total bulk
Barcode Frequency
Clonotypes
Isolated B cells
Barcode Frequency
Clonotypes

B.

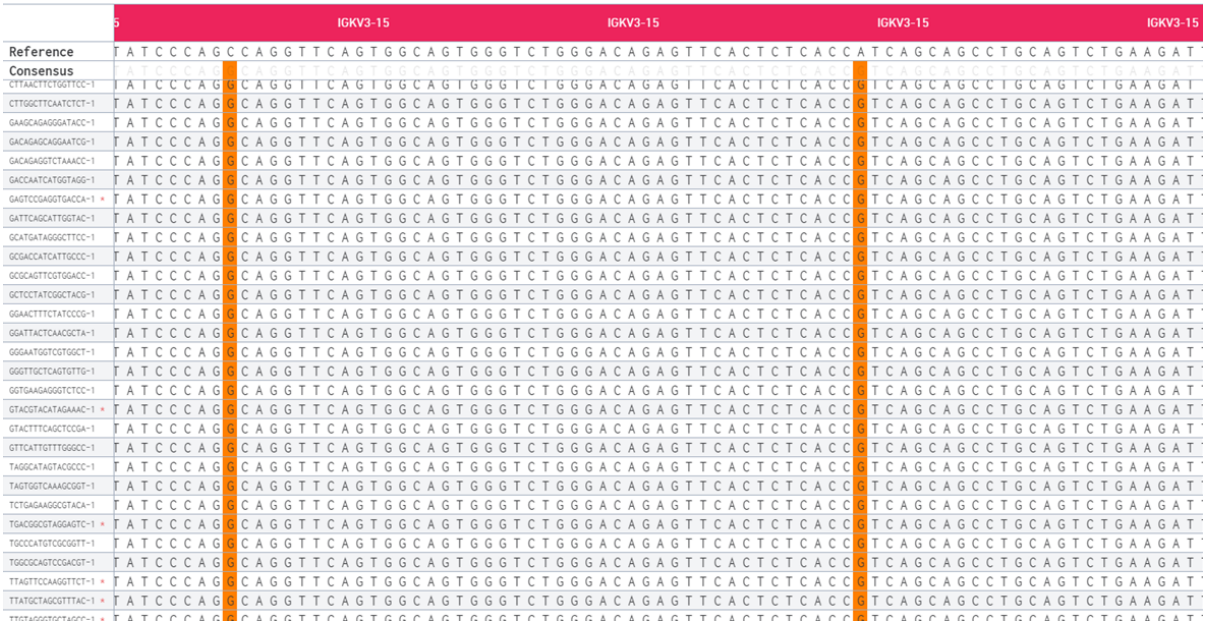
IGKV3-15
IGKV3-15
IGKV3-15
IGKV3-15
Reference
Consensus

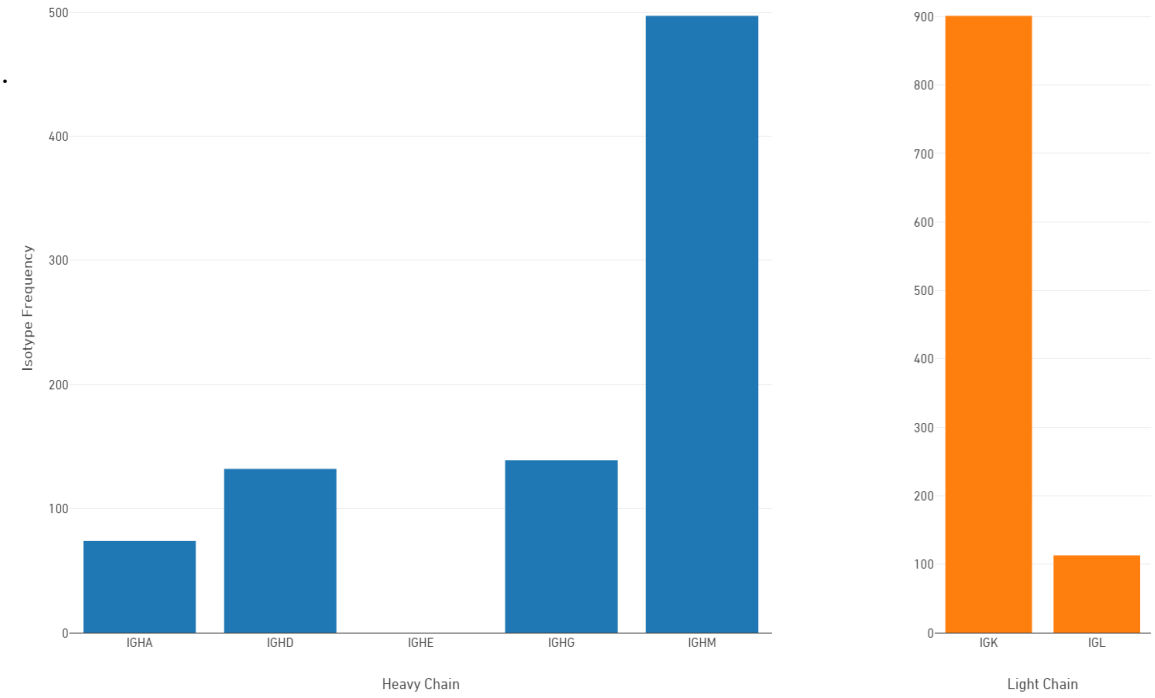

Figure 23: Analysis of single cell B cell receptor sequencing from ovarian carcinoma sample

A. Clonotype abundance comparison between B cells from total tumor bulk with B cells from isolated fraction (using CD19 and CD138 microbeads). B. Sequence alignment between different cells to determine intraclonal diversity. Orange represents mutation in the clone in comparison to the germ line sequence. An exemplary part of the sequence is shown from the light chain Igκ from the isolated fraction. C. Isotype distribution among all cells sequenced from isolated B cells.

3.9 Antibody generation and specificity validation on primary tumor samples

To generate a recombinant antibody with the specificity of the top clone, the heavy and light chain sequences were extracted from the 10X loupe browser and were cloned into 2 vectors, one expressing the light chain, the other expressing the heavy chain. Using a standardized in-house process (confidential), starting with a co-transfection of both vectors, a stable antibody producing cell pool was generated in an (approximately) 10 weeks protocol. The recombinant antibody was purified using protein-A beads and then concentrated to use it further for conjugation steps. Antibody was named as OvCa_1.

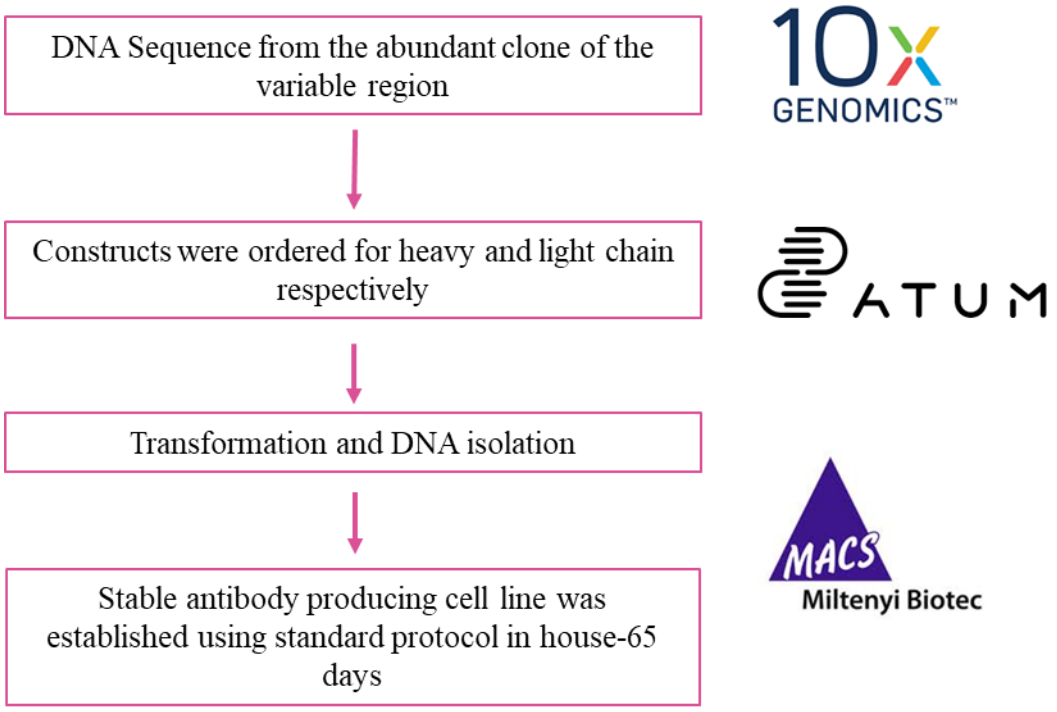

Figure 24: Flowchart explaining steps for recombinant antibody generation

Heavy and light chain sequences were extracted and cloned in respective vectors. Following this, a stable cell line was generated using an in-house protocol.

For conjugation, the antibody was coupled to Vio667, a dye which offers the advantage of being brighter than for example FITC, but also small, so that it does not cause problems in course of intracellular staining protocols. To obtain a monomeric form, a single molecule of antibody was conjugated to a single Vio-667 dye.

As the top clone was identified as IgM, which is usually present in pentamer form, a second approach was set up for comparison. Here, it was tried to mimic this pentameric configuration by bringing more antibodies together on one PE molecule. Using standard PE-coupling procedure with modifications, the PE molecule was activated to have free binding sites, while on the other side the antibody was reduced to have free thiol groups. Final coupling of PE with antibodies was done and the number of antibody molecules conjugated with one PE molecule was calculated using

absorbance values. It was found that one PE had four antibodies bound at the end, called tetramer form.

As a next step, the specificity of the antibody was tested on human ovarian cell lines. Pure antibody was used as negative control. Pure antibody with monomer/tetramer form was used as blocking, to check the nonspecific binding of the antibody. No binding was observed with flow staining in ovarian cell lines (Figure25a). In addition to that, the specificity of the antibody was tested on an acetone fixed tumor tissue section from the same patient, from where also the BCR clone was obtained. In this section, EpCAM was used to mark tumor cells. Section from another ovarian carcinoma patient was used as negative control, in case the antibody was binding to patient specific clone. No specific binding was observed in the PE channel for the OvCA_1 antibody (Figure25b). Due to limited availability of tumor tissue from the patient, only the tetramer form of the antibody was tested.

At last, testing of antibody was performed on freshly thawed tumor cells from the same patient dissociated tumor digest using flow cytometry. Florescence minus one (FMO) was used as a control and for gating of the OvCa_1 binding population. A PE-signal enhancer kit was also used, in case the signal was too low to be detected. With the OvCa1 monomer 0.38% positive cells could be detected, while with the Ovca1-PE 0.17% were detectable, indicating that the antibody is binding only to a small subset of tumor cells (Figure 25c).

A. On OvCa cell lines

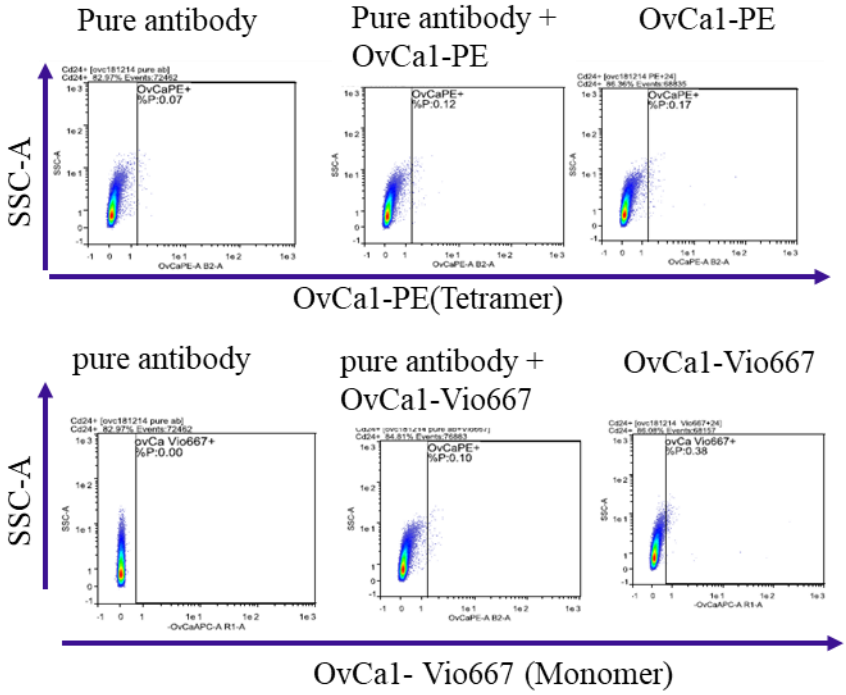

B. On tumor tissue from the patient

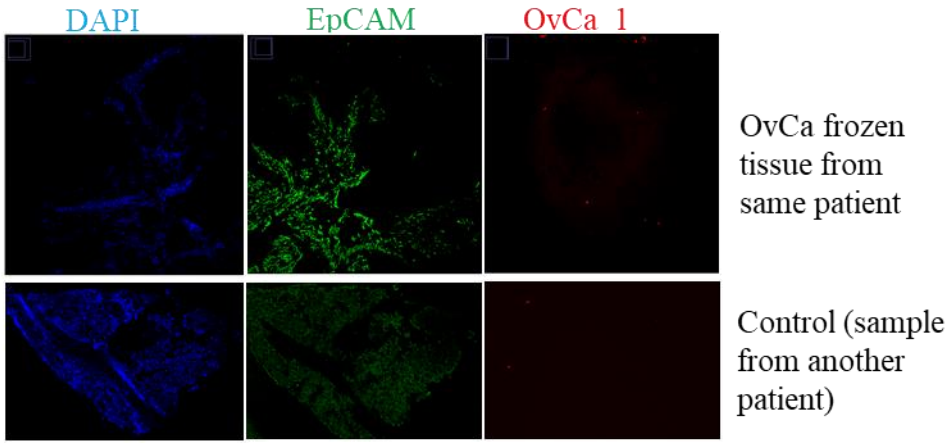

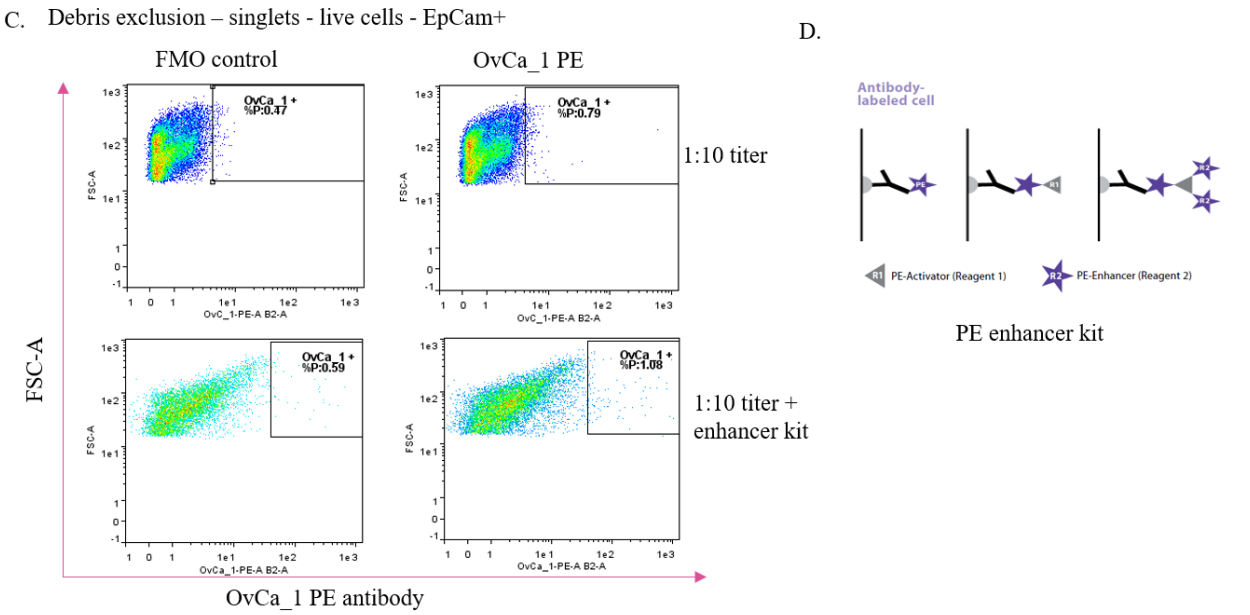

Figure 25: Validation of OvCa_1 antibody

A. Testing of antibody on ovarian cell lines generated from primary tissues in-house, with pure antibody used as negative control. Flow cytometry data was measured on MACS Quant and analyzed in Flow Logic software. B. Screening of antibody on frozen tumor tissue section from the same patient. EpCAM is represented in green, DAPI in blue and OvCA_1 antibody in red. C. Testing of OvCa_1 antibody on tumor cells from the same patient. D. Graphical abstract of enhancer kit mechanism from Miltenyi datasheet.

3.10 Gene expression profiling of tumor infiltrating B cells

Along with BCR sequencing, using the 10X genomics platform, single cell RNA sequencing (scRNA seq) was performed on the same patient material. In total, 1,429 cells were sequenced. Data was analyzed using the Loupe Cell Browser, where along with the expression analysis of cells, one can look at clonotypes within a gene expression cluster and compare clonotype distributions between clusters. Seven clusters were identified in the sample and a list of the top 50 significant genes from each cluster were extracted. Based on the expression profiles of the genes the clusters were then categorized (Figure 26). Two distinct B cell clusters were observed.

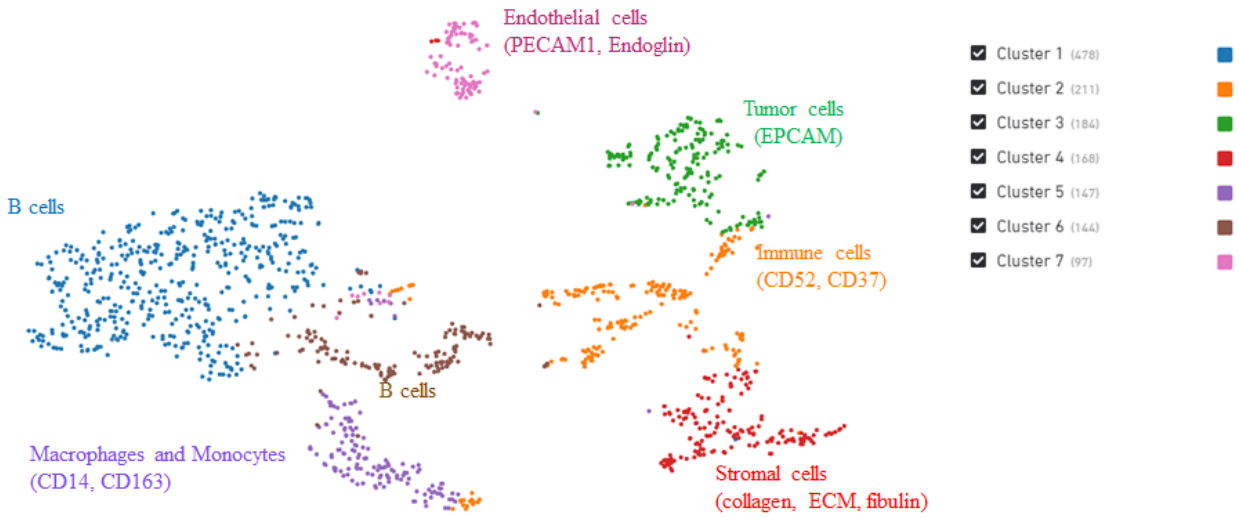

Figure 26: Distinct cell clusters were identified by gene expression profiling of B cells from ovarian carcinoma sample

T-SNE plot showing seven different cluster from scRNA seq data. Cluster were characterized based on their expression profiles. The standard 10X chromium protocol for gene expression was followed and analysis was done using 10X Loupe Cell Browser.

As for this work, the focus was on B cells, expression pattern of CD20 was checked among the clusters (Figure 27A). It was found that most of the cells in both B cell clusters were expressing CD20. Expression of classical B cell markers such as CD19, CD22 and CXCR4 was found to be on the same cells as CD20 (Figure 27b). Expression of other B cell related genes and factors was analyzed, among which expression of PAX5, a B cell–specific transcription factor, BACH1 and EBF1, factors expressed on B cells from early stages of development on, was found to be specifically expressed on these subset of B cells. Distribution of BCR isotypes was also analyzed among $CD20^{+}$ B cells and plasma cells. It was found in agreement with scBCR data that IgM was present in highest abundance with 48% to 41% of the B cells in both B cells and plasma cells being IgM+. Interestingly, the percentage of IgG1 was increased in plasma cells to 25% from 8% in B cells.

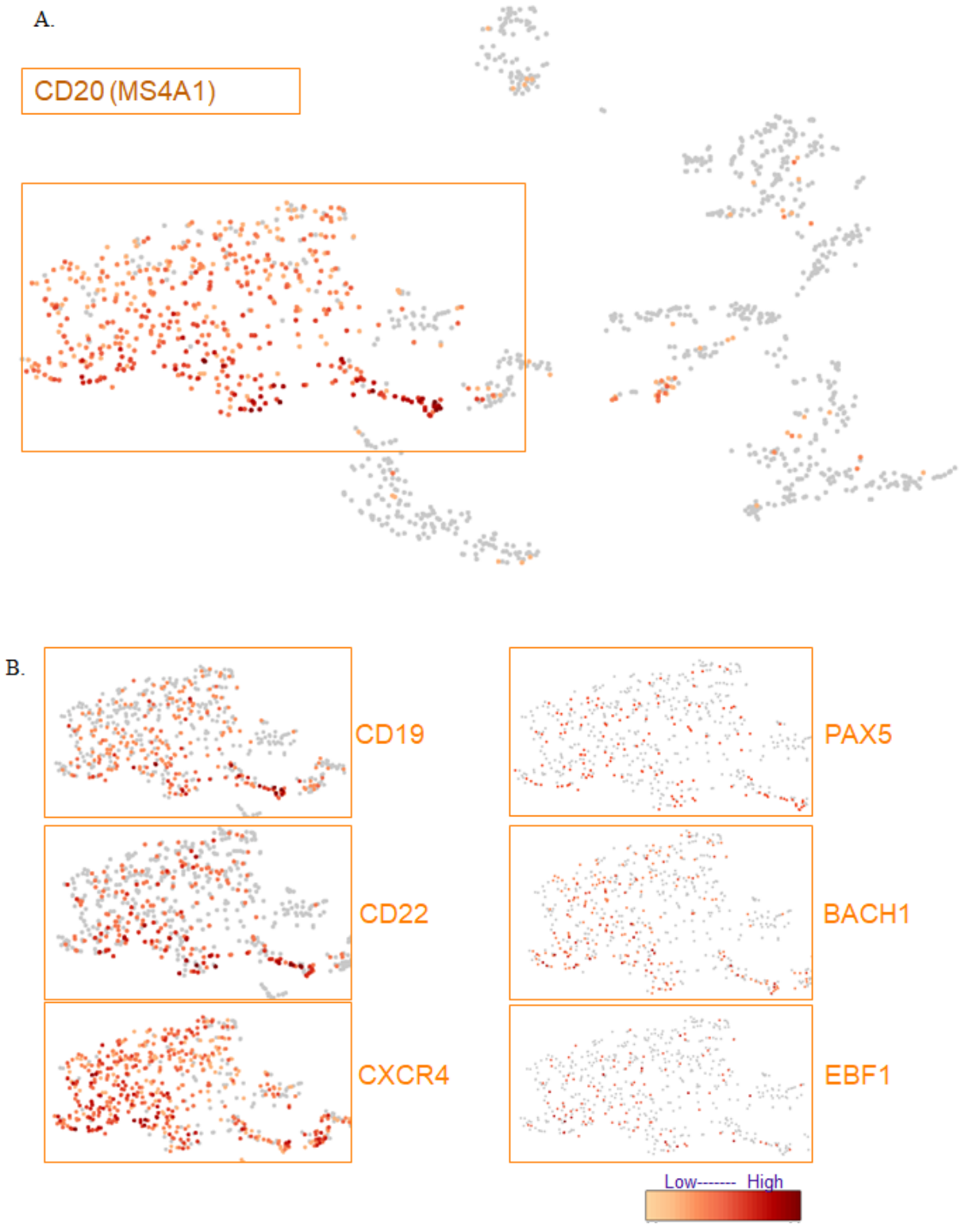
A.
CD20 (MS4A1)
B.
CD19
CD22
CXCR4
PAX5
BACH1
EBF1
Low------- High

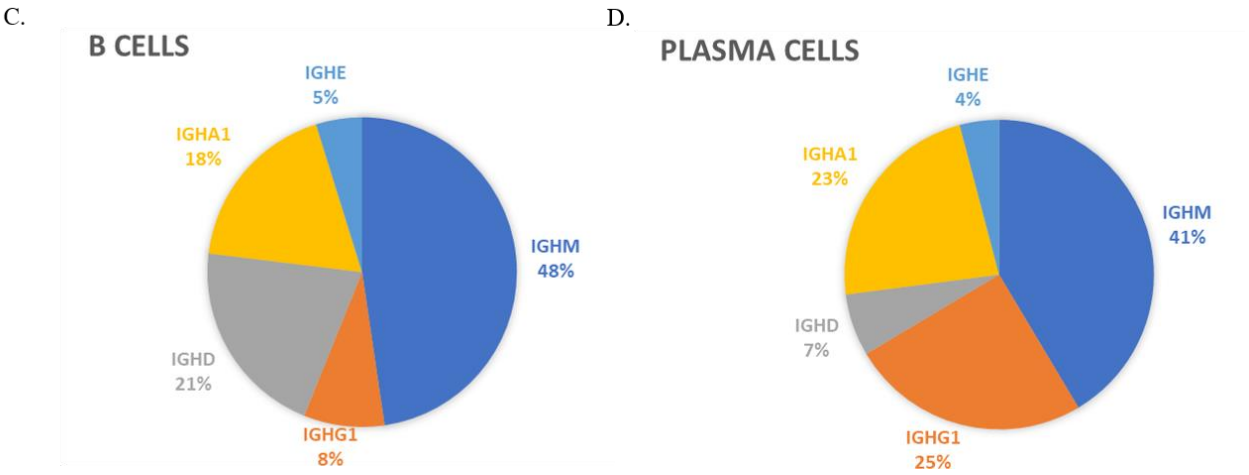

Figure 27: Characterization of B cell cluster from scRNA seq

A. Expression of CD20 among different clusters obtained from scRNA seq of B cells from human an ovarian carcinoma sample using the 10X Loupe browser software B. Expression of classical B cell related genes observed in the cluster. Gradient of orange color corresponds to intensity of the gene expression. C and D. Pi-chart showing percentage of isotypes present in B cells and plasma cells, respectively.

To investigate the B cell phenotype of the cells with BCR sequence, data from single cell BCR sequencing was mapped back on to the scRNA seq data and most of the cells were found to be lying in the same area as the cells in the $CD20^{+}$ cluster (Figure 28a). Following this, the top clone of the scBCR data was investigated in context of the scRNA seq data, indicated in the Figure as the dark blue cells (Figure 28b).

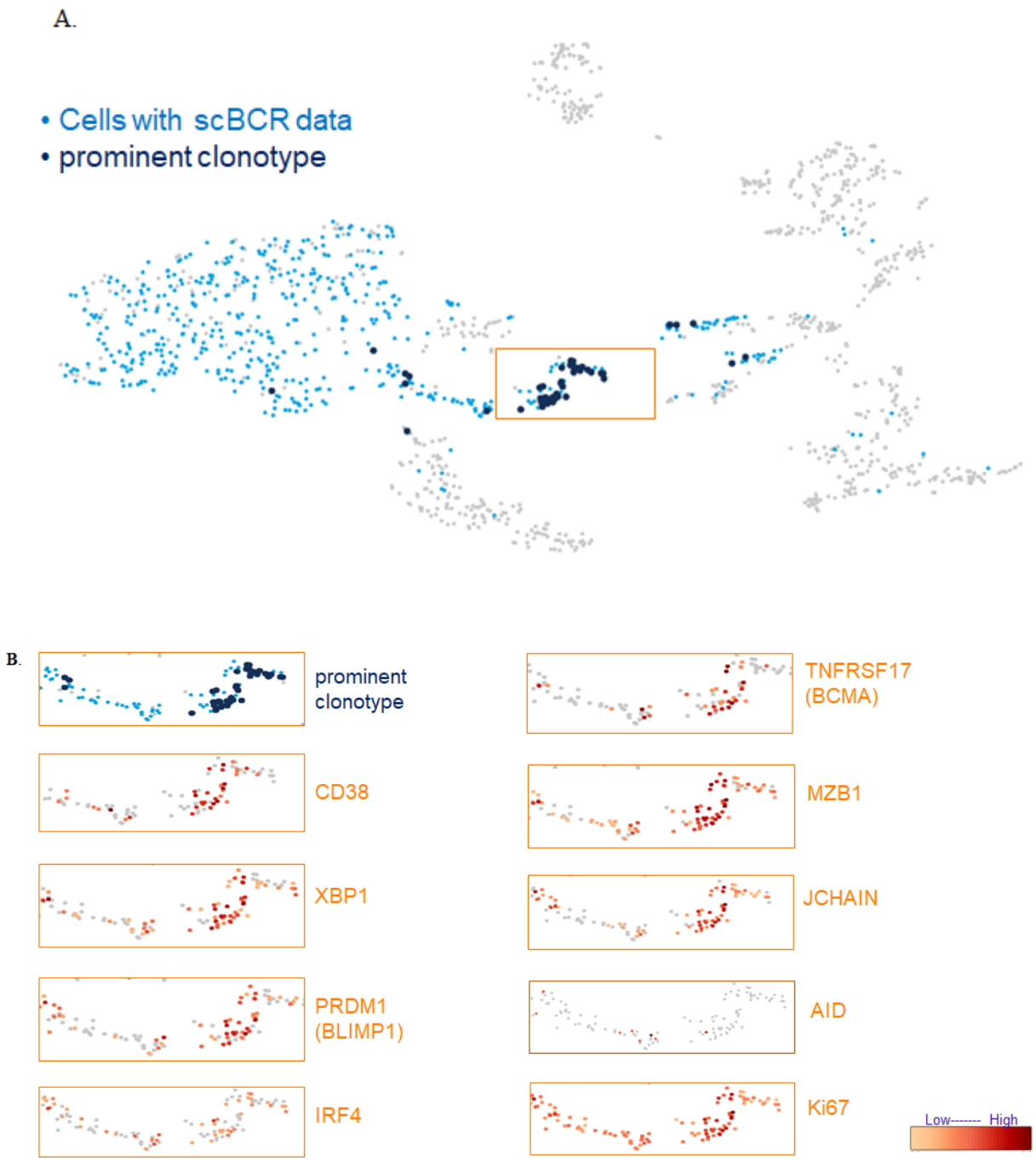

Figure 28: Characterization of the BCR top clone with scRNA data

A. Mapping back of data from scBCR sequencing to scRNA seq using which software. Light blue shows all B cells from scBCR sequencing, dark blue represent the abundant clone. B. Expression profile of the top clone. Gradient of orange color corresponds to intensity of the gene expression.

Expression of B cell related genes and transcription factors was then analyzed. The cells in this cluster were found to be positive for CD38, a marker which is expressed with CD138 on plasma cells. In addition, they were expressing X-Box protein 1 (XBP1), BLIMP1 and B-cell maturation antigen (BCMA), factors expressed exclusively on late stage B cells and plasma cells. Interferon regulatory factor 4 (IRF-4) among the B-cell lineage has been found to be restricted to plasmablast-like germinal center B cells and plasma cells. Besides this, the top clone was also expressing marginal zone B1 (MZB1) which has been shown to have a role in regulating calcium homeostasis and antibody secretion. JCHAIN has been reported to be expressed by plasma cells and it helps in secretion IgA and IgM antibody, and this comes in alignment with expression of it in our top clone which expresses IgM. No expression of AID was found, confirming absence of germinal center cells in the sample. Moreover, these cells were positive for Ki67 suggesting that the cells are in a proliferating stage.

Taken together, these data suggest that there are two distinct B cell clusters, one expressing a classical, general B cell phenotype, indicated by CD20, CD22, and PAX-5, while the abundant clonotype from the BCR possess mostly specific characteristics of plasma cells.

4. Discussion

In several studies, immune cells have been described to infiltrate solid tumors, mainly characterized by high infiltrates of $CD8^+/CD3^+$ T cells (Hadrup and others, 2013). The role of T cell in mediating antitumor immune responses has been studied extensively and consequently, most of the new immunotherapeutic approaches have been developed on T cell (Wang and others, 2014). In contrast to T cells, considerably less is deciphered about TIBs. Studies relating to TIBs are inconsistent, and both tumor-inhibitory as well as tumor-promoting roles of B cells have been reported in many malignancies, but the exact function of B cells has not been satisfactorily evaluated so far (Flynn and others, 2017). In this project, we assess the distribution and phenotype of TIBs in frozen and fresh tumor samples using microscopy and flow cytometry techniques. With the aid of single-cell sequencing of B cells, a state of the art method has been developed to identify and characterize the clonal composition and differentiation stage of TIBs and to identify tumor specific antibodies.

B cells were detected in 21% of all frozen human ovarian carcinoma tissues screened. This is in line with current literature which describes a frequency of 40% B cell infiltration in high-grade serous ovarian cancer (Nelson, 2010). In several experiments, we found that T cells are infiltrating the tumor tissue at a much higher frequency and constitute most of the immune infiltrates in tumors. Besides T cells, macrophages are also described to infiltrate the tumor microenvironment and are mostly reported to be associated with a worse outcome (Jayasingam and others, 2019). After cancer initiation the tumor microenvironment is mainly hypoxic (Vaupel and Mayer, 2007). Hypoxia is one of the hallmarks of malignant cancer progression and associated with therapy resistance and poor clinical outcome (Harris, 2002; Semenza, 2012). Within this environment aerobic glycolysis is the main source for ATP production and the generation of acidic products lead to lower pH (Stubbs and others, 2000). Next to this, the stromal compartment is highly desmoplastic and with the help of cytokines and growth factors, it becomes immunosuppressive (Rabinovich and others, 2007). This kind of high immunosuppressive microenvironment of tumor is detrimental to the activation of immune cells (Magalhaes and others, 2019). These observations could be one of the reasons, why B cells need specific chemokines or factors for their recruitment and to pose anti-tumor effect (Workel and Lubbers, 2019).

Within tumors, B cells show heterogeneity in their phenotype and function, and here with the help of MACSima technology, we have characterized the TIBs keeping the spatial information of the tumor microenvironment intact. This technology allows us to look for more than 90 markers

at the same area within a fixed tissue, providing an opportunity to decipher cell-cell mediated interactions and protein colocalizations, which could help us in unravelling many biological questions. With the help of the marker CD20, which is expressed by all mature B cells, except plasma cells, B cells were identified. It was observed that dense areas of lymphocytes had clusters of B cells resembling lymphoid structure surrounded by mostly T cells, while the lower infiltrated area had single scattered B cells.

The tumor microenvironment (TME) is a networking system composed of not only tumor cells but also stroma, vasculature, fibroblast, infiltrating immune cells and other noncellular tissues (Wagner and others, 2019). Prominent immune cells in TME include macrophages, myeloid cells, dendritic cells, natural killer cells, T cells and B cells (Gun and others, 2019). In the same line, we could identify a cluster of $CD45^+$ leukocytes next to $CD326^+$ tumor cells (epithelial cell adhesion molecule, EpCAM), surrounded by $CD14^+$ myeloid cells, $CD163^+$ macrophages and $CD105^+$ blood vessels. Among the lymphocytes, a predominant abundance of $CD4^+$ T cells, surrounded by $CD20^+$ B cells, was observed. $CD138^+$ plasma cells were found in the vicinity, together with $CD8^+$ T cells.

In solid tumors, the existence of structured lymphocytic infiltrates has been frequently reported. Generally referred to as TLS, they mimic structurally secondary lymphoid organs and might serve to enhance anti-tumor immune responses. Along with a network of dendritic cells and CD4 and CD8 T cells, B cells are a major component of TLS. In tumors, TLS can indicate a source for the recruitment of lymphocytes and may promote the production of memory T and B cells (Teillaud and Dieu-Nosjean, 2017). This can be observed in our study on ovarian carcinoma tissue. An accumulation of memory B and T cells could indicate a maturation stage which normally is driven by B cells encountering their specific antigen. In line with this, TLS have been described as a signature for better prognosis in several tumor types like colon cancer (Shimabukuro-Vornhagen and others, 2014), ovarian carcinoma (Montfort and others, 2017) and breast cancer (Song and others, 2017). We were able to observe clusters of $CD20^+$ B cells adjacent to $CD21^+$ fDCs and $CD3^+$ T cells, predominantly $CD4^+$ T cells with some $CD8^+$ T cells confirming TLS structures in the sample. Also, MECA-79–expressing high endothelial venules (HEVs), $CD64^+$ macrophages and $CD138^+$ plasma cells were found in the surrounding. Interestingly, these plasma cell were present at relatively high amounts in the periphery, this is in line with the previous observation that many memory B cells can be detected in the tumor tissue, strengthening the assumption that affinity maturation may be taking place within the TLS in the tumor microenvironment, and suggesting that these cells could be secreting tumor specific antibodies. Underlying this hypothesis, in triple-

negative breast cancer patients, a high frequency of plasma cells was correlated with a higher number of TLS, suggesting a functional role for B cells in survival (Astorri and others, 2010). In patients with esophagogastric adenocarcinoma, B cells in TLS were reported to produce tumor-specific antibodies (Schlößer and others, 2019). Taken together, these data demonstrate a functional role for TLS-associated B cells in anti-tumor response and makes them an important cell population to further look into.

Several bioinformatic tools were tested and optimized for segmentation and quantification of the images generated through the MACSima technology. As cells are very tightly packed within the tissue, segmenting them into individual cells is a challenging task. Also, because of close localization of the cells, it is tricky to differentiate and allocate the signals to the respective individual cells, making exact quantification of signal intensity difficult. There is the strong need of establishing an automated pipeline for image segmentation, quantification of signal intensity, their respective normalization and clustering into further subsets to draw meaningful biological interpretation.

B cell formation starts in the bone marrow and undergoes several developmental stages before and after antigen mediated stimulation. B cells can be categorized by a variety of markers for their differentiation stages. Additionally, numerous phenotypical and functionally diverse subsets of B cells have been acknowledged (Jackson and others, 2008). TLS are involved in the differentiation of antigen-specific B cells and as mentioned above in the generation of memory responses (Montfort and others, 2017). In our study, the abundance of the memory B cell phenotype has been found within the microscopic as well as the flow cytometric data. This indicates that either there is an ongoing germinal center reaction in the TLS from where these memory B cells originate or, with the help of a chemokine axis involving factors such as CXCL10, CXCL12, CXCL13, CCL19, and CCL21 (Guo and Cui, 2019; Lee and others, 2016), these memory B cells could penetrate the tumor and depending on antigen availability they have the potential to switch to plasma cells upon stimulation. Enrichment of plasmablasts and plasma cells in periphery, points in the direction that B cells can provide anti-tumor immunity by producing antigen specific antibodies (Sharonov and others, 2020). It could be also speculated that these plasma cells originated from the pool of memory B cells in the TLS. In this context, secretion of cytokines and production of antibodies targeting tumor antigens could be a potential way to provide immune cytotoxic response by B cells. To test these assumptions, one has to test Ig isotypes present in fresh tissue supernatants and plasma and to perform profiling for cytokines, including IFN-γ, TNF-α, IL-1β, IL-4, IL-5, IL-

6, IL-10, IL-13 and IL-21. Furthermore, more samples need to be examined to draw stronger conclusions.

Along with secreting antibodies, B cells can also perform a variety of other immunological functions, such as presenting antigens to T cells initiating their further activation. Here, we observed expression of costimulatory molecules like CD40, HLA-DQ and HLA-DR which suggests that B cells possess an antigen presenting function in the tumor tissue analyzed. In comparison to dendritic cells, B cells are not as efficient in priming T cells (Hilpert and others, 2016), but in context of the tumor microenvironment B cells as antigen presenting cells could have advantages. They can detect even low amounts of antigens with the help of their specific B cell receptor. Memory B cells are derived from germinal center B cells that have undergone affinity maturation so that these cells are optimized to detect antigen even at low concentrations. The presence of a higher proportion of memory B cells could therefore allow a more potent antigen presentation if the antigen is only present at low level.

A distinct subset of B cells, called B-reg cells, has come into light in recent decades. This subset shows immune-modulatory functions mostly through the production of the immunosuppressive cytokines TGFβ and IL-10 (Mizoguchi and others, 2002). As discussed in the Introduction, B-reg cells can promote metastasis by switching resting $CD4^+$ T cells into T-reg cells. In our study, enrichment of $CD4^+$ T cells is observed next to $CD20^+$ B cells, it could be that these are B -regs and T-regs. Staining of markers such as IL-10, FoxP3 or TGFβ could help in unravelling this question. Within this study this could not be investigated as technical problems did not allow a clear staining. Further optimization in this regard is needed to enable more profound characterizations.

Terminally differentiated B cells, i.e. plasma cells, are primarily known for producing antibodies. Multiple lines of evidence currently made it clear that B cells undergo clonal proliferation, isotype switching and selection for high affinity clones within tumor-linked TLS and in less organized structures, finally differentiating into memory B cells or plasma cells (Cipponi and others, 2012; Pimenta and Barnes, 2014). Studies done on breast cancer, melanoma and ovarian cancer have shown that plasma cells may reside locally and produce huge amount of antibodies against tumor epitopes (Pavoni and others, 2007). Antibodies can mediate opsonization, ADCC via natural killer cells, complement mediated lysis of cancer cells or phagocytosis by macrophages (Vargas-Inchaustegui and Robert-Guroff, 2013). Keeping this background in mind, we performed single cell sequencing of B cells infiltrating ovarian carcinoma. As the frequency of B cells is very

limited in solid tumors, B cells were enriched using CD19 and CD138 microbeads. B cells undergo clonal expansion upon encounter with cognate antigen. Our hypothesis was that the most abundant B cell clone within the enriched B cell fraction could exhibit the highest likelihood of being directed against a tumor-specific antigen. Our data obtained from single cell sequencing demonstrated that there was abundance of BCR clones in the enriched B cell fraction compared to the non-isolated, original fraction, suggesting that pre-enrichment of B cells is a good strategy to search for abundant and therefore potentially tumor-specific clones.

An important parameter of whether an antibody will have antitumor or protumor effects is determined by the antibody isotype it possesses. Tumor-specific IgG production by plasma cells was linked with an antitumor role in ovarian cancer (Montfort and others, 2017). In hepatocellular carcinoma, IgG^+ memory B cells have been shown to produce granzyme B and TRAIL, which can cause toxicity to tumor cells (Shi and others, 2013). In the RNAseq data, analyzed in this study, we observed that IgG isotype distribution was significantly increased in plasma cells (17%) compared to overall B cells, suggesting that these clones could have more potent anti-tumor effect, provided that it would be tumor antigen specific. Due to low availability of viable B cells, we didn't have the option to differentiate between B cells and plasma cells for the BCR sequencing. Therefore, the most abundant clone was taken, which consisted of an IgM isotype, and was used to clone and produce a recombinant antibody. Natural IgM has been reported to bind preferentially to post-transcriptionally modified cell surface antigens that are tumor-specific, recognizing the conserved structure of carbohydrate epitopes (Brändlein and others, 2003; Díaz-Zaragoza and others, 2015). In our hands, the recombinantly produced antibody did not show strong binding to ovarian carcinoma cell lines, nor primary tumor cells obtained from the same patient. In case of the primary patient material, the antibody was binding to only very few tumor cells, suggesting either the produced antibody is not specific for a tumor antigen or the antibody is targeting a very small subset of cells in the tumor. This would argue against it as a suitable antibody, because a potential candidate should on the one hand bind specifically to a tumor epitope, but additionally should be expressed on the majority of the tumor cells to be as efficient as possible in generating an antitumor immune response. Nevertheless, the procedure in itself represent a promising approach, but to allow a more efficient selection of potential candidates, a higher throughput of samples has to be run as well as more clones have to be tested. To improve the efficacy, the B cell pool has to be more carefully selected. An option would be to enrich only the plasma cells and use them for single cell

BCR sequencing. In this way we would enrich the antibody secreting cells locally in the tumor and the chances of them being tumor antigen specific would be higher.

A combination of DNA-based and RNA-based immunoglobulin repertoire profiling was applied to estimate both B cell clonal and immunoglobulin composition within a tumor sample. The clusters observed from RNA sequencing data display cells from tumor microenvironment such as stromal cells, endothelial cells, macrophages and immune cells. There are two distinct B cell clusters, one expressing classical B cell phenotype markers while the other one displays a plasma cell phenotype, notably exhibiting the dominant clone from BCR sequencing. The second cluster clearly expresses markers of late differentiation stages like BLIMP1, TACI, XBP1, and IRF4. Surface markers from microscopy or flow data like CD138, and CD38 could not be used for comparison, as often the cells express low amounts of RNA for surface proteins, which can be below the detection level of RNA sequencing. Taken together, with this study we were able to develop and establish a pipeline which in the future can be used to investigate tumor infiltrating B cells and especially plasma cells in more detail in regard to their capacity to serve as a source for anti-tumor specific antibodies. Even though a tumor specific antibody could not be generated, it indicates that especially a higher throughput of sample and assessment of multiple potential promising clones has to be performed to increase the probability of tumor specific antibody. Furthermore, the analysis of the B cell subsets by MACSima technology has to be bioinformatical intensified to allow investigations and characterization of smaller B cell subsets which could be a potential source for a tumor-specific subset similar to what has been described for CD137 in T cells (Wölfl and others, 2008)

B cells can contribute in various ways to the generation of a potent anti-tumor response. Through their intrinsic capabilities to secrete antibodies, or to work as APCs or by secreting cytokines they have proven to assist adaptive immune functions. The discrepancies in the role of B cells in tumors could be due to alterations in tumor microenvironment provided by varieties of tumor entities mediated by distinct immune cells, cytokines and chemokines. However, as we could demonstrate, B cell studies are challenging due to their low abundance in solid tumors. Studies like this which focus on a step by step characterization of antibody expression, functional phenotyping of intratumoral B cells and their interaction with other cells within intact spatial localization might provide new understandings about the role of B cells in tumor immunology. With the help of robust phenotypic markers, therapeutic strategies aiming to, for example, deplete, inhibit or strategically target B regs will make a valuable contribution towards immunotherapy, reducing and potentially

remodeling the immunosuppressive microenvironment. Advanced knowledge about the role of specific B cell subsets might provide important information to differentiate patients who may profit from depletion or activation of B cell-dependent therapies. As chimeric antigen receptor (CAR) therapies contain an antibody part for target recognition, a potential new tumor-specific antigen which fulfills all the above mentioned requisites could be used for developing new and more efficient CAR treatments.

5. Summary

Current immunotherapies focus mostly on immune cells designated as $CD8^+$ cytotoxic T cells to fight cancer. Despite growing appreciation to the role of B cells in solid tumor microenvironments, most of the immune checkpoint blockade therapy targets are developed with the purpose to act on T cells and induce their activation. Up to now, a heterogenous impact has been ascribed to B cells infiltrating solid tumors. The presence of B cells within tumors has been correlated with improved patient survival in several studies, however, there are also investigations which describe pro-tumor roles of B cells and severe disease progression. These varying observations depend on the tumor entity and B cell subset investigated, but the exact underlying mechanisms and regulations are still only poorly understood and remain to be fully elucidated.

The aim of this project is to characterize tumor infiltrating B cells phenotypically in solid tumor entities. For this purpose, the MACSima technology is used to investigate the marker expression pattern of B cells present in solid tumors in context to their spatial localization. B cells could be detected in 21% of the samples screened. Here, tertiary lymphoid structures (TLS) like structures were identified consisting of mainly B and T cells, but also $CD64^+$ macrophages, high endothelial venules and $CD21^+$ follicular dendritic cells. Even though no new B cell subset could be identified to this point, the interesting observation could be made that the B cells within the TLS like structure show a prevalence of a memory B cell phenotype. In line with that, similar observation were made by flow cytometry analysis of freshly dissociated solid tumor. Interestingly, additional to that, a distinctive $CD138^+CD38^+$ plasma cell population was detected in the surrounding of the TLS like structure within the tumor by MACSima which could as well be validated by flow cytometric and RNA sequencing analysis of dissociated tumor samples. Observation of many memory B cells and plasma cells strengthens the assumption that affinity maturation might be taken place within the TLS in the tumor microenvironment, and suggesting that these cells could be secreting tumor specific antibodies. Therefore, BCR single cell sequencing was used to identify tumor-specific antibodies, combined with RNA expression profiling. Strikingly, clear abundance of BCR clones were found in pre-enriched B cell fractions, and the most dominant clone was displaying a plasma cell phenotype, characterized by expression of late B cell differentiation marker patterns. The recombinant production of the selected, most abundant antibody clone did not show binding to a majority of the respective primary tumor sample, neither to human ovarian cell lines. More tumor samples and B cell clones have to be screened and tested to increase the throughput and therefore the likelihood of identifying a suitable clone which meets

the requirements for a potential future therapeutic application. These are particularly: tumor specificity while exhibiting low off tumor effects and targeting an epitope that is present on a high percentage of tumor cells and in best case shared by a substantial group of patients. Furthermore, the identification of tumor specific B cell markers contains the potential to isolate or target specific B cells. Altogether, these data augment and further validate the information about B cell phenotypes in tumors, and continued effort in this direction will pave the way for novel development B cells based immunotherapies.

6. Zusammenfassung

Aktuelle Immuntherapien konzentrieren sich hauptsächlich auf Immunzellen zur Krebsbekämpfung, die als $CD8^+$ zytotoxische T-Zellen bezeichnet werden. Trotz wachsender Würdigung der Rolle der B-Zellen in dem Mikromilieu solider Tumore werden die meisten Immunkontrollpunkte-Blockade-Therapien mit dem Ziel entwickelt, auf T-Zellen einzuwirken und ihre Aktivierung zu induzieren. Bislang wurde den B-Zellen, die in solide Tumore eindringen, eine heterogene Wirkung zugeschrieben. Die Präsenz von B-Zellen innerhalb von Tumoren korrelierte in mehreren Studien mit einem verbesserten Überleben der Patienten. Es gibt jedoch auch Untersuchungen, die die Pro-Tumor-Rolle der B-Zellen und das Fortschreiten der Krankheit beschreiben. Diese unterschiedlichen Beobachtungen hängen von der untersuchten Tumorentität und B-Zell-Untergruppen ab, aber die genauen, dem zugrunde liegenden Mechanismen und Regulationen sind nur unzureichend verstanden und müssen noch vollständig aufgeklärt werden.

Das Ziel dieses Projekts ist es, tumorinfiltrierende B-Zellen in soliden Tumorentitäten phänotypisch zu charakterisieren. Zu diesem Zweck wird die MACSima-Technologie eingesetzt, um das Marker-Expressionsmuster von B-Zellen in soliden Tumoren im Zusammenhang mit ihrer räumlichen Lokalisation zu untersuchen. B-Zellen konnten in 21% der untersuchten Proben nachgewiesen werden. Dabei wurden TLS-ähnliche Strukturen identifiziert, die hauptsächlich aus B- und T-Zellen, aber auch aus $CD64^+$-Makrophagen, hochendothelialen Venolen und $CD21^+$ follikulären dendritischen Zellen bestehen. Auch wenn bis zu diesem Zeitpunkt keine neue Untergruppe von B-Zellen eindeutig identifiziert werden konnte, konnte die interessante Beobachtung gemacht werden, dass die B-Zellen innerhalb der TLS-ähnlichen Struktur eine Prävalenz eines Gedächtnis-B-Zell-Phänotyps aufweisen. In Übereinstimmung damit wurden ähnliche Beobachtungen durchflusszytometrisch an frisch dissoziierten soliden Tumoren gemacht. Interessanterweise konnte zusätzlich dazu mit der MACSima-Technologie eine ausgeprägte $CD138^+CD38^+$-Plasmazellpopulation in der Umgebung der TLS-ähnlichen Struktur innerhalb des Tumors nachgewiesen werden, die darüber hinaus durch durchflusszytometrische und RNA-Sequenzierungsanalysen dissoziierter Tumorproben validiert werden konnte. Die Beobachtung vieler Gedächtnis-B-Zellen und Plasmazellen bestärkt die Vermutung, dass innerhalb der tertiären lymphatischen Strukturen im Mikromilieus des Tumors eine Affinitätsreifung stattfinden könnte, und lässt vermuten, dass diese Zellen tumorspezifische Antikörper sezernieren. Daher wurde die BCR-Einzelzell-Sequenzierung zur Identifizierung tumorspezifischer Antikörper verwendet, kombiniert mit einer RNA-Expressionsanalyse. Erwähnenswert ist, dass eine deutlich erhöhte

Anzahl von BCR-Klonen in vorangereicherten B-Zellfraktionen gefunden wurde und der dominanteste Klon einen Plasmazell-Phänotyp zeigt, der durch die Expression von einem späten B-Zelldifferenzierungsmarker-Muster gekennzeichnet ist. Die rekombinante Produktion des ausgewählten, am häufigsten vorkommenden Antikörperklons zeigte keine Bindung an einen Großteil der jeweiligen Primärtumorprobe und auch nicht an humane Ovariazelllinien. Es müssen mehr Tumorproben und B-Zell-Klone gescreent und getestet werden, um den Durchsatz und damit die Wahrscheinlichkeit zu erhöhen, einen geeigneten Klon zu identifizieren, der die Anforderungen an ein mögliches zukünftiges Therapeutikum erfüllt. Diese sind insbesondere: hohe Tumorspezifität bei gleichzeitig geringer Spezifität für ein unter normalen Umständen im gesunden Körper vorkommendes Epitop. Außerdem sollte das Epitop auf einem hohen Prozentsatz von Tumorzellen vorhanden sein und im besten Fall von einer beträchtlichen Gruppe von Patienten geteilt wird. Darüber hinaus beinhaltet die Identifizierung tumorspezifischer B-Zell-Marker die Möglichkeit, spezifische B-Zellen zu isolieren oder gezielt anzusprechen. Insgesamt ergänzen diese Daten die Informationen über die B-Zell-Phänotypen in Tumoren und validieren sie weiter. Weiterführende Anstrengungen in diese Richtung bieten das Potenzial den Weg für neue Immuntherapien auf der Basis von B-Zellen zu entwickeln und zu ebnen.

7. References

10XGenomics. 2020. Sequencing Requirements for Single Cell V(D)J.

Al-Shibli KI, Donnem T, Al-Saad S, Persson M, Bremnes RM, Busund LT. 2008. Prognostic effect of epithelial and stromal lymphocyte infiltration in non-small cell lung cancer. Clinical cancer research : an official journal of the American Association for Cancer Research 14(16):5220-5227.

Alberts B JA, Lewis J, et al. 2002. Molecular Biology of the Cell. 4th ed: New York: Garland Science.

Ammirante M, Luo JL, Grivennikov S, Nedospasov S, Karin M. 2010. B-cell-derived lymphotoxin promotes castration-resistant prostate cancer. Nature 464(7286):302-305.

Andreu P, Johansson M, Affara NI, Pucci F, Tan T, Junankar S, Korets L, Lam J, Tawfik D, DeNardo DG and others. 2010. FcRgamma activation regulates inflammation-associated squamous carcinogenesis. Cancer cell 17(2):121-134.

Astorri E, Bombardieri M, Gabba S, Peakman M, Pozzilli P, Pitzalis C. 2010. Evolution of ectopic lymphoid neogenesis and in situ autoantibody production in autoimmune nonobese diabetic mice: cellular and molecular characterization of tertiary lymphoid structures in pancreatic islets. Journal of immunology 185(6):3359-3368.

Bar-Or A, Oliveira EM, Anderson DE, Krieger JI, Duddy M, O'Connor KC, Hafler DA. 2001. Immunological memory: contribution of memory B cells expressing costimulatory molecules in the resting state. Journal of immunology 167(10):5669-5677.

Barbera-Guillem E, Nelson MB, Barr B, Nyhus JK, May KF, Jr., Feng L, Sampsel JW. 2000. B lymphocyte pathology in human colorectal cancer. Experimental and clinical therapeutic effects of partial B cell depletion. Cancer immunology, immunotherapy : CII 48(10):541-549.

Batista FD, Harwood NE. 2009. The who, how and where of antigen presentation to B cells. Nature reviews Immunology 9(1):15-27.

Bindea G, Mlecnik B, Angell HK, Galon J. 2014. The immune landscape of human tumors: Implications for cancer immunotherapy. Oncoimmunology 3(1):e27456.

Bindea G, Mlecnik B, Tosolini M, Kirilovsky A, Waldner M, Obenauf AC, Angell H, Fredriksen T, Lafontaine L, Berger A and others. 2013. Spatiotemporal dynamics of intratumoral immune cells reveal the immune landscape in human cancer. Immunity 39(4):782-795.

Bodogai M, Moritoh K, Lee-Chang C, Hollander CM, Sherman-Baust CA, Wersto RP, Araki Y, Miyoshi I, Yang L, Trinchieri G and others. 2015. Immunosuppressive and Prometastatic Functions of Myeloid-Derived Suppressive Cells Rely upon Education from Tumor-Associated B Cells. Cancer research 75(17):3456-3465.

Bomben R, Dal-Bo M, Benedetti D, Capello D, Forconi F, Marconi D, Bertoni F, Maffei R, Laurenti L, Rossi D and others. 2010. Expression of mutated IGHV3-23 genes in chronic lymphocytic leukemia identifies a disease subset with peculiar clinical and biological features. Clinical cancer research : an official journal of the American Association for Cancer Research 16(2):620-628.

Brändlein S, Pohle T, Ruoff N, Wozniak E, Müller-Hermelink HK, Vollmers HP. 2003. Natural IgM antibodies and immunosurveillance mechanisms against epithelial cancer cells in humans. Cancer research 63(22):7995-8005.

Brink R. 2014. The imperfect control of self-reactive germinal center B cells. Current opinion in immunology 28:97-101.

Cabrita R, Lauss M, Sanna A, Donia M, Skaarup Larsen M, Mitra S, Johansson I, Phung B, Harbst K, Vallon-Christersson J and others. 2020. Tertiary lymphoid structures improve immunotherapy and survival in melanoma. Nature 577(7791):561-565.

Carmi Y, Spitzer MH, Linde IL, Burt BM, Prestwood TR, Perlman N, Davidson MG, Kenkel JA, Segal E, Pusapati GV and others. 2015. Allogeneic IgG combined with dendritic cell stimuli induce antitumour T-cell immunity. Nature 521(7550):99-104.

Casola S, Perucho L, Tripodo C, Sindaco P, Ponzoni M, Facchetti F. 2019. The B-cell receptor in control of tumor B-cell fitness: Biology and clinical relevance. Immunological reviews 288(1):198-213.

Cipponi A, Mercier M, Seremet T, Baurain JF, Theate I, van den Oord J, Stas M, Boon T, Coulie PG, van Baren N. 2012. Neogenesis of lymphoid structures and antibody responses occur in human melanoma metastases. Cancer research 72(16):3997-4007.

Colbeck EJ, Ager A, Gallimore A, Jones GW. 2017. Tertiary Lymphoid Structures in Cancer: Drivers of Antitumor Immunity, Immunosuppression, or Bystander Sentinels in Disease? Frontiers in immunology 8:1830.

Cooper MD, Peterson RDA, Good RA. 1965. Delineation of the Thymic and Bursal Lymphoid Systems in the Chicken. Nature 205(4967):143-146.

Cooper MD, Raymond DA, Peterson RD, South MA, Good RA. 1966. The functions of the thymus system and the bursa system in the chicken. The Journal of experimental medicine 123(1):75-102.

Cottrell TR, Taube JM. 2018. PD-L1 and Emerging Biomarkers in Immune Checkpoint Blockade Therapy. Cancer journal (Sudbury, Mass) 24(1):41-46.

Coventry BJ, Baume D, Lilly C. 2015. Long-term survival in advanced melanoma patients using repeated therapies: successive immunomodulation improving the odds? Cancer management and research 7:93-103.

Crawford A, Macleod M, Schumacher T, Corlett L, Gray D. 2006. Primary T cell expansion and differentiation in vivo requires antigen presentation by B cells. Journal of immunology 176(6):3498-3506.

de Visser KE, Korets LV, Coussens LM. 2005. De novo carcinogenesis promoted by chronic inflammation is B lymphocyte dependent. Cancer cell 7(5):411-423.

Deola S, Panelli MC, Maric D, Selleri S, Dmitrieva NI, Voss CY, Klein H, Stroncek D, Wang E, Marincola FM. 2008. Helper B cells promote cytotoxic T cell survival and proliferation independently of antigen presentation through CD27/CD70 interactions. Journal of immunology 180(3):1362-1372.

Díaz-Zaragoza M, Hernández-Ávila R, Viedma-Rodríguez R, Arenas-Aranda D, Ostoa-Saloma P. 2015. Natural and adaptive IgM antibodies in the recognition of tumor-associated antigens of breast cancer (Review). Oncology reports 34(3):1106-1114.

Dieu-Nosjean MC, Goc J, Giraldo NA, Sautès-Fridman C, Fridman WH. 2014. Tertiary lymphoid structures in cancer and beyond. Trends in immunology 35(11):571-580.

Dong HP, Elstrand MB, Holth A, Silins I, Berner A, Trope CG, Davidson B, Risberg B. 2006. NK- and B-cell infiltration correlates with worse outcome in metastatic ovarian carcinoma. American journal of clinical pathology 125(3):451-458.

Fanoni D, Tavecchio S, Recalcati S, Balice Y, Venegoni L, Fiorani R, Crosti C, Berti E. 2011. New monoclonal antibodies against B-cell antigens: possible new strategies for diagnosis of primary cutaneous B-cell lymphomas. Immunology letters 134(2):157-160.

Farkona S, Diamandis EP, Blasutig IM. 2016. Cancer immunotherapy: the beginning of the end of cancer? BMC medicine 14:73.

Fillatreau S, Sweenie CH, McGeachy MJ, Gray D, Anderton SM. 2002. B cells regulate autoimmunity by provision of IL-10. Nature immunology 3(10):944-950.

Flynn NJ, Somasundaram R, Arnold KM, Sims-Mourtada J. 2017. The Multifaceted Roles of B Cells in Solid Tumors: Emerging Treatment Opportunities. Targeted Oncology 12(2):139-152.

Folkman J. 1971. Tumor angiogenesis: therapeutic implications. The New England journal of medicine 285(21):1182-1186.

Fremd C, Schuetz F, Sohn C, Beckhove P, Domschke C. 2013. B cell-regulated immune responses in tumor models and cancer patients. Oncoimmunology 2(7):e25443.

Fridman WH, Zitvogel L, Sautès-Fridman C, Kroemer G. 2017. The immune contexture in cancer prognosis and treatment. Nature reviews Clinical oncology 14(12):717-734.

Gu-Trantien C, Loi S, Garaud S, Equeter C, Libin M, de Wind A, Ravoet M, Le Buanec H, Sibille C, Manfouo-Foutsop G and others. 2013. $CD4^+$ follicular helper T cell infiltration predicts breast cancer survival. The Journal of clinical investigation 123(7):2873-2892.

Gun SY, Lee SWL, Sieow JL, Wong SC. 2019. Targeting immune cells for cancer therapy. Redox biology 25:101174.

Gunderson AJ, Coussens LM. 2013. B cells and their mediators as targets for therapy in solid tumors. Experimental cell research 319(11):1644-1649.

Guo FF, Cui JW. 2019. The Role of Tumor-Infiltrating B Cells in Tumor Immunity. Journal of oncology 2019:2592419.

Hadrup S, Donia M, thor Straten P. 2013. Effector CD4 and CD8 T Cells and Their Role in the Tumor Microenvironment. Cancer Microenvironment 6(2):123-133.

Hagn M, Schwesinger E, Ebel V, Sontheimer K, Maier J, Beyer T, Syrovets T, Laumonnier Y, Fabricius D, Simmet T and others. 2009. Human B cells secrete granzyme B when recognizing viral antigens in the context of the acute phase cytokine IL-21. Journal of immunology 183(3):1838-1845.

Hansen MH, Nielsen HV, Ditzel HJ. 2002. Translocation of an intracellular antigen to the surface of medullary breast cancer cells early in apoptosis allows for an antigen-driven antibody response elicited by tumor-infiltrating B cells. Journal of immunology 169(5):2701-2711.

Harris AL. 2002. Hypoxia--a key regulatory factor in tumour growth. Nature reviews Cancer 2(1):38-47.

Heise N, De Silva NS, Silva K, Carette A, Simonetti G, Pasparakis M, Klein U. 2014. Germinal center B cell maintenance and differentiation are controlled by distinct NF-κB transcription factor subunits. The Journal of experimental medicine 211(10):2103-2118.

Helmink BA, Reddy SM, Gao J, Zhang S, Basar R, Thakur R, Yizhak K, Sade-Feldman M, Blando J, Han G and others. 2020. B cells and tertiary lymphoid structures promote immunotherapy response. Nature 577(7791):549-555.

Hilpert C, Sitte S, Matthies A, Voehringer D. 2016. Dendritic Cells Are Dispensable for T Cell Priming and Control of Acute Lymphocytic Choriomeningitis Virus Infection. Journal of immunology 197(7):2780-2786.

Hsueh EC, Essner R, Foshag LJ, Ollila DW, Gammon G, O'Day SJ, Boasberg PD, Stern SL, Ye X, Morton DL. 2002. Prolonged Survival After Complete Resection of Disseminated Melanoma and Active Immunotherapy With a Therapeutic Cancer Vaccine. Journal of Clinical Oncology 20(23):4549-4554.

Hwang WT, Adams SF, Tahirovic E, Hagemann IS, Coukos G. 2012. Prognostic significance of tumor-infiltrating T cells in ovarian cancer: a meta-analysis. Gynecologic oncology 124(2):192-198.

Iglesia MD, Vincent BG, Parker JS, Hoadley KA, Carey LA, Perou CM, Serody JS. 2014. Prognostic B-cell signatures using mRNA-seq in patients with subtype-specific breast and ovarian cancer. Clinical cancer research : an official journal of the American Association for Cancer Research 20(14):3818-3829.

Intlekofer AM, Thompson CB. 2013. At the bench: preclinical rationale for CTLA-4 and PD-1 blockade as cancer immunotherapy. Journal of leukocyte biology 94(1):25-39.

Jackson SM, Wilson PC, James JA, Capra JD. 2008. Human B cell subsets. Advances in immunology 98:151-224.

Jacquelot N, Roberti MP, Enot DP, Rusakiewicz S, Ternès N, Jegou S, Woods DM, Sodré AL, Hansen M, Meirow Y and others. 2017. Predictors of responses to immune checkpoint blockade in advanced melanoma. Nature communications 8(1):592.

Janeway C. 2012. Janeway's immunobiology. New York, Garland Science.

Jayasingam SD, Citartan M, Thang TH, Mat Zin AA, Ang KC, Ch'ng ES. 2019. Evaluating the Polarization of Tumor-Associated Macrophages Into M1 and M2 Phenotypes in Human Cancer Tissue: Technicalities and Challenges in Routine Clinical Practice. Frontiers in oncology 9:1512.

Karasuyama H, Rolink A, Shinkai Y, Young F, Alt FW, Melchers F. 1994. The expression of Vpre-B/lambda 5 surrogate light chain in early bone marrow precursor B cells of normal and B cell-deficient mutant mice. Cell 77(1):133-143.

Kemp TJ, Moore JM, Griffith TS. 2004. Human B cells express functional TRAIL/Apo-2 ligand after CpG-containing oligodeoxynucleotide stimulation. Journal of immunology 173(2):892-899.

Kitamura D, Kudo A, Schaal S, Müller W, Melchers F, Rajewsky K. 1992. A critical role of lambda 5 protein in B cell development. Cell 69(5):823-831.

Königsberger S, Weis V, Prodöhl J, Stehling M, Hobeika E, Reth M, Kiefer F. 2015. Suboptimal B-cell antigen receptor signaling activity in vivo elicits germinal center counterselection mechanisms. European journal of immunology 45(2):603-611.

Kräutler NJ, Suan D. 2017. Differentiation of germinal center B cells into plasma cells is initiated by high-affinity antigen and completed by Tfh cells. J Exp Med
214(5):1259-1267.

Kumar S, Mohan A, Guleria R. 2009. Prognostic implications of circulating anti-p53 antibodies in lung cancer--a review. European journal of cancer care 18(3):248-254.

Kurosaki T. 2011. Regulation of BCR signaling. Molecular immunology 48(11):1287-1291.

Kurosaki T, Shinohara H, Baba Y. 2010. B cell signaling and fate decision. Annual review of immunology 28:21-55.

Lebien TW, Tedder TF. 2008. B lymphocytes: how they develop and function. Blood 112 5:1570-1580.

Lee-Chang C, Rashidi A, Miska J, Zhang P, Pituch KC, Hou D, Xiao T, Fischietti M, Kang SJ, Appin CL and others. 2019. Myeloid-Derived Suppressive Cells Promote B cell-Mediated Immunosuppression via Transfer of PD-L1 in Glioblastoma. Cancer immunology research 7(12):1928-1943.

Lee HJ, Park IA, Song IH, Shin SJ, Kim JY, Yu JH, Gong G. 2016. Tertiary lymphoid structures: prognostic significance and relationship with tumour-infiltrating lymphocytes in triple-negative breast cancer. Journal of clinical pathology 69(5):422-430.

Liao W, Hua Z, Liu C, Lin L, Chen R, Hou B. 2017. Characterization of T-Dependent and T-Independent B Cell Responses to a Virus-like Particle. Journal of immunology 198(10):3846-3856.

Lindner S, Dahlke K, Sontheimer K, Hagn M, Kaltenmeier C, Barth TF, Beyer T, Reister F, Fabricius D, Lotfi R and others. 2013. Interleukin 21-induced granzyme B-expressing B cells infiltrate tumors and regulate T cells. Cancer research 73(8):2468-2479.

Linton PJ, Bautista B, Biederman E, Bradley ES, Harbertson J, Kondrack RM, Padrick RC, Bradley LM. 2003. Costimulation via OX40L expressed by B cells is sufficient to determine the extent of primary CD4 cell expansion and Th2 cytokine secretion in vivo. The Journal of experimental medicine 197(7):875-883.

Lund FE. 2008. Cytokine-producing B lymphocytes-key regulators of immunity. Current opinion in immunology 20(3):332-338.

Luo JL, Tan W, Ricono JM, Korchynskyi O, Zhang M, Gonias SL, Cheresh DA, Karin M. 2007. Nuclear cytokine-activated IKKalpha controls prostate cancer metastasis by repressing Maspin. Nature 446(7136):690-694.

Luther SA, Lopez T, Bai W, Hanahan D, Cyster JG. 2000. BLC expression in pancreatic islets causes B cell recruitment and lymphotoxin-dependent lymphoid neogenesis. Immunity 12(5):471-481.

Magalhaes I, Yogev O, Mattsson J, Schurich A. 2019. The Metabolic Profile of Tumor and Virally Infected Cells Shapes Their Microenvironment Counteracting T Cell Immunity. Frontiers in immunology 10:2309.

Martin F, Chan AC. 2006. B cell immunobiology in disease: evolving concepts from the clinic. Annual review of immunology 24:467-496.

Messina JL, Fenstermacher DA, Eschrich S, Qu X, Berglund AE, Lloyd MC, Schell MJ, Sondak VK, Weber JS, Mulé JJ. 2012. 12-Chemokine gene signature identifies lymph node-like structures in melanoma: potential for patient selection for immunotherapy? Scientific reports 2:765.

Milne K, Köbel M, Kalloger SE, Barnes RO, Gao D, Gilks CB, Watson PH, Nelson BH. 2009. Systematic analysis of immune infiltrates in high-grade serous ovarian cancer reveals CD20, FoxP3 and TIA-1 as positive prognostic factors. PloS one 4(7):e6412.

Mizoguchi A, Mizoguchi E, Takedatsu H, Blumberg RS, Bhan AK. 2002. Chronic intestinal inflammatory condition generates IL-10-producing regulatory B cell subset characterized by CD1d upregulation. Immunity 16(2):219-230.

Montfort A, Pearce O, Maniati E, Vincent BG, Bixby L, Böhm S, Dowe T, Wilkes EH, Chakravarty P, Thompson R and others. 2017. A Strong B-cell Response Is Part of the Immune Landscape in Human High-Grade Serous Ovarian Metastases. Clinical cancer research : an official journal of the American Association for Cancer Research 23(1):250-262.

Nedergaard BS, Ladekarl M, Nyengaard JR, Nielsen K. 2008. A comparative study of the cellular immune response in patients with stage IB cervical squamous cell carcinoma. Low numbers of several immune cell subtypes are strongly associated with relapse of disease within 5 years. Gynecologic oncology 108(1):106-111.

Nelson BH. 2010. CD20+ B cells: the other tumor-infiltrating lymphocytes. Journal of immunology 185(9):4977-4982.

Nieuwenhuis P, Opstelten D. 1984. Functional anatomy of germinal centers. The American journal of anatomy 170(3):421-435.

Nutt SL, Hodgkin PD, Tarlinton DM, Corcoran LM. 2015. The generation of antibody-secreting plasma cells. Nature reviews Immunology 15(3):160-171.

Oettinger MA, Schatz DG, Gorka C, Baltimore D. 1990. RAG-1 and RAG-2, adjacent genes that synergistically activate V(D)J recombination. Science (New York, NY) 248(4962):1517-1523.

Okazaki T, Maeda A, Nishimura H, Kurosaki T, Honjo T. 2001. PD-1 immunoreceptor inhibits B cell receptor-mediated signaling by recruiting src homology 2-domain-containing tyrosine phosphatase 2 to phosphotyrosine. Proceedings of the National Academy of Sciences of the United States of America 98(24):13866-13871.

Olkhanud PB, Baatar D, Bodogai M, Hakim F, Gress R, Anderson RL, Deng J, Xu M, Briest S, Biragyn A. 2009. Breast cancer lung metastasis requires expression of chemokine receptor CCR4 and regulatory T cells. Cancer research 69(14):5996-6004.

Olkhanud PB, Damdinsuren B, Bodogai M, Gress RE, Sen R, Wejksza K, Malchinkhuu E, Wersto RP, Biragyn A. 2011. Tumor-evoked regulatory B cells promote breast cancer metastasis by converting resting $CD4^+$ T cells to T-regulatory cells. Cancer research 71(10):3505-3515.

Pardoll DM. 2012. The blockade of immune checkpoints in cancer immunotherapy. Nature reviews Cancer 12(4):252-264.

Pavoni E, Monteriu G, Santapaola D, Petronzelli F, Anastasi AM, Pelliccia A, D'Alessio V, De Santis R, Minenkova O. 2007. Tumor-infiltrating B lymphocytes as an efficient source of highly specific immunoglobulins recognizing tumor cells. BMC biotechnology 7:70.

Pillai S, Baltimore D. 1987. Formation of disulphide-linked mu 2 omega 2 tetramers in pre-B cells by the 18K omega-immunoglobulin light chain. Nature 329(6135):172-174.

Pimenta EM, Barnes BJ. 2014. Role of Tertiary Lymphoid Structures (TLS) in Anti-Tumor Immunity: Potential Tumor-Induced Cytokines/Chemokines that Regulate TLS Formation in Epithelial-Derived Cancers. Cancers 6(2):969-997.

Pioli C, Gatta L, Ubaldi V, Doria G. 2000. Inhibition of IgG1 and IgE production by stimulation of the B cell CTLA-4 receptor. Journal of immunology 165(10):5530-5536.

Postow MA, Callahan MK, Wolchok JD. 2015. Immune Checkpoint Blockade in Cancer Therapy. Journal of clinical oncology : official journal of the American Society of Clinical Oncology 33(17):1974-1982.

Rabinovich GA, Gabrilovich D, Sotomayor EM. 2007. Immunosuppressive strategies that are mediated by tumor cells. Annual review of immunology 25:267-296.

Reuschenbach M, von Knebel Doeberitz M, Wentzensen N. 2009. A systematic review of humoral immune responses against tumor antigens. Cancer immunology, immunotherapy : CII 58(10):1535-1544.

Richards CH, Flegg KM, Roxburgh CS, Going JJ, Mohammed Z, Horgan PG, McMillan DC. 2012. The relationships between cellular components of the peritumoural inflammatory response, clinicopathological characteristics and survival in patients with primary operable colorectal cancer. British journal of cancer 106(12):2010-2015.

Sautes-Fridman C, Petitprez F, Calderaro J, Fridman WH. 2019. Tertiary lymphoid structures in the era of cancer immunotherapy. Nature reviews Cancer 19(6):307-325.

Schatz DG, Oettinger MA, Baltimore D. 1989. The V(D)J recombination activating gene, RAG-1. Cell 59(6):1035-1048.

Schlößer HA, Thelen M, Lechner A, Wennhold K, Garcia-Marquez MA, Rothschild SI, Staib E, Zander T, Beutner D, Gathof B and others. 2019. B cells in esophago-gastric adenocarcinoma are highly differentiated, organize in tertiary lymphoid structures and produce tumor-specific antibodies. Oncoimmunology 8(1):e1512458.

Schmidt M, Böhm D, von Törne C, Steiner E, Puhl A, Pilch H, Lehr HA, Hengstler JG, Kölbl H, Gehrmann M. 2008. The humoral immune system has a key prognostic impact in node-negative breast cancer. Cancer research 68(13):5405-5413.

Schrama D, thor Straten P, Fischer WH, McLellan AD, Bröcker EB, Reisfeld RA, Becker JC. 2001. Targeting of lymphotoxin-alpha to the tumor elicits an efficient immune response associated with induction of peripheral lymphoid-like tissue. Immunity 14(2):111-121.

Selitsky SR, Mose LE, Smith CC, Chai S, Hoadley KA, Dittmer DP, Moschos SJ, Parker JS, Vincent BG. 2019. Prognostic value of B cells in cutaneous melanoma. Genome medicine 11(1):36.

Semenza GL. 2012. Hypoxia-inducible factors: mediators of cancer progression and targets for cancer therapy. Trends in pharmacological sciences 33(4):207-214.

Sharonov GV, Serebrovskaya EO, Yuzhakova DV, Britanova OV, Chudakov DM. 2020. B cells, plasma cells and antibody repertoires in the tumour microenvironment. Nature reviews Immunology 20(5):294-307.

Shen P, Fillatreau S. 2015. Antibody-independent functions of B cells: a focus on cytokines. Nature reviews Immunology 15(7):441-451.

Shen P, Roch T, Lampropoulou V, O'Connor RA, Stervbo U, Hilgenberg E, Ries S, Dang VD, Jaimes Y, Daridon C and others. 2014. IL-35-producing B cells are critical regulators of immunity during autoimmune and infectious diseases. Nature 507(7492):366-370.

Shi JY, Gao Q, Wang ZC, Zhou J, Wang XY, Min ZH, Shi YH, Shi GM, Ding ZB, Ke AW and others. 2013. Margin-infiltrating CD20(+) B cells display an atypical memory phenotype and correlate with favorable prognosis in hepatocellular carcinoma. Clinical cancer research : an official journal of the American Association for Cancer Research 19(21):5994-6005.

Shimabukuro-Vornhagen A, Schlößer HA, Gryschok L, Malcher J, Wennhold K, Garcia-Marquez M, Herbold T, Neuhaus LS, Becker HJ, Fiedler A and others. 2014. Characterization of tumor-associated B-cell subsets in patients with colorectal cancer. Oncotarget 5(13):4651-4664.

Siliņa K, Soltermann A, Attar FM, Casanova R, Uckeley ZM, Thut H, Wandres M, Isajevs S, Cheng P, Curioni-Fontecedro A and others. 2018. Germinal Centers Determine the Prognostic Relevance of Tertiary Lymphoid Structures and Are Impaired by Corticosteroids in Lung Squamous Cell Carcinoma. Cancer research 78(5):1308-1320.

Song IH, Heo SH, Bang WS, Park HS, Park IA, Kim YA, Park SY, Roh J, Gong G, Lee HJ. 2017. Predictive Value of Tertiary Lymphoid Structures Assessed by High Endothelial Venule Counts in the Neoadjuvant Setting of Triple-Negative Breast Cancer. Cancer research and treatment : official journal of Korean Cancer Association 49(2):399-407.

Stubbs M, McSheehy PM, Griffiths JR, Bashford CL. 2000. Causes and consequences of tumour acidity and implications for treatment. Molecular medicine today 6(1):15-19.

Teillaud JL, Dieu-Nosjean MC. 2017. Tertiary Lymphoid Structures: An Anti-tumor School for Adaptive Immune Cells and an Antibody Factory to Fight Cancer? Frontiers in immunology 8:830.

Teng MW, Galon J, Fridman WH, Smyth MJ. 2015. From mice to humans: developments in cancer immunoediting. The Journal of clinical investigation 125(9):3338-3346.

Thibult ML, Mamessier E, Gertner-Dardenne J, Pastor S, Just-Landi S, Xerri L, Chetaille B, Olive D. 2013. PD-1 is a novel regulator of human B-cell activation. International immunology 25(2):129-137.

Tirosh I, Izar B, Prakadan SM, Wadsworth MH, 2nd, Treacy D, Trombetta JJ, Rotem A, Rodman C, Lian C, Murphy G and others. 2016. Dissecting the multicellular ecosystem of metastatic melanoma by single-cell RNA-seq. Science (New York, NY) 352(6282):189-196.

Tobón GJ, Izquierdo JH, Cañas CA. 2013. B lymphocytes: development, tolerance, and their role in autoimmunity-focus on systemic lupus erythematosus. Autoimmune diseases 2013:827254.

Vargas-Inchaustegui DA, Robert-Guroff M. 2013. Fc receptor-mediated immune responses: new tools but increased complexity in HIV prevention. Current HIV research 11(5):407-420.

Vaupel P, Mayer A. 2007. Hypoxia in cancer: significance and impact on clinical outcome. Cancer metastasis reviews 26(2):225-239.

Wagner J, Rapsomaniki MA, Chevrier S, Anzeneder T, Langwieder C, Dykgers A, Rees M, Ramaswamy A, Muenst S, Soysal SD and others. 2019. A Single-Cell Atlas of the Tumor and Immune Ecosystem of Human Breast Cancer. Cell 177(5):1330-1345.e1318.

Wang M, Yin B, Wang HY, Wang RF. 2014. Current advances in T-cell-based cancer immunotherapy. Immunotherapy 6(12):1265-1278.

Wejksza K, Lee-Chang C, Bodogai M, Bonzo J, Gonzalez FJ, Lehrmann E, Becker K, Biragyn A. 2013. Cancer-produced metabolites of 5-lipoxygenase induce tumor-evoked regulatory B cells via peroxisome proliferator-activated receptor α. Journal of immunology 190(6):2575-2584.

Whitmire JK, Asano MS, Kaech SM, Sarkar S, Hannum LG, Shlomchik MJ, Ahmed R. 2009. Requirement of B cells for generating CD4+ T cell memory. Journal of immunology 182(4):1868-1876.

Wölfl M, Kuball J, Eyrich M, Schlegel PG, Greenberg PD. 2008. Use of CD137 to study the full repertoire of CD8+ T cells without the need to know epitope specificities. Cytometry Part A : the journal of the International Society for Analytical Cytology 73(11):1043-1049.

Woo JR, Liss MA, Muldong MT, Palazzi K, Strasner A, Ammirante M, Varki N, Shabaik A, Howell S, Kane CJ and others. 2014. Tumor infiltrating B-cells are increased in prostate cancer tissue. Journal of translational medicine 12:30.

Workel HH, Lubbers JM. 2019. A Transcriptionally Distinct CXCL13(+)CD103(+)CD8(+) T-cell Population Is Associated with B-cell Recruitment and Neoantigen Load in Human Cancer. Cancer Immunol Res 7(5):784-796.

Yanaba K, Bouaziz JD, Matsushita T, Magro CM, St Clair EW, Tedder TF. 2008. B-lymphocyte contributions to human autoimmune disease. Immunological reviews 223:284-299.

Yang J, Reth M. 2016. Receptor Dissociation and B-Cell Activation. Current topics in microbiology and immunology 393:27-43.

Yuen GJ, Demissie E, Pillai S. 2016. B lymphocytes and cancer: a love-hate relationship. Trends in cancer 2(12):747-757.

Zhang Y, Eliav Y, Shin SU, Schreiber TH, Podack ER, Tadmor T, Rosenblatt JD. 2013. B lymphocyte inhibition of anti-tumor response depends on expansion of Treg but is independent of B-cell IL-10 secretion. Cancer immunology, immunotherapy : CII 62(1):87-99.

8. Acknowledgment

I am so overwhelmed while writing this, that I don't know from where to start. Firstly, I would like to thank Andrzej Dzionek and Mario Assenmacher for providing me the opportunity to work on this exciting project. I would like to extend a deep sense of gratitude and respect to my supervisor Daniela Vorholt for her support and encouragement at crucial stages of my PhD tenure which has made this academic landmark achievable. She always has the right combination of encouragement and critics and her belief in my potentials helped a lot in my independent growth as a researcher. It was my privilege to work with her and I could not have asked for a better mentor.

I warmly express my special thanks to Bianca and Elvira for their collaboration on solid tumor samples part. Our brainstorming sessions on utilizing every bit of tissues really helped in developing an optimal workflow which is mandatory for projects like this, based on human samples. Special thanks to Elvira for always helping me in screening and dissociation of tumor samples, I think we make a good team.

I express my deepest gratitude to my academic supervisor, Prof. Dr. Ralf Küppers. His profound knowledge of B cells and critical input helped me a lot in giving direction and making the final conclusion for the story. He is the live example of the phrase "just a call/mail away". Despite his busy schedule, he always responded promptly, positively and precisely, just the perfect way, which assisted me during lows of the project to be optimistic and to always give my best. I feel honored to have him as my Doctoral father. I also would like to thank Prof. Dr. Jan Dürig for agreeing to be my second supervisor. I appreciate a lot of his support.

Heartfelt thanks to "MICS team" including Vanessa, Lara, Christiane, Maurice and Kathrin, for always helping me with the materials and special inputs of the critical parts of the experiments.

All these data would not have been possible without support from "MACSima team" including Jan and Markus, who provided me with the time and help during the runs. I am also grateful to Prof. Werner Müller, who always helped me with the bioinformatic analysis of the data. Special thanks to Andre for designing the InspectorCell tool and helping in the analysis.

Sincere thanks to Nadine and Ruth for their help in single-cell sequencing experiments. Special thanks to Nadine for providing me with the detailed protocol for the 10X part. Heartfelt thanks to Stefan for his assistance and comments in the analysis of 10X data.

I profusely thank Meike Bartl for helping me in the generation of antibody, I learnt a lot and especially I enjoyed my time in the group. Special thanks to Anne and David for providing me ovarian cell lines.

I would also like to thank all members of the Students club for their critical comments and fruitful discussion that helped me to grow scientifically over the last years.

Special and heartfelt thanks to "H13 PhD squad" including Daniel, Jona, Janina, Jonathan, Alba and Asia. Thank you for providing me with the emotional support, for always hearing me out. Thank you for making me feel "home away from home".

I would like to acknowledge support from my friends Hamiz, Nischal and Gaurav for always being there for me. This journey wouldn't have been possible without their trust and believe in me.

Words fall short to mention the assorted and benevolent presence of my parents and my sisters Anamika and Ankita who inspired me to achieve the best in life. Even though I was not able to visit and spend time with them during the last years, the never-ending love and encouragement from their side made me be the person who I am today.

The space available is limited but I express my gratitude to all responsible for the success of the present endeavor. With the completion of this study, I feel one can achieve anything, if they have support of the right people around. Thank you all!

13.08.2020 Apu 😊

The curriculum vitae is not included for data protection reasons

The curriculum vitae is not included for data protection reasons

9. Declarations

Declaration:

In accordance with § 6 (para. 2, clause g) of the Regulations Governing the Doctoral Proceedings of the Faculty of Biology for awarding the doctoral degree Dr. rer. nat., I hereby declare that I represent the field to which the topic “Characterization of tumor-infiltrating B cells in solid tumors” is assigned in research and teaching and that I support the application of Aparajita Singh.

Essen, date _____ Prof. Ralf Küppers _____

Name of the scientific supervisor/member of the University of Duisburg-Essen

Signature of the supervisor/ member of the University of Duisburg-Essen

Declaration:

In accordance with § 7 (para. 2, clause d and f) of the Regulations Governing the Doctoral Proceedings of the Faculty of Biology for awarding the doctoral degree Dr. rer. nat., I hereby declare that I have written the herewith submitted dissertation independently using only the materials listed, and have cited all sources taken over verbatim or in content as such.

Essen, date _____ _____

Signature of the doctoral candidate

Declaration:

In accordance with § 7 (para. 2, clause e and g) of the Regulations Governing the Doctoral Proceedings of the Faculty of Biology for awarding the doctoral degree Dr. rer. nat., I hereby declare that I have undertaken no previous attempts to attain a doctoral degree, that the current work has not been rejected by any other faculty, and that I am submitting the dissertation only in this procedure.

Essen, date _____ _____

Signature of the doctoral candidate

DOI: 10.17185/duepublico/73505
URN: urn:nbn:de:hbz:465-20231031-080508-1